Photodynamic Activity of a Glucoconjugated Silicon(IV) Phthalocyanine on Human Colon Adenocarcinoma

CHAN, Man Hung

A Thesis Submitted in Partial Fulfillment

of the Requirements for the Degree of

Master of Philosophy

In

Biochemistry (Science)

The Chinese University of Hong Kong

July 2009

Examination Committee List

Professor Siu-Kai Kong (Chair)

Professor Wing-Ping Fong (Thesis Supervisor)

Professor Kwok-Nam Leung (Committee Member)

Professor Nai-Ki Mak (External Examiner)

I declare that the assignment here submitted is original except for source material explicitly acknowledged, and that the same or related material has not been previously submitted for another course. I also acknowledge that I am aware of University policy and regulations on honesty in academic work, and of the disciplinary guidelines and procedures applicable to breaches of such policy and regulations, as contained in the website.

Signature

30th July 2007
Date

Chan Man Hung
Name

07019230
Student ID

BCH 806R
Course code

Thesis Research
Course title

Acknowledgements

I would like to express my sincere gratitude to my supervisor Prof. Wing-Ping Fong for providing me with this precious opportunity to study the M.Phil degree in CUHK. The experience of doing research here is invaluable for my life. I also want to give thanks for his patient guidance throughout my study. Finally I would like to thank my supervisor again who has reviewed and provided invaluable suggestions for the improvement of this thesis.

I would like to thank Prof. Dennis Kei-Pui Ng and Prof. Pui-Chi Lo, Department of Chemistry, The Chinese University of Hong Kong. They have kindly provided me the chemical SiPcGlu for this study and given me support and help in the field of chemistry.

I particularly want to express my thanks to Ms. Judy Wong, Mr. Chun-Pong Wong, Ms. Esther Yeung and Ms. Anna Cheang for their always spiritual and technical support throughout my study. Special thanks should also be given to Mr. Stanley Leung, Ms. Elaine Chan, Ms. Michel Chan and Mr. Cheung-Wai So. They all helped me a lot when I first entered this laboratory.

I also want to give special gratitude to my family who always support me throughout my study. I would also like to take this opportunity to give my thanks to my husband Daniel who I am deeply in love and treasure with. He has given me the most support throughout these two years, both spiritually and technically.

Lastly, I must give thanks to my Lord who has led me here, given me the chance to learn, to grow and provided me everything I need.

摘要

光動力療法已經成爲一種有望治療癌症、濕性老年性黃斑變性及傳染病的方法。光動力療法透過在光的作用下，激活原來無毒的光敏劑，產生殺害的效用。本研究小組研製了一系列嶄新的第二或三代光敏劑，當中以葡萄糖復合矽酞菁藍(SiPcGlu)被視爲有潛力的光敏劑。在試管研究中，它對人類大腸腺癌細胞產生高度殺傷力，我們亦成功証明由第一及二類光作用反應所產生的活性氧是引致細胞死亡的重要因素。

本小組透過以下幾個測定參數，包括脫氧核糖核苷酸末端轉移酶介導的缺口末端標記、磷酯結合蛋白/碘化丙啶雙染及 DNA 梯形電泳圖譜分析法，証明 SiPcGlu 在光的激活作用下能引起細胞凋亡。另外透過亞細胞定位分析我們亦發現 SiPcGlu 定位於線粒體及內質網，並在光作用下會立刻導致線粒體膜去極化及使其產生活性氧，及至釋放細胞色素 c，激活半胱氨酸蛋白酶 3 及切割二磷酸腺苷核糖多聚酶。另外內質網應激分子伴侶—葡萄糖調節蛋白 78 的蛋白表達及胞漿游離鈣濃度亦相對增加，以上的研究結果顯示線粒體及內質網是光損傷的最初位置。

我們亦在後天性免疫力嚴重缺乏小鼠身上種植大腸腺癌腫瘤，從而評估 SiPcGlu 光動力治療殺死癌細胞的功效及分析其生物分佈。研究結果顯示，雖然 SiPcGlu 的葡萄糖部分未能令其靶向癌細胞組織，但利用醫學用的激光瞄準癌腫瘤，被激活的 SiPcGlu 能顯著地抑制癌細胞的增長。內在的毒性測試結果顯示 SiPcGlu 在有無光的作用下均不會

對後天性免疫力嚴重缺乏小鼠產生肝臟及心臟的損傷，這個測試顯示 SiPcGlu 是臨床的光動力治療上安全的候選光敏劑。

Abstract

Photodynamic therapy (PDT) has emerged as a promising therapeutic modality for cancer, wet age-related macular degeneration and infectious disease. PDT involves the use of a non-toxic photosensitizer which, in the presence of light, is activated to produce the killing effect. We have synthesized a number of novel second or third generation photosensitizers, among them the glucoconjugated silicon(IV) phthalocyanine SiPcGlu is a promising candidate. In the *in vitro* studies, it is highly photocytotoxic against HT29 human colon adenocarcinoma. We have successfully demonstrated that reactive oxygen species (ROS) initiated cell death via Type I and Type II photoreactions.

Photoactivation of SiPcGlu induced apoptosis in HT29 as measured by several parameters, including TUNEL, annexin V & propidium iodide staining and DNA laddering assays. Subcellular localization studies revealed that SiPcGlu exhibited a partial localization in mitochondria and endoplasmic reticulum. After PDT, immediate mitochondrial membrane depolarization and ROS production were resulted, followed by release of cytochrome c, activation of caspase-3 and PARP cleavage. Expression of the ER-stress chaperone protein GRP78 was induced and the level of cytosolic Ca^{2+} was elevated. The above findings showed that mitochondria and ER are the primary sites of photodamage.

The efficacy of SiPcGlu-PDT and the drug's biodistribution in HT29 tumor-bearing nude mice were also evaluated. Though the glucose moiety failed to target SiPcGlu towards tumor tissue, photoactivation of SiPcGlu by spotting medical laser onto the tumor can significantly inhibit tumor growth. Analysis of intrinsic toxicity also revealed that SiPcGlu with or without irradiation did not cause any apparent hepatic and cardiac injuries to the nude mice, indicating that SiPcGlu is a safe candidate for clinical PDT.

List of Abbreviations

%ID	% initial dose
A431	Human epidermoid carcinoma
Ac-DEVD-AMC	N-Acetyl-Asp-Glu-Val-Asp-7-amino-4-methylcoumarin
AlPcS(4)	Aluminum phthalocyanine tetrasulfonate
ALT	Alanine aminotransferase
ANOVA	Analysis of variance
Apaf-1	Apoptotic protease activating factor 1
AST	Aspartate aminotransferase
ATX-S10(Na)	13,17-Bis(1-carboxypropionyl)carbamoylethyl-8-ethenyl-2-hydroxy-3-hydroxyiminoethylidene-2,7,12,18-tetramethylporphyrin sodium salt
BAM-SiPc	A bisamino silicon(IV) phthalocyanine
CK	Creatine kinase
DCFDA	2',7'-Dichlorofluorescein diacetate
DMF	N,N-Dimethylformamide
EGF	Epidermal growth factor
EMT6	Murine mammary sarcoma
ER	Endoplasmic reticulum
FITC-dUTP	Fluorescein-2'-deoxyuridine 5'-triphosphate
GLUT	Glucose transporter
GRP78	78-kDa Glucose-regulated protein
HepG2	Hepatocarcinoma
HpD	Hematoporphyrin derivatives

HT29	Human colorectal adenocarcinoma
IL	Interleukin
LDL	Low-density lipoprotein
MTT	3-(4,5-Dimethylthiazole-2-yl)-2,5-diphenyl tetrazolium bromide
PACT	Photodynamic antimicrobial chemotherapy
PARP	Poly (ADP-ribose) polymerase
PBS	Phosphate buffered saline
PDT	Photodynamic therapy
ROS	Reactive oxygen species
scFv	Antibody fragment
SDS	Sodium dodecyl sulfate
$SERCA_2$	Sarco/endoplasmic reticulum Ca^{2+} ATPase
SiPcGlu	Glucoconjugated silicon(IV) phthalocyanine
TdT	Terminal deoxynucleotidyl transferase
TUNEL	Terminal deoxynucleotidyl transferase-mediated dUTP nick end labeling
UPR	Unfolded protein response
V79	Chinese hamster lung fibroblasts

List of Figures

List of Table

Table of Content

Chapter 1
Introduction

1.1 Background of photodynamic therapy (PDT)

1.1.1 History of PDT

Treatments using light and light-activated compounds were reported in ancient times and were used to treat a variety of disorders and malaise. The therapeutic use of light was first reported by Niels R. Finsen in the late nineteenth century. He discovered that light treatment could control skin manifestations of tuberculosis and the 1903 Nobel Prize was awarded to him for his work on phototherapy (Bonnett, 1995). Throughout the 20th century, a few attempts were made to treat tumor tissue with photosensitizing agents, mainly with non-porphyrin photosensitizers. The first clinical application of PDT was described by Hermann von Tappeiner and Albert Jesionek who applied eosin topically to basal cell carcinomas prior to illumination (MacDonald and Dougherty, 2001). They later defined PDT as a dynamic interaction among light, photosensitizing agent and oxygen resulting in tissue destruction. In the 1960s, Richard Lipson and Samuel Schwartz isolated a tumor localizing impurity hematoporphyrin derivative (HpD), and used it as a tumor detecting agent and later recognized it as a photosensitizer to destroy tumor tissue (Lipson et al., 1961). In the 1970s, Thomas J. Dougherty discovered that when placing radiation sensitizing agents in cell culture near laboratory windows, significant cell death was observed. He isolated and found that HpD in combination with red light could completely eradicate mouse mammary tumor growth (Allison et al., 2004). He injected a mixture of

porphyrins into the bloodstream of the mice with mammary tumors. After waiting a few days, the porphyrins accumulated in tumors and he shone red light on them. At that time, the experimental setup was primitive, using simply an old slide projector through a 35 mm red-colored slide to pass the light. In almost every case, the tumors turned out to be blackened and died after light treatment (Dougherty et al., 1975). The active fractions of HpD was later isolated and identified as a purified version named Photofrin®. Clinical studies were done in the following years with Photofrin® to treat patients with bladder and skin cancers. After these successful clinical studies, the approval of PDT, using Photofrin®, Axcan Pharma Inc., Mont-Saint-Hilaire, Canada was granted in 1993 and later in Japan, USA and parts of Europe for the treatment of esophageal, bladder, head and neck, skin and some stages of lung cancers (Lane, 2003).

1.1.2 Photochemistry

Upon absorption of light, the photosensitizer in the ground state is promoted to the short-lived excited singlet state and then converted to the more stable triplet state through electron spin conversion. The triplet state is long-lived enough to elicit chemical reactions and most part of the photodynamic actions take place at this stage. There are two types of photodynamic reactions (Figure 1.1). In the Type I photoreaction, the triplet photosensitizer can react directly with substrate, such as the cell membrane, and transfer a hydrogen atom

or electron to form radicals. The radicals can interact with oxygen to produce oxygenated products ($^1O_2$) such as superoxide anions(O_2^-), hydroperoxyls (HO_2), hydrogen radicals (·OH) and hydrogen peroxide (H_2O_2). These are reactive intermediates harmful to cells. Thereby the photosensitizer returns to the ground state. Alternately, the triplet photosensitizers can undergo Type II photoreaction in which they undergo an electron spin exchange with ground-state triplet oxygen ($^3O_2$) to produce a cytotoxic singlet oxygen ($^1O_2$), a highly reactive oxygen species (ROS) which is the most damaging species generated during PDT (Calzavara-Pinton et al., 2007; Dolmans et al., 2003; Triesscheijn et al., 2006). The effects of almost all PDT drugs are oxygen-dependent. ROS are known to initiate a number of reactions with biomolecules, including amino acid residues (e.g. tryptophan) in proteins; unsaturated lipids, cholesterol and nucleic acid bases, particularly guanosine and guanine derivatives with the latter base more susceptible to ROS (Josefsen and Boyle, 2008a).

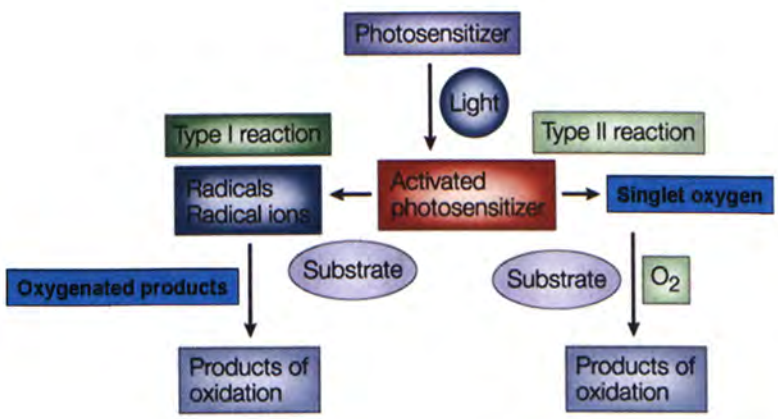

Figure 1.1 Mechanisms of action of PDT (Dolmans et al., 2003)

1.1.3 Principal stages of PDT

PDT is a treatment requiring injection of photosensitizer (in syringe or tube) (Stage I). The injection of drug can be done locally by subcutaneous injection or systemically by intravenous injection. The drug then accumulates in tumors (Stage II). After a certain time interval, the drug is activated by external illumination (Stage III), which is very often done on an outpatient basis. This induces cell death and tumor destruction (Stage IV) (Figure 1.2) (Chatterjee et al., 2008).

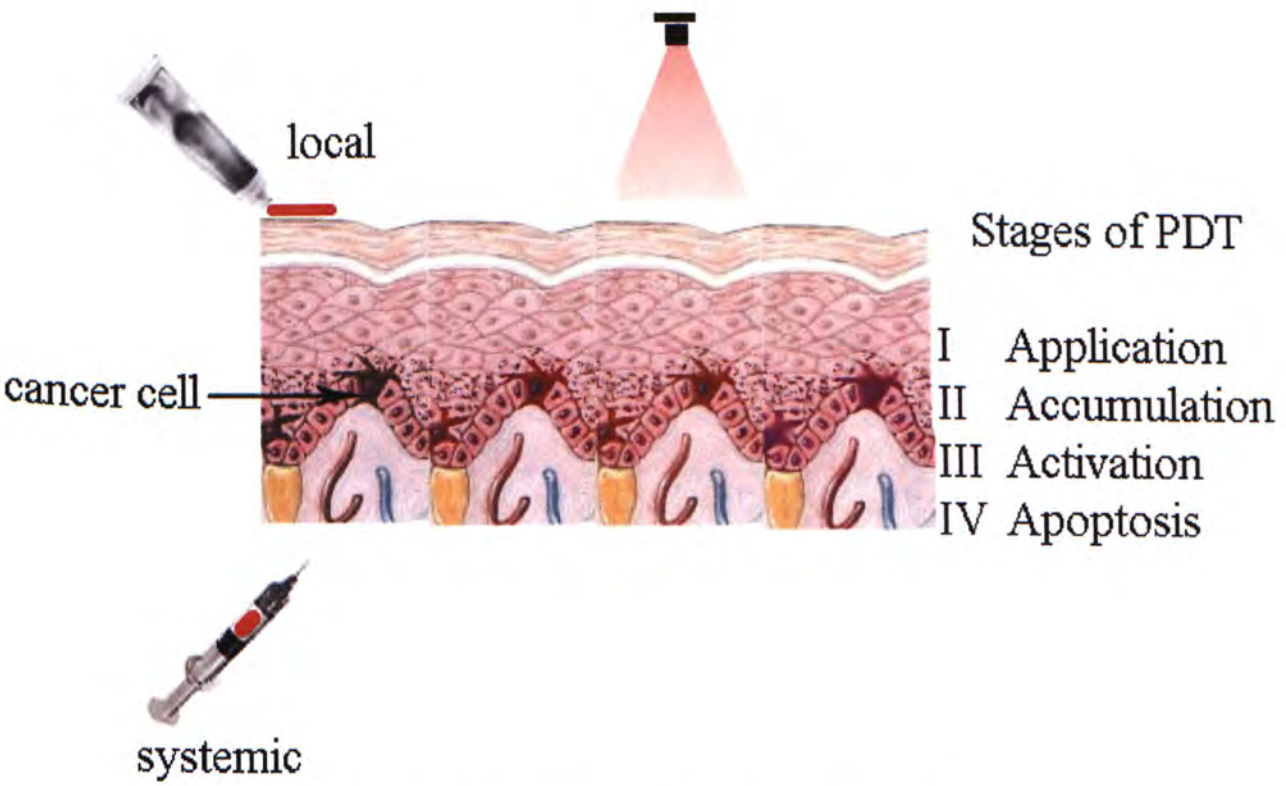

Figure 1.2 Principle stages of PDT (Chatterjee et al., 2008)

1.1.4 Light sources of PDT

The efficacy of light sources for PDT is determined by two factors. The first one is the absorption spectrum of the photosensitizer. A light source with an emission spectrum that corresponds to the absorption spectrum of the photosensitizer gives the higher efficacy. The second factor is the wavelength and penetration power of the light. Light with longer wavelength can penetrate into skin more deeply (Figure 1.3). Therefore, light in the far-red region is usually adopted for PDT as red light with wavelength > 650 nm can penetrate deeply into the skin down to the subcutaneous layers.

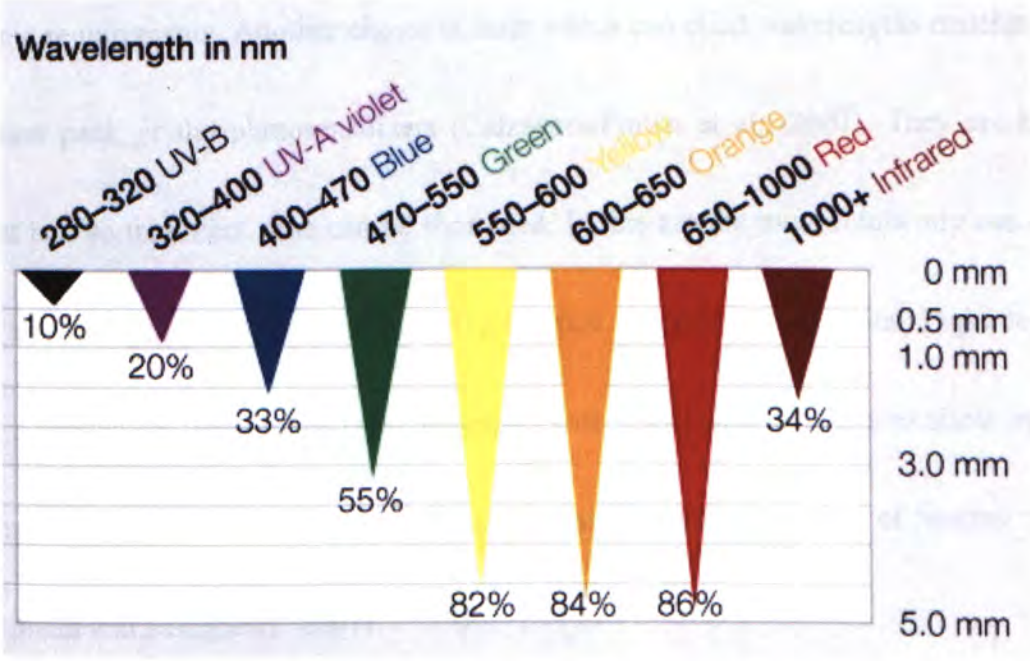

Figure 1.3 Depth of penetration of light with different wavelengths (Adapted from http://www.bundp.net/?q=en/node/219)

There are three major groups of light source: broadband lamps, diode lamps and lasers. The traditionally used light sources in PDT are broad-spectrum lamps. Non-coherent broad-spectrum light sources in red and blue wavelengths, together with porphyrins, was the earliest and most frequently used light sources in PDT for cutaneous diseases. Nowadays, metal halogen lamps are frequently used as they are cheap and have high power intensity, therefore a reasonable light exposure time can be achieved. Moreover, they can be equipped with optical filter to cut off the shorter wavelengths which cannot be absorbed into skin. Diode lamps are small solid-state semiconductors with a high and reliable emission in a narrow bandwidth of 20-50 nm. They are simple to use and do not have any special electronic requirements. Another choice is laser which can elicit wavelengths matching the absorption peak of the photosensitizers (Calzavara-Pinton et al., 2007). They are highly efficient and so treatment time can be shortened. Lasers are the most frequently used light source as it can produce monochromatic light which is highly homogenous. Light delivery can be achieved by fiber-optics cable equipped with lenses and diffusers to allow optimal illumination of the tissues to be treated and minimize the illumination of healthy tissues (MacDonald and Dougherty, 2001).

1.2 Anti-tumor effect of PDT

1.2.1 Mode of cell death after PDT

The crucial factors determining the types of cell death are cell type, subcellular localization and light dose (Castano et al., 2006). The subcellular localization of the photosensitizers determines the primary site of photodamage which triggers different types of cell death. Moreover, singlet oxygen can diffuse only 20 nm during its lifetime (half life: < 0.04 μs). It can only damage biomolecules in its close proximity (Castano et al., 2004). Cellular structures having high photosensitizer and oxygen concentrations will preferentially be damaged. Therefore, the subcellular localization of photosensitizers triggers different pathways to cell death. In general, the photosensitizers with preferred localization in mitochondria (e.g. porphyrin-related compounds) will activate the apoptotic pathways within a certain threshold of oxidative stress (Agostinis et al., 2004). For photosensitizers localized in the plasma membrane, the photosensitization process can rapidly switch towards necrosis due to the loss of plasma membrane integrity and rapid depletion of intracellular ATP (Kessel and Poretz, 2000). The plasma membrane-localized Photofrin® can render the death phenotype to be more necrosis like in human epidermoid carcinoma A431 (Hsieh et al., 2003).

Besides subcellular localization, light dose also determines the mode of cell death. It is believed that a lower dose of light leads to apoptosis, while higher dose leads to necrosis (Plaetzer et al., 2002). With the use of the amphiphilic photosensitizer 13,17-bis(1-carboxypropionyl)carbamoylethyl-8-ethenyl-2-hydroxy-3-hydroxyiminoethylidene-2,7,12,18-tetramethylporphyrin sodium salt [ATX-S10(Na)], light doses that led to < 70% cytotoxicity induced mainly apoptosis in human malignant melanoma cells, while doses which led to 99% cytotoxicity induced necrosis (Nagata et al., 2003).

1.2.2 PDT-induced anti-tumor immunity

An ideal cancer therapy would destroy not only the primary tumor, but also trigger the immune system to recognize, track down and destroy remaining tumor cells (Castano et al., 2006). A lot of evidence showed that the outcome of PDT is greatly dependent on the contribution of host response (Korbelik, 2006). Treatment of tumors by PDT results in an oxidative stress at the targeted site associated with a wide range of photooxidative lesions produced in the membrane and cytoplasm of cancer cells, tumor vasculature and other stroma elements. Tumor destruction is experienced by the host as a local trauma threatening the integrity and homeostasis at the affected site. Therefore the host is provoked to launch canonical response to deal with the localized injury to prevent spreading of tissue damage, remove the dead and damaged tissue and restore tissue function, which are orchestrated by the

innate immune system and characterized by the activation of inflammation and acute phase response (Korbelik, 2006). The occurrence of inflammation may be induced by expression of two transcription factors, nuclear factor κB and activator protein 1, which are known to be activated by cellular oxidative stress (Sun and Xiao, 2003). At the therapeutic point of view, the host response can amplify the PDT instigated eradication of tumors, which can uncover the tumor-specific antigens and lead to their presentation for the recognition and response by adaptive immune system targeted to the tumor. *In vitro* studies showed that PDT can have effects on monocyte/macrophage and lymphocyte cell lineage which are easily killed by PDT (Castano et al., 2006). In the *in vivo* studies, inflammatory cytokines and chemokines were also detected in the serum of mice that have received PDT directed at a subcutaneous tumor or to an area of normal skin (Gollnick et al., 2003). In clinical studies, increased levels of interleukin (IL) 1, 6, 8 and 10 were also detected in patients after surgery and PDT for mesothelioma (Yom et al., 2003). Korbelik et al. (1996) has shown that PDT treatment of murine EMT6 mammary sarcoma using Photofrin® and light cured all lesions growing in BALB/c mice. In contrast, the same treatment produced initial ablation but no long-term cures of EMT6 tumors growing in either Severe Combined Immunodeficiency (SCID) or nude mice, which suggested that the activity of host lymphoid populations was essential for preventing the recurrence of EMT6 tumors following PDT treatment used in this study.

1.3 Clinical applications of PDT

1.3.1 Photofrin®

Photofrin® (HpD, porfimer sodium) is commercially available from Axcan Pharma., Inc. and has the longest clinical history and patient track record. It remains the most common photosensitizer for the treatment of non-dermatological tumors (Brown et al., 2004). Photofrin® can be easily synthesized by reacting hematoporphyrin in a mixture of sulfuric and acetic acids to form hematoporphyrin IX (di- and mono-) acetates. Hydrolytic treatment with base yields a crude mixture commonly referred to as HpD. Figure 1.4 shows the structure of Photofrin®. Commercially available Photofrin® is made by removing components with low-molecular weight. The purified fraction is composed of monomers, dimers, trimers and larger oligomers up to eight to nine porphyrin units (MacDonald and Dougherty, 2001). A wide variety of neoplasms and even 'benign' lesions can be treated on an outpatient basis with Photofrin® (Allison et al., 2004). The advantages of Photofrin® are first it destroys tumors effectively; and second it is non-toxic in the absence of light and can be easily formulated in a water-soluble preparation for intravenous injection. Since this drug has been used for more than 20 years and no long-term safety issues have emerged (Brown et al., 2004), Photofrin® does not appear to succumb to multi-drug resistance and has no known cumulative dose ceiling as radiation and chemotherapy do. Thus patients can be treated repeatedly as needed.

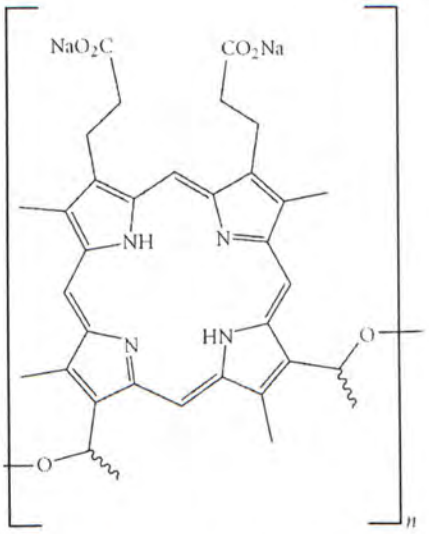

Figure 1.4 Structure of Photofrin®, n = 1-9 (Josefsen and Boyle, 2008a)

Photofrin® is a mixture of hematoporphyrin products with several absorption peaks. Since the absorption peak with the longest wavelength at 630 nm is the weakest, a high light dose of 100-200 J/cm^2 is required for tumor control which always comes with skin photosensitivity for 4 to 12 weeks (Triesscheijn et al., 2006). Moreover, since Photofrin® also appears to be taken up by other rapidly proliferating tissues like skin, therefore a possible complication caused by severe photoreaction such as sunburn or skin rashes might be resulted. As a result, patients need to avoid sunlight for about 6 weeks after treatment (MacDonald and Dougherty, 2001).

1.3.2 Clinical applications of PDT

Over the past 3 decades, PDT has been proven to be successful in treating different types of cancers. Besides, PDT has also been approved for other applications such as wet age-related macular degeneration which is the major cause of blindness in the aged populations. Many approved photosensitizers have been developed for different clinical applications in different countries (Table 1.1). Other treatments avenues are also being explored. One ingenious idea is photoangioplasty to treat coronary artery disease by using a tiny light source to illuminate the artery, particularly targeting at the plaque and destroying it. Due to the increasingly widespread diffusion of antibiotic-resistant microbial strains, photodynamic antimicrobial chemotherapy (PACT) offers favorable features for the treatment for bacterial, fungal, parasitic, and viral infections, such as the broad spectrum of antimicrobial action and low risk of developing photoresistant strains. At present, PACT appears to be especially convenient for the treatment of localized infections, such as oral candidosis, periodontitis or chronic wounds (Calzavara-Pinton et al., 2005; Jori, 2006; Konopka and Goslinski, 2007). In our laboratory, previous study was done to investigate the antifungal effect of an bisamino silicon(IV) phthalocyanine BAM-SiPc and it was found that BAM-SiPc-PDT is effective in killing *Candida albicans* (So et al., 2009).

Table 1.1 Summary of a range of photosensitisers and their clinical applications

(Josefsen and Boyle, 2008a).

TRADE NAME	MARKETING COMPANY	PRE-/CLINICAL APPLICATION	COUNTRIES APPROVED IN
Photofrin (sodium porfimer)	QLT Phototherapeutics	Oesophageal, lung, bladder and cervical dysplasia; Barrett's esophagus	Canada (1993), The Netherlands (1994), Japan (1994), USA (1995), France (1996), Germany (1997), Finland (1999), UK (1999) Sweden (2000), Italy (2000), Ireland (2000), Poland (2000)
Levulan (5-aminolevulinic acid)	DUSA Pharmaceuticals	Actinic keratosis, actinic keratosis and basal cell carcinoma	USA (1999), Sweden (2001), Europe (2001), Korea (2007)
Visudyne (benzoporphyrin derivative)	QLT Phototherapeutics	Wet aged-related macular degeneration, subfoveal choroidal neovascularisation	Europe (2001), USA (2000), Canada (2000), Europe (2001), USA(2001), Canada (2001), Japan (2003), Brazil (2006)
ATMPn (acetoxy-tetrakis-(methoxyethyl)-porphycene)	GlaxoWellcome and Cytopharm	Psorasis and non-melanoma skin cancer	Germany (1997)
Purlytin (tin ethyl etiopurpurin)	Miravant Medical Technologies	Psorasis and restenosis	USA (1998)
Foscan (meso-tetra-hydroxy-phenyl-chlorin)	BioLitec Pharmaceuticals	Head and neck cancers	Europe (2001)
Metvix	Photocure ASA	Actinic keratosis and basal cell carcinoma	Sweden (2001), Europe (2001)

1.3.3 Challenges of PDT for clinical applications

PDT offers several advantages over conventional therapies. In contrast to weeks or months of radiotherapy or chemotherapy or prolonged hospitalization of surgery, PDT offers an advantage of being an outpatient therapy. PDT can induce immune response and provide long term control of tumor growth. It is also cost-effective and has high cure rates. However, acceptance of PDT is still limited by the high cost of setup, lack of standardized protocol from randomized trials, limited accessibility to deep-penetrated tumors and possibility of photosensitivity over a long period following treatment. To realize the popularity of PDT, more efforts should be done to overcome the above challenges. Another limitation of conventional PDT approach for cancer treatment is its lack of selectivity towards tumor tissues in terms of cellular localization and cytotoxicity. The ideal photosensitizer should enable selective accumulation within the tumor tissue. Unfortunately, the majority of the photosensitizers are taken up non-specifically by all cell types. Therefore, in recent years, lots of efforts have been spent to improve the specificity of the photosensitizers for more effective therapeutic outcomes and less side-effects. Many new second and third generation photosensitizers are being synthesized in an attempt to create more specific photosensitizers (Triesscheijn et al., 2006).

1.4 The development of new photosensitizers

1.4.1 Targeted PDT

One major obstacle for the development of PDT is its lack of specificity to tumor tissues. For the treatment of tumors, a widespread uptake of photosensitizers has limited its ability to target specifically to localized lesions in the body. Photosensitizers may accumulate in the skin and lead to photosensitivity. Therefore, in order to reach the full potential of PDT, there is a need for numerous targeting motifs so that tumor tissues can be selectively destroyed. A lot of efforts have been spent on the development of photosensitizers which can be more specifically targeted to malignant tissues and increase the uptake of the dye by target cells. One approach is to conjugate photosensitizers with biomolecules. Conjugating photosensitizers with saccharides such as glucose and galactose can prevent aggregation of photosensitizers, increase their water solubility and biological efficacy (Maillard et al., 1989). Our laboratory has previously described the preparation of silicon(IV) phthalocyanine conjugated to galactose via axial coordination and found that this compound is highly soluble in most organic solvents and remains essentially non-aggregated in solution. Moreover, it shows an improvement in cellular uptake which may explain its high photocytotoxicity against the hepatocarcinoma (HepG2) cells (Lee et al., 2005).

Targeted PDT can also be achieved via receptor-mediated delivery system, such as via low-density lipoproteins (LDL), gastrin-releasing peptide and epidermal growth factor (EGF)

receptors. LDL is an attractive vehicle for drug targeting, since highly proliferating tumor cells overexpress LDL receptors. Previous study has reported that the reconstituted LDL-naphthalocyanine is able to maintain the size and shape of native LDL, retain their LDL receptor-mediated uptake by cancer cells and has a preferential uptake by tumor vs normal tissue *in vivo* (Song et al., 2007). Another study has shown that by conjugating aluminum phthalocyanine tetrasulfonate AlPcS(4) with bombesin (gastrin-releasing peptide) and targeting it to gastrin-releasing peptide receptor which is early expressed in prostate tumor development, the *in vitro* photodynamic efficacy against human prostate cancer cells can be improved by 2.5 fold over the non-conjugated AlPcS(4) (Dubuc et al., 2008).

Photoimmunotherapy combines phototoxicity of the photosensitizers with the selectivity of monoclonal antibodies directed against tumor-associated antigens by conjugating multiple photosensitizers with antibody fragments (scFvs). The treatment of human breast cancer xenografts with a photoimmunoconjugate comprising an anti-epidermal growth factor 2 (anti-HER2) receptor 2 scfv linked to 8-10 molecules of pyropheophorbide a leads to significant tumor regression (Bhatti et al., 2008). Hemotoporphyrin conjugated with antibodies with vascular endothelial growth factor (VEGF) was also previously synthesized and this conjugate exhibited a stronger anti-tumor effect *in vivo* when compared with the native hematoporphyrin. The development of cellular characteristics will eventually lead to the discovery of targeting mechanisms (Novichenko et al., 2008). Research is still ongoing to

develop various photosensitizers and numerous targeting motifs so that each disease type can be targeted on an individual basis (Sharman et al., 2004).

Carriers for drug such as liposomes and nanoparticles are also made possible to enhance efficacy of photosensitizers (Chatterjee et al., 2008; Sibani et al., 2008). Previous study has shown that encapsulating methylene blue in nanoparticles can increase its nuclear localization and result in enhanced DNA damage, which significantly potentiate the cytotoxicity of methylene blue-mediated PDT (Khdair et al., 2008). Nishiyama et al. (2009) showed that the dendrimer phthalocyanine with polymeric micelle (DPc/m) can efficiently induce cell death and significantly enhance *in vivo* antitumor efficacy, when compared with the dendrimer phthalocyanine without polymeric micelle (DPc), indicating that polymeric micelle can be an effective nanocarrier for drug delivery.

1.4.2 Phthalocyanine

Phthalocyanine has been extensively examined as photosensitizers. They are synthesized by joining four benzene rings to the β-pyrrolic positions of porphyrins and substituting methane-bridge carbons with nitrogen (Figure 1.5). Polar substituents are often linked to avoid solubility problems caused by their strong hydrophobicity. The presence of aluminium, zinc(II), silicon(IV) and other ions gives hexacoordination and guarantees a satisfactory yield of singlet oxygen generation (Calzavara-Pinton et al., 2007). The

photophysical properties of phthalocyanine are of utmost interests since they exhibit very strong absorption at longer wavelengths than porphyrins as they have a larger macrocycle ring system (Miller et al., 2007). With a very strong absorption peak in the far-red region of the visible spectra, tissue penetration can be improved. Apart from its non-aggregated nature, phtahlocyanine does not exist as structural isomers (Lo et al., 2004). Its chemical synthesis and structure allow the addition of substituents to both the central metal and the periphery of the hydrophobic phthalocyanine macrocycle to change its physical properties which determine its cellular uptake, subcellular localization and phototoxicity (Allen et al., 2002).

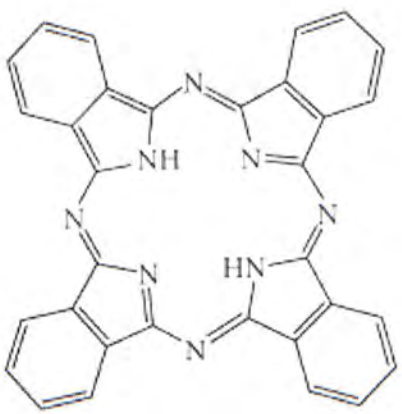

Figure 1.5 Structure of phthalocyanine (Josefsen and Boyle, 2008a)

Besides having desirable physical properties, phthalocyanine also exhibits high photodynamic activities, both *in vitro* and *in vivo,* against a range of model cancer cell lines

and tumors. Bis(cholesteryloxy) derivative of silicon(IV) phthalocyanine exhibits half lethal dose at 6-8 nM via early activation of mitochondria-mediated apoptosis (Barge et al., 2004). In our laboratory a number of silicon(IV) and zinc(II) phthalocyanines were synthesized. Most of them possess desirable physical properties and potent photodynamic activities in killing cancer cells (IC_{50} ranged from 0.03 to 4.7μM against both HepG2 and HT29) (Choi et al., 2008; Liu et al., 2009; Lo et al., 2008).

Silicon(IV) phthalocyanines are also effective in the treatment of SW480 human colon cancer xenografts and skin papillomas in *in vivo* studies (Kalka et al., 2000; Whitacre et al., 2000). They have been studied in clinical applications. Phase I clinical trials have been performed and the preliminary results were promising with a subset of patients responded to therapy showing improvement in the treated lesions, as evidenced by the thinning and decreased erythema. Both the responders and non-responders tolerated the treatment well, with no side effects or pain reported (Miller et al., 2007).

1.5 Objective of my study

Over the past few years, a number of modified phthalocyanines have been studied in our laboratory. SiPcGlu (Figure 1.6) was chosen for the present study as it is one of the most potent phthalocyanines. Human colorectal adenocarcinoma HT29 was used to study its photocytotoxicity. It is believed that the action mechanism of PDT is via the production of ROS. Therefore, the production of ROS after SiPcGlu-PDT and its role in triggering cell death by the use of various antioxidants were investigated. Furthermore, the mode of cell death initiated by SiPcGlu-PDT was also evaluated. Since the subcellular localization of photosensitizer determines the primary site of photodamage and cell death pathways, confocal microscopic investigations with the use of organelle-specific probes were performed to study the intracellular localization of SiPcGlu.

To evaluate whether SiPcGlu has the potential for clinical PDT, a HT29 tumor-bearing nude mice model was developed to investigate the *in vivo* efficacy of SiPcGlu-PDT to eradicate tumor. Biodistribution of SiPcGlu was also performed to investigate whether its glucose moiety can target it to tumor specifically, through the over-expressed glucose transporters (GLUTS) in cancer cells. Finally, the safety use of the drug was evaluated by analyzing levels of plasma enzyme markers for any possible hepatic or cardiac injuries.

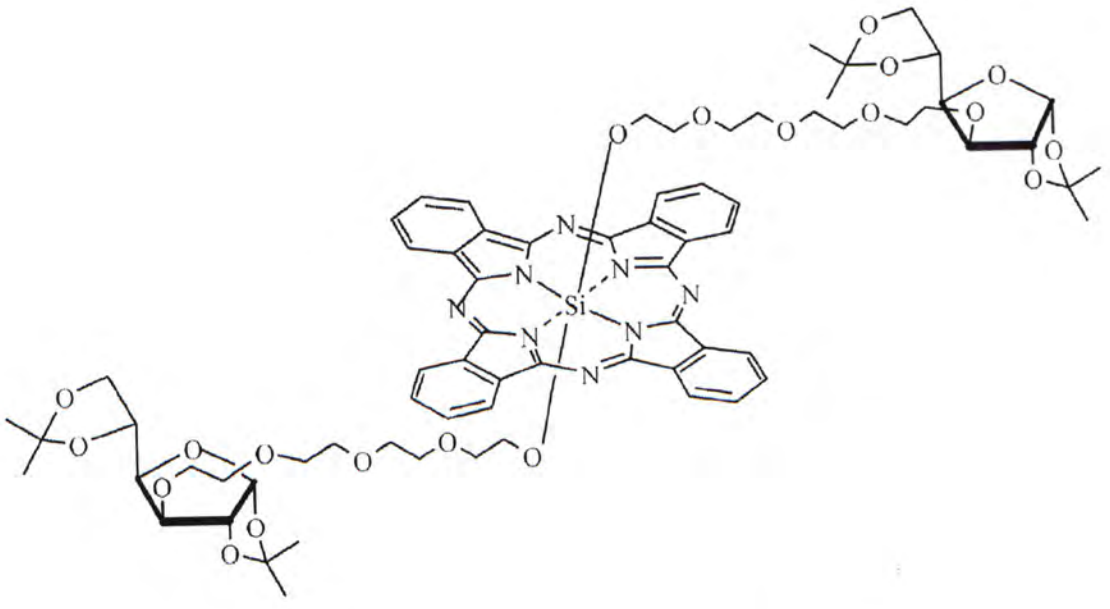

Figure 1.6 Chemical Structure of SiPcGlu

Chapter 2
Materials and Methods

2.1 Synthesis of glucoconjugated silicon(IV) phthalocyanine (SiPcGlu)

SiPcGlu was kindly provided by Prof. Dennis K.P. Ng from the Department of Chemistry, The Chinese University of Hong Kong. The procedures of the synthesis were summarized as follow. A mixture of silicon phthalocyanine dichloride (1.02 g, 1.7 mmol), protected glucose (3.73 g, 8.6 mmol) and NaH (60% in mineral oil, 0.83 g, 20.8 mmol) in toluene (80 mL) was refluxed for 2 days. After evaporating the solvent *in vacuo*, the residue was subjected to column chromatography on neutral alumina using $CHCl_3$ as eluent, followed by gel permeation chromatography using THF as eluent. The crude product was then chromatographed again on neutral alumina using CH_2Cl_2, and then $CHCl_3/CH_2Cl_2$ (1:4) as eluent. The product (0.3 g, 0.22 mM) was collected as a blue solid. The product yield is 13% from the precursor silicon phthalocyanine dichloride. The purity of the product is confirmed by proton nuclear magnetic resonance (^{1}H NMR) spectroscopy and elemental analysis.

2.2 *In vitro* studies

2.2.1 Cell line and culture conditions

The human colorectal adenocarcinoma HT29 cells were originally obtained from American Type Culture Collection (ATCC Number: HTB-38). They were maintained in

Dulbecco's Modified Eagle's Medium (DMEM) supplemented with 10% fetal bovine serum, 100 units/ml penicillin, 100 μg/ml streptomycin, 2 mM L-glutamine and 10 μg/ml transferrin (Sigma-Aldrich, USA) in 5% CO_2, 95% air in a humidified incubator at 37 °C. All reagents were purchased from Invitrogen, USA unless otherwise specified.

2.2.2 Photodynamic treatment

SiPcGlu was first dissolved in N,N-dimethylformamide (DMF, Sigma-Aldrich) to give a 1.5 mM solution and then diluted to 80 μM with an aqueous solution of Cremaphor EL (0.047g/ml in water, Sigma-Aldrich). The solution was then filtered with 0.2 μm *Acrodisc*® Syringe Filters with *Supor*® Membrane (Pall Gelman Laboratory, USA) and then diluted to appropriate concentrations with culture medium. For the photodynamic treatment with Photofrin®, Photofrin® was dissolved in culture medium directly. Cells (3×10^4) were seeded in each well of the 96-well plates and incubated overnight in 5% CO_2, 95% air in a humidified incubator at 37 °C. After incubation, the cells were rinsed with 100 μl phosphate buffered saline (PBS). Different concentrations of SiPcGlu (100 μl) were added to each well and incubated for 2 h in 5% CO_2, 95% air in a humidified incubator at 37 °C in darkness. The cells were then rinsed with PBS and refed with 100 μl culture medium, followed by illumination for 20 min with a 300 W halogen lamp through a color glass filter (Newport, USA) which cuts off light below 610 nm so that only a narrow region of light (at ca. 610-

700 nm) can be absorbed by the compound to initiate the photodynamic action (Figure 1.2). The fluence rate for the illumination was 40 mW/cm^2 so that an illumination of 20 min will lead to a total fluence of 48 J/cm^2.

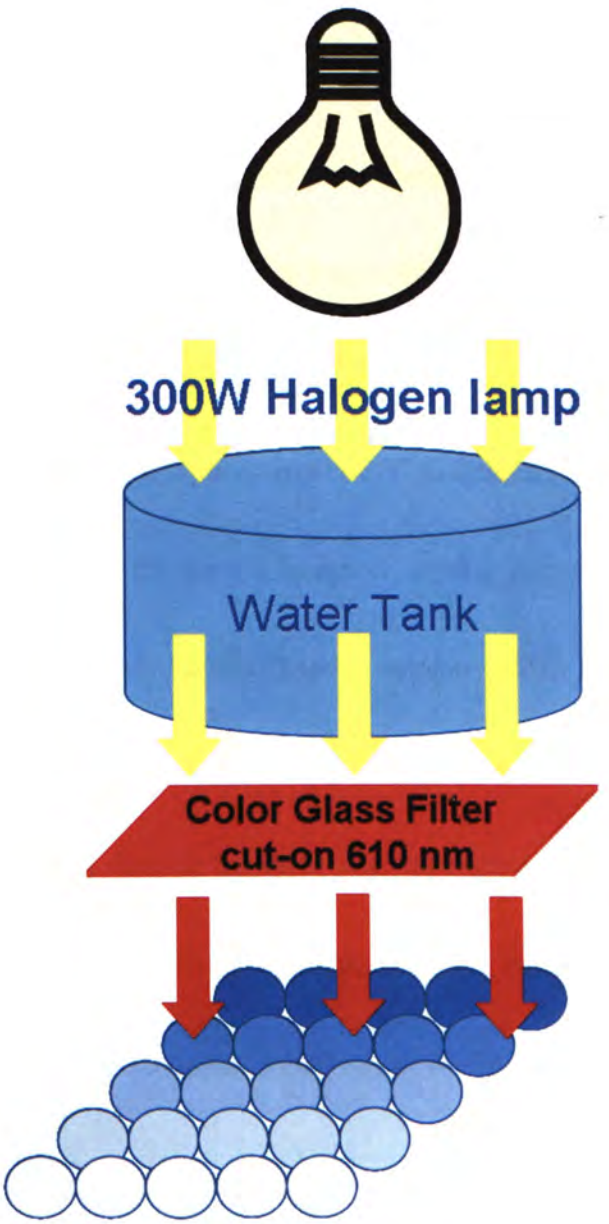

Figure 2.1 Schematic diagram showing the setup for illumination of the HT29 cells

2.2.3 Cell viability assay

After photodynamic treatment, the cells were incubated for 24 h in 5% CO_2, 95% air in a humidified incubator at 37 °C in darkness. After incubation, the cell viability was determined by the colorimetric 3-(4,5-dimethylthiazole-2-yl)-2,5-diphenyl tetrazolium bromide (MTT, USB Corporation, USA) assay. The PDT-treated cells were first rinsed with PBS. MTT solution (50 µl, 3 mg/ml in PBS) was then added to each well followed by incubation for 2 h in 5% CO_2, 95% air in a humidified incubator at 37 °C in darkness. Afterwards, 50 µl sodium dodecyl sulfate (SDS, 10% w/v, USB) was added to each well. The plate was incubated for 30 min in an oven at 60 °C to lyse the cells, and then 80 µl *iso*-propanol was added to dissolve the purple formazan crystal formed inside the cells. The plate was agitated on a Microplate Reader (Model number: 3550, Bio-rad, USA) at room temperature for 10 s and the absorbance of 540 nm was taken. The average absorbance of the blank wells, which did not contain the cells, was subtracted from the readings of other wells. The cell viability was then determined by the following equation:

$$\% \text{ Viability} = (OD_{540(\text{treated cells})} - OD_{540(\text{blank})} / (OD_{540(\text{control})} - OD_{540(\text{blank})}) \times 100\%$$

2.2.4 Light dose effect on the photocytotoxicity of SiPcGlu-PDT

Halogen lamp and a diode laser were used to study the effect of light dose or light source on the cytotoxicity induced by SiPcGlu-PDT. For halogen lamp, the fluence rate for

the illumination was 40 mW/cm^2 so that an illumination of 20 min will lead to a total fluence of 48 J/cm^2. For diode laser, continuous wave laser was generated from the Ceralas PDT 675 medical laser system (bandwidth 675 nm ± 3 nm, power range 0.1 – 1 W) coupled with a frontal light distributor (CeramOptec GmbH, Germany) (Figure 2.2). The fluence rate for illumination was 200 mW/cm^2 and the time for illumination is 10 and 40 s to give a total fluence of 2 and 8 J/cm^2 respectively.

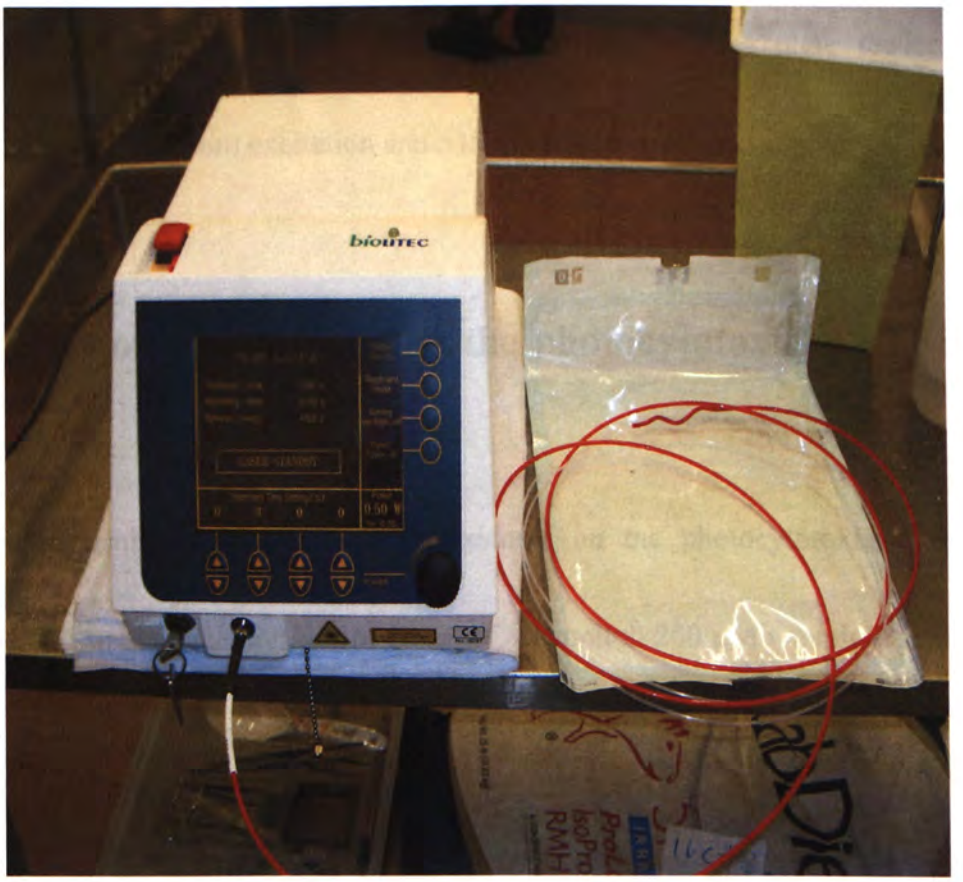

Figure 2.2 Setup of the PDT laser system

2.2.5 Determination of reactive oxygen species (ROS) production by SiPcGlu-PDT

ROS production during SiPcGlu-PDT was determined by using 2',7'-dichlorofluorescein diacetate (DCFDA, Molecular Probes, USA). Cells were incubated with various concentrations of SiPcGlu. After rinsing with PBS, 100 μl of 10 μM DCFDA was added to each well followed by incubation for 30 min in 5% CO_2, 95% air in a humidified incubator at 37 °C in darkness. The cells were then illuminated for 20 min with the halogen lamp. Fluorescence measurements were made by fluorescence plate reader (TECAN Polarion, UK) with 485 nm excitation and 535 nm emission filters.

2.2.6 Effect of antioxidants on the photocytotoxicity of SiPcGlu-PDT

To determine the effects of antioxidants on the photocytotoxicity induced by SiPcGlu-PDT, final concentrations of 50 mM D-mannitol, 200 μM vitamin C or 100 μM L-histidine (all purchased from Sigma-Aldrich) were added and incubated with different concentrations of SiPcGlu for 2 h, followed by illumination with halogen lamp to trigger photodynamic reactions. After 24 h, cell viability was determined by MTT assay.

2.2.7 Determination of reactive oxygen species (ROS) production after SiPcGlu-PDT

To determine the ROS production after PDT, the cells were rinsed with PBS immediately after illumination with halogen lamp. DCFDA was then added to each well, followed by incubation in 5% CO_2, 95% air in a humidified incubator at 37 °C in darkness for 1 h. Fluorescence measurements were made by fluorescence plate reader.

2.2.8 Glucose competitive assay

The potential role of GLUTS in the uptake of the photosensitizer was studied by a glucose competitive assay. Glucose solutions (1 or 100 mM in PBS) were added and incubated with different concentrations of SiPcGlu formulated in PBS for 2 h, followed by rinsing with PBS. The same experimental setup with halogen lamp was used for illumination of the cells. After 24 h, cell viability was determined by MTT assay.

2.2.9 Terminal deoxynucleotidyl transferase-mediated dUTP nick end labeling (TUNEL) assay

Cells (1 x 10^6) were seeded in 35 mm tissue culture dish and incubated overnight in 5% CO_2, 95% air in a humidified incubator at 37 °C. After incubation, the cells were rinsed with 100 μl PBS. Different concentrations of SiPcGlu (1 ml) were added to each dish and

incubated for 2 h. The cells were rinsed with PBS and refed with culture medium, followed by illumination with halogen lamp. Twenty-four h after PDT, the presence of DNA breaks were detected by using the *In Situ* Cell Death Detection Kit, Fluorescein (Roche, Germany) according to the manufacturer's instructions. In brief, the cells were trypsinized, washed with PBS for 3 times, resuspended in 100 μl of 2% Fixation Solution (4% paraformaldehyde in PBS, pH 7.4) and incubated for 60 min at room temperature with gentle shaking to avoid cell clumping. The cells were then centrifuged at 300 *g* for 10 min to remove the fixative and rinsed with PBS twice. Afterwards, the cells were resuspended in Permeabilization Solution (0.1% Triton-X in 0.1% sodium citrate) for 2 min on ice and washed with PBS twice. Finally the cells were labeled with 50 μl TUNEL reaction mixture and further incubated for 60 min at 37 °C in darkness. The 488 nm laser was used for excitation. The samples were then analyzed by the FITC channel of the BD FACSCanto™ flow cytometer (Becton Dickinson, USA) and 10,000 cells were counted. The data were analyzed with the Program WinMDI.

2.2.10 DNA fragmentation analysis by gel electrophoresis

Twenty-four h after PDT, the cells were trypsinized and washed with PBS for three times. The cells were lysed in 400 μl lysis buffer (200 mM Tris-HCl, pH 8.3, 100 mM EDTA, 1% SDS). After adding 20 μl of 10 mg/ml proteinase K (USB), the cells were

incubated at 37 °C for 2 h to digest the protein. The samples were then cooled to room temperature. Saturated NaCl (150 µl) was added and mixed by vigorously shaking the tube followed by centrifugation at 2,700 *g* at room temperature for 15 min. One ml of cold absolute ethanol was added to the supernatant and they were mixed by inverting the tubes. DNA was centrifuged out at 20,817 *g* at 4 °C for 20 min and the DNA pellet was washed with 70% ethanol and allowed to dry in oven. DNA was resuspended in 20 µl TE buffer (10 mM Tris-HCl, pH 8.0, 1 mM EDTA) containing 0.2 mg/ml RNase (Roche) and incubated at 37 °C for 90 min. One µg of DNA preparation was loaded into each lane of a 2% agarose (USB) gel containing ethidium bromide (0.4 µg/ml). Electrophoresis was carried out at 90 V for 2 h. Image of gel was captured with a MultiImage™ Light Cabinet (Alpha Innotech Corporation, USA).

2.2.11 Annexin-V & propidium iodide staining assay

Twenty-four h after PDT, the cells were trypsinized and washed with PBS for three times and then resuspended in 0.5 ml 1X binding buffer (0.01 M HEPES/NaOH, pH 7.4, 140 mM NaCl, 25 mM $CaCl_2$). The cells were labeled with 5 µl Annexin V solution (BD Pharmingen™, USA) as well as 4 µg/ml propidium iodide solution (Sigma-Aldrich) and allowed to incubate at room temperature in darkness for 15 and 5 min respectively. The

fluorescence of the cells was analyzed with a dot plot (PE vs FITC) of the BD FACSCanto™ flow cytometer and 10,000 cells were counted.

2.2.12 Subcellular localization studies

Cells (3×10^5) were seeded in a 35 mm glass bottom culture dish (MatTek, USA). The cells were first rinsed with PBS and incubated with 0.5 μM SiPcGlu for 90 min. The cells were then stained with 200 nM MitoTracker® Green FM, 10 μM ER-Tracker™ Green, 2 μM BODIPY® FL C5-ceramide or 4 μM LysoTracker® Green Probes (all purchased from Molecular Probes) for 30 min. After rinsing with PBS, the cells were refed with culture medium and viewed with Leica SP5 Confocal Laser Scanning Microscope (Leica Microsystems GmbH, Germany). The argon/krypton laser with a wavelength of 488 nm and the helium/neon laser with a wavelength of 633 nm were used to excite the organelle-specific probes and SiPcGlu respectively. A water immersion objective with magnification of 63 was used for image capturing. Their emitted fluorescences (at 516 nm for organelle-specific probes and 673 nm for SiPcGlu) were captured and further analyzed by using LAS AF software. The subcellular localization of SiPcGlu was revealed by drawing the fluorescence intensity profiles of SiPcGlu and the organelle-specific probes.

2.2.13 Detection of mitochondrial superoxide production

Immediately after SiPcGlu-PDT, 5 μM MitoSOX™ Red mitochondrial superoxide indicator (Molecular Probes) was added to stain the cells for 30 min. After incubation, the cells were trypsinized and washed in PBS for three times. The emitted fluorescence due to superoxide production in mitochondria was detected by the PE channel of the BD FACSCanto™ flow cytometer and 10,000 cells were counted.

Alternatively, 3 x 10^5 cells were seeded in 35 mm glass bottom culture dish and after PDT, the cells were labeled with 5 μM MitoSOX™ Red mitochondrial superoxide indicator for 15 min and washed with PBS for 3 times and re-fed with culture medium. The cells were viewed with Leica SP5 Confocal Laser Scanning Microscope. MitoSOX™ Red was excited by argon/krypton laser with wavelength of 514 nm. The emitted fluorescence was detected at 580 nm.

2.2.14 Assessment of mitochondrial membrane potential

After PDT, the cells were trypsinized and washed with PBS for three times followed by resuspension in 1 ml culture medium. The cells were then stained with 2 μM JC-1 staining solution (Molecular Probes) and incubated at 37 °C. The cells were then pelleted by centrifugation and resuspended in 500 μl PBS. Mitochondrial depolarization is indicated by the decrease in the red/green fluorescence ratio which can be analyzed with a contour plot

(PE vs FITC) of the BD FACSCanto™ flow cytometer. The data were analyzed with the Program WinMDI.

2.2.15 Caspase-3 activity assay

The activation of caspase-3 can be detected by a commercially available caspase-3 assay kit (BD Pharmingen^{TM}). The assays were done according to the manufacturer's instructions. Twenty-four h after PDT, the cells were trypsinized and washed with PBS for three times followed by resuspension in 200 μl cold cell lysis buffer and incubation on ice for 30 min. For each sample, 15 μl reconstituted N-acetyl-Asp-Glu-Val-Asp-7-amino-4-methylcoumarin (Ac-DEVD-AMC) was added to the tube containing 1 ml 1X HEPES buffer. Cell lysate (100 μl) was added to the mixture and incubated for 1 h at 37 °C. For inhibitor control, the cells were treated with 12nM SiPcGlu-PDT and 20 μg/ml Ac-DEVD-CHO, a synthetic inhibitor of caspase-3 activity. The amount of AMC liberated from Ac-DEVD-AMC by active caspase-3 was measured using a fluorescence spectrofluorometer (Perkin Elmer, USA) with excitation and emission wavelengths of 380 and 440 nm respectively.

2.2.16 Western blot analyses for cytochrome c, caspase-3, PARP and glucose-regulated protein 78 (GRP78)

Twenty-four h after PDT, the cells were trypsinized and washed with PBS for three times. For the analysis of cytochrome c, the Cytosol/Particulate Rapid Separation Kit (BioVision, USA) was used to obtain the cytosolic fraction, according to the manufacturer's instructions. For the analyses of caspase-3, poly (ADP-ribose) polymerase (PARP) and GRP78, whole cell lysate was used. Cells (4×10^6) were incubated in 50 μl lysis buffer [75 mM NaCl, 1 mM NaH_2PO_4, 250 mM sucrose, 8 mM Na_2HPO_4 and 4 μl protease inhibitor cocktail (Sigma-Aldrich)] in the presence of 8 μg/μl digitonin (Sigma-Aldrich) and then vortexed immediately for 30 s. The whole cell lysate was obtained by centrifugation at 20,817 *g* for 1 min at 4 °C. For electrophoresis, 25 μg protein (determined by the bicinchoninic acid method) per lane was mixed with sample buffer (65.5 mM Tris-HCl, pH 6.8, 0.11% glycerol, 2.1% SDS, 2.6% β-mercaptoethanol and 0.13% bromophenol blue) in a 12% polyacrylamide gel with 5% stacking gel. After electrophoresis, the proteins were transferred to immobilon-P transfer membrane (Millipore, USA) using a semi-dry transfer system (Bio-rad). Membranes were blocked with 5% skim milk in TBS-T (TBS with 0.1% Tween-20). Target proteins were incubated with mouse monoclonal antibodies against cytochrome c (1:1000, BD Pharmingen™) and caspase-3 (1:500, Zymed, USA), rabbit polyclonal antibodies against GRP78 (1:200, Santa Crux Biotechnology, USA) and PARP

(1:200, Santa Cruz) for 18 h at 4 °C, and rabbit polyclonal antibodies against β-actin (1:1000, Sigma-Aldrich) for 2 h at room temperature. After several washes with TBS-T, the signal was developed by incubating with anti-mouse or anti-rabbit horseradish peroxidase-conjugated secondary antibodies (1:1000, Amersham Bioscience, USA) for 1 h. Enhanced chemiluminescence detection reagents (Amersham Pharmacia, England) were used for detecting the signal.

2.2.17 Ca^{2+} release from endoplasmic reticulum (ER)

After PDT, the cells were trypsinized and washed with PBS for three times followed by incubation with 2.5 μM Fluo-3, AM (Molecular Probes) for 60 min at 37 °C. Before fluorescence measurements, cells were washed with culture medium to remove any dye that is nonspecifically associated with the cell surface, and then incubated for 30 min to allow complete de-esterification of intracellular AM esters. The emitted fluorescence due to Ca^{2+} release from ER was then detected by FITC channel of the BD FACSCanto™ flow cytometer and the data were analyzed with the Program WinMDI.

2.3 *In vivo* studies

2.3.1 HT29 tumor-bearing nude mice model

The nude mice (20 - 25 g) were obtained from the Laboratory Animal Services Centre (LASEC) at The Chinese University of Hong Kong. All experiments on tumor-bearing nude mice were approved by the Animal Experimentation Ethics Committee, The Chinese University of Hong Kong. Mice were bred under pathogen-free condition with free access of food and water. In developing the tumor model, HT29 cells (1×10^7) were subcutaneously inoculated at the back of the nude mice. Measurement of the tumor size started on Day 8 after inoculation of tumor cells (Figure 2.3). Three parameters of the tumor, viz. length, width and thickness, were measured by micrometer digital caliper (SCITOP Systems, Hong Kong). The tumor volume was calculated by the following formula:

Tumor volume = π x (Length x Width x Thickness) / 6

Figure 2.3 HT29 tumor- bearing nude mice (8 days after inoculation).

2.3.2 *In vivo* photodynamic treatment

On day 9, SiPcGlu (1 μmole/kg body weight, 0.2 ml) was intravenously injected into the tail vein of the tumor-bearing nude mice. Twenty-four h after the injection, laser was spotted onto the tumor with a fluence rate of 0.1 W/cm^2 for 5 min, giving a total fluence of 30 J/cm^2. Tumor size of the nude mice were followed for the next 15 days.

2.3.3 Biodistribution of SiPcGlu

SiPcGlu (1 μmole/kg body weight, 0.2 ml) was intravenously injected into the tumor-bearing nude mice. After 24 h, the mice were anesthetized with an intra-peritoneal injection of 0.2 ml ketamine/xylazine cocktail solution (0.1 mg ketamine and 0.01 mg xylazine/g body weight). The major organs/tissues of the mice were excised, rinsed with PBS and blotted dry. The excised organs/tissues were homogenized with DMF (10-fold volume of the organs/tissues) by a Biospec Biohomogenizer (Fisher Scientific, USA). Homogenates were centrifuged at 2,450 *g* for 20 min to remove the large debris. Supernatants were collected and subjected to fluorescence measurement. The peak fluorescence intensity was recorded by scanning the fluorescence emission spectrum from 610 nm to 900 nm using an excitation wavelength at 608 nm with a fluorescence spectrofluorometer (Perkin Elmer, USA). Amount of SiPcGlu present in the sample was determined with reference to the standard curves in different organs/tissues. The amount

was expressed in % initial dose (% ID) per gram of tissue as calculated by the following formula.

$$\% \text{ ID per gram of tissue} = \frac{(\text{amount of SiPcGlu} / \text{weight of the tissue})}{\text{Initial injection dose}} \times 100\%$$

Ketamine and xylazine solution were obtained from LASEC, The Chinese University of Hong Kong.

2.3.4 Assay for plasma enzyme activities

Blood was obtained by intra-cardiac puncture with a heparinized syringe. Heparin (1250 USP units/ml, Sigma-Aldrich) was added to prevent blood coagulation. The blood samples were centrifuged at 1,700 *g* for 5 min to obtain the supernatant which represents the plasma. The activities of alanine aminotransferase (ALT), aspartate aminotransferase (AST) (both purchased from Thermo Electron Corporation, Australia) and creatine kinase (CK, Biosystems, Spain) were assayed by the commercially available assay kits. Fifty μl plasma was added to 1 ml of ALT, AST and CK assay reagents. Enzyme activities were then determined by monitoring the absorbance change at 340 nm for 3 min. The enzyme activity was expressed as U/L.

2.4 Statistical analysis

Differences in the tumor volume and caspase-3 activity were analyzed for significance by One-way Analysis of Variance (ANOVA, with Holm-Sidak method) and Student's *t*-test respectively. Difference between the values was considered significant when $p < 0.05$. All statistical analysis was done by SigmaStat (Systat Software, San Jose).

Chapter 3
Results

3.1 *In vitro* studies

3.1.1 SiPcGlu-PDT induced cytotoxicity on HT29 cells

In order to investigate the *in vitro* photocytotoxicity induced by the SiPcGlu-PDT and see whether it is essentially non-toxic to the HT29 cells in darkness, the cell survival after SiPcGlu-PDT was determined by MTT assay at 24 h post irradiation. Figure 3.1 shows the cell survival curves of HT29 after treatment with SiPcGlu-PDT, in the presence or absence of red light illumination. From the cell survival curve of HT29 in the absence of light, the cell survival was unaffected and remained ~100%. The cell survival of HT29 cells in the solvent itself is also unaffected with a viability of 91.23 ± 1.96%. On the contrary, in the presence of red light, the cell survival of HT29 was significantly reduced in a dose-dependent manner and the IC_{50} and IC_{90} values are about 6 and 12 nM respectively.

To compare the efficacy of SiPcGlu with that of Photofrin®, the HT29 cells were treated with Photofrin®, in the presence or absence of light, using the same experimental setup. In the absence of light, the cell survival of HT29 was unaffected and remained ~100%. However, in the presence of light, Photofrin®-PDT produced a dose-dependent cytotoxicity on HT29 cells. The IC_{50} value is ~5 μg/ml (Figure 3.2). When compared with the IC_{50} of SiPcGlu-PDT 6 nM, i.e. 7.8 ng/ml, SiPcGlu-PDT is much more potent than Photofrin® in killing HT29.

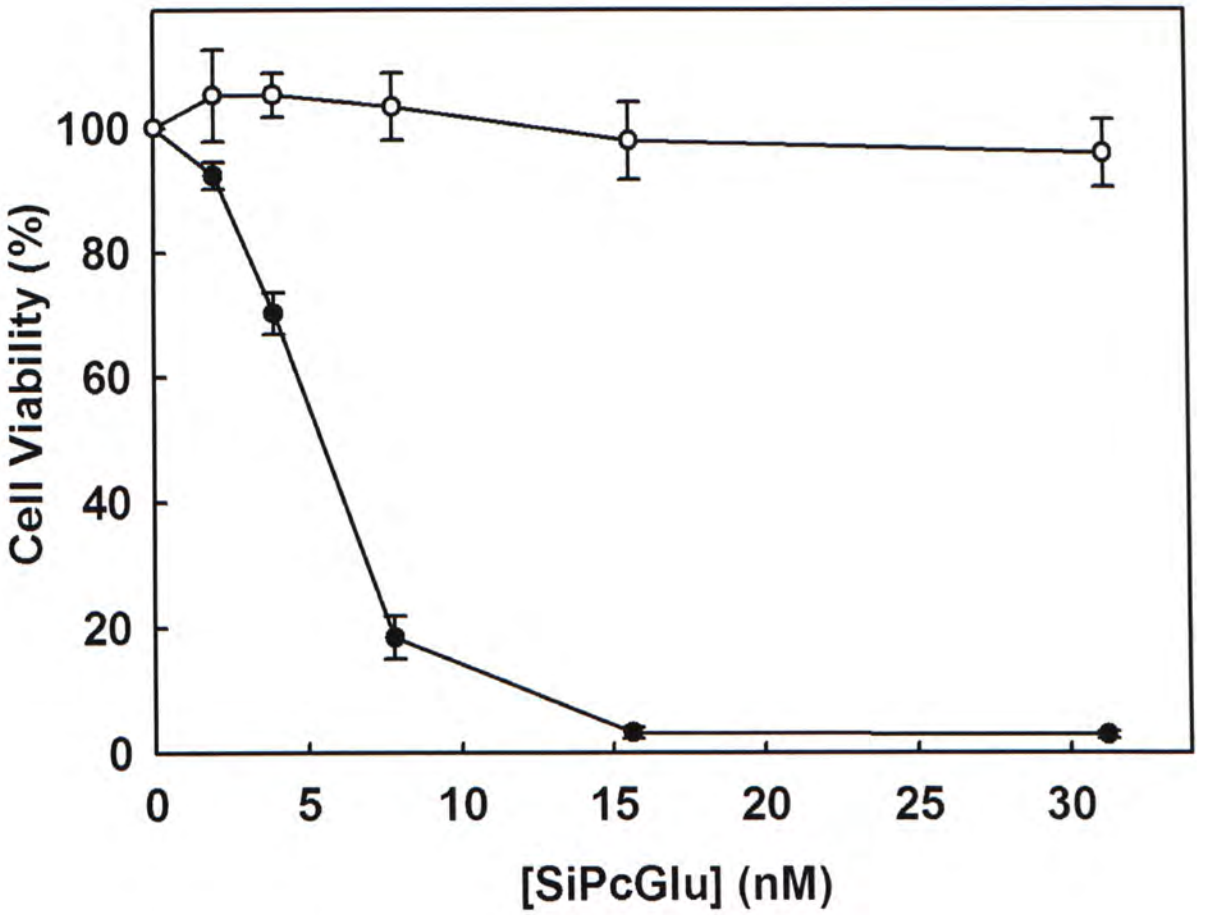

Figure 3.1 SiPcGlu-PDT-induced cytotoxicity in HT29 cells. The cells were treated with different concentrations of SiPcGlu in the presence (●) or absence (○) of light illumination with halogen lamp (48 J/cm^2). Cell viability was determined by MTT assay. The data are Mean ± S.E.M. from three independent experiments, each performed in quadruplicates.

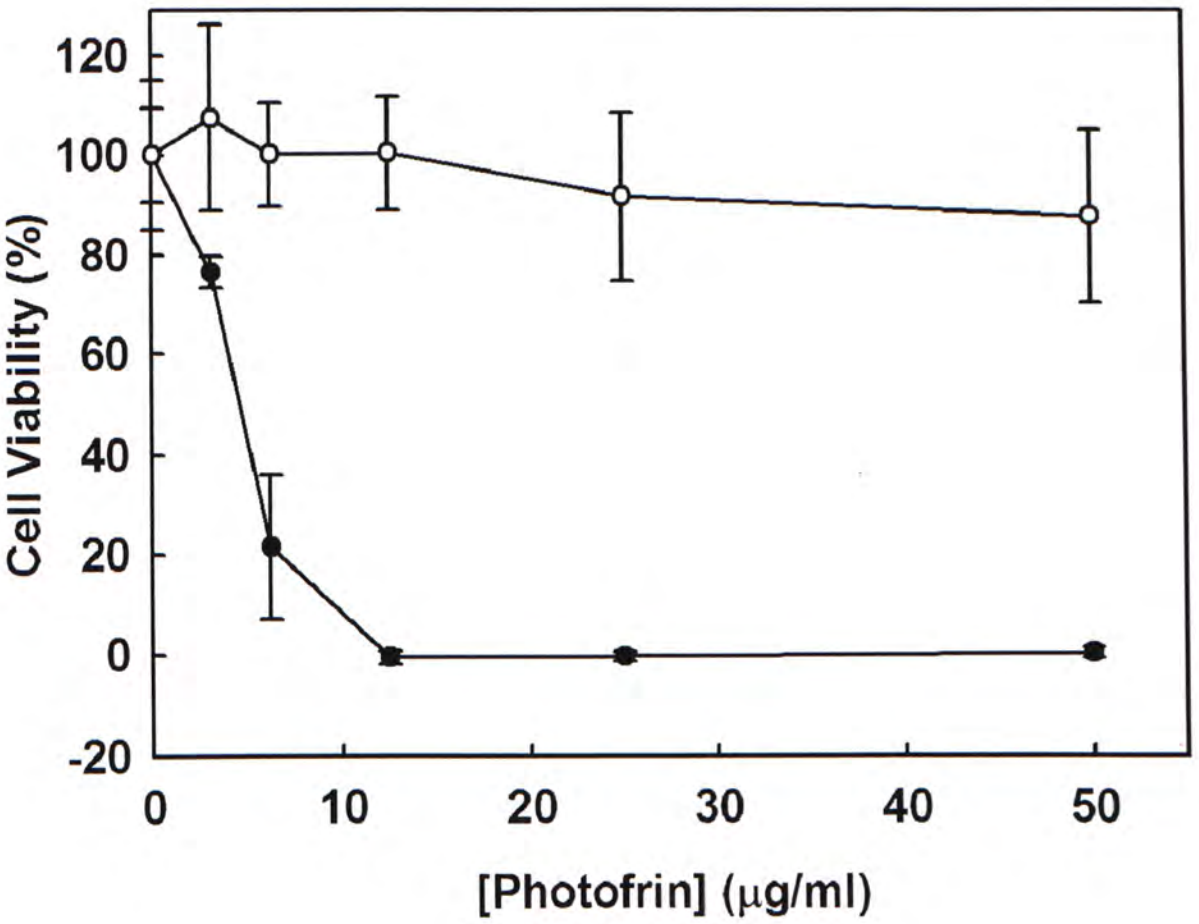

Figure 3.2 Photofrin®-PDT-induced cytotoxicity in HT29 cells. The cells were treated with different concentrations of Photofrin® in the presence (●) or absence (○) of light illumination with halogen lamp (48 J/cm^2). Cell viability was determined by MTT assay. The data are Mean ± S.D., n = 4.

3.1.2 Light dose effect on cytotoxicity by SiPcGlu-PDT

Halogen lamp and diode laser were used to study the effect of light dose on the photocytotoxicity induced by SiPcGlu-PDT. A total fluence of 48 J/cm^2 was delivered to the cells with halogen lamp. For diode laser, 2 light doses, 2 and 8 J/cm^2 were used. With a total fluence of 8 J/cm^2, the IC_{50} produced by the diode laser was similar to that produced by the halogen lamp. By reducing the total fluence to 2 J/cm^2, the photoactivity was lowered, giving an IC_{50} value of 46 nM (Figure 3.3).

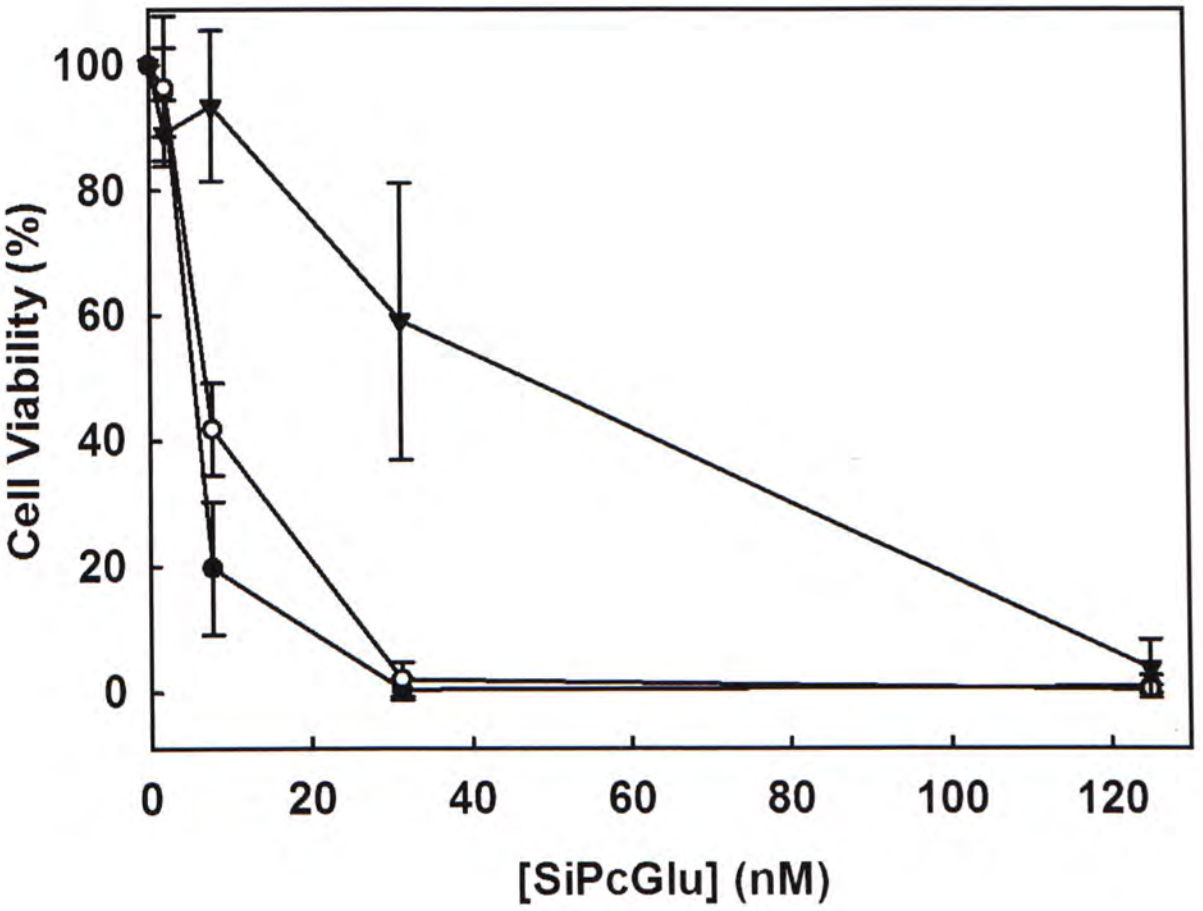

Figure 3.3 Light dose effect on photocytotoxicity induced by SiPcGlu-PDT. After incubating the cells with SiPcGlu, the cells were illuminated with halogen lamp of 48 J/cm^2 (●) or a diode laser of 2 (▼) or 8 J/cm^2 (○). Cell viability was determined by MTT assay. The data are Mean ± S.E.M. from three independent experiments, each performed in quadruplicates.

3.1.3 SiPcGlu-PDT induced ROS production

To study the action mechanism of SiPcGlu-PDT in triggering cell death, the SiPcGlu-treated cells were subjected to DCFDA staining to investigate the ROS production during photodynamic treatment. Figure 3.4 shows the ROS production curves in the presence or absence of red light illumination. In darkness, the ROS production was unaffected while in the presence of light, the ROS production was increased in a dose-dependent manner and had ~4-fold increase at concentration of ca. 30 nM.

3.1.4 SiPcGlu-PDT induced cell death through Type I and II photoreactions

In order to investigate whether Type I or Type II reactions are involved in the photodynamic action by SiPcGlu-PDT, the hydroxyl radical scavenger D-mannitol and singlet oxygen scavengers L-histidine and vitamin C were used to investigate whether they can protect the cells from photocytotoxicity. HT29 cells were pretreated with antioxidants and SiPcGlu and subjected to light illumination. Their cell viabilities were determined. The cell survival curves show that both the hydroxyl radical and singlet oxygen scavengers can slightly protect the cells from photodamage (Figure 3.5), indicating that SiPcGlu-PDT triggers cell death via both Type I and Type II photoreactions.

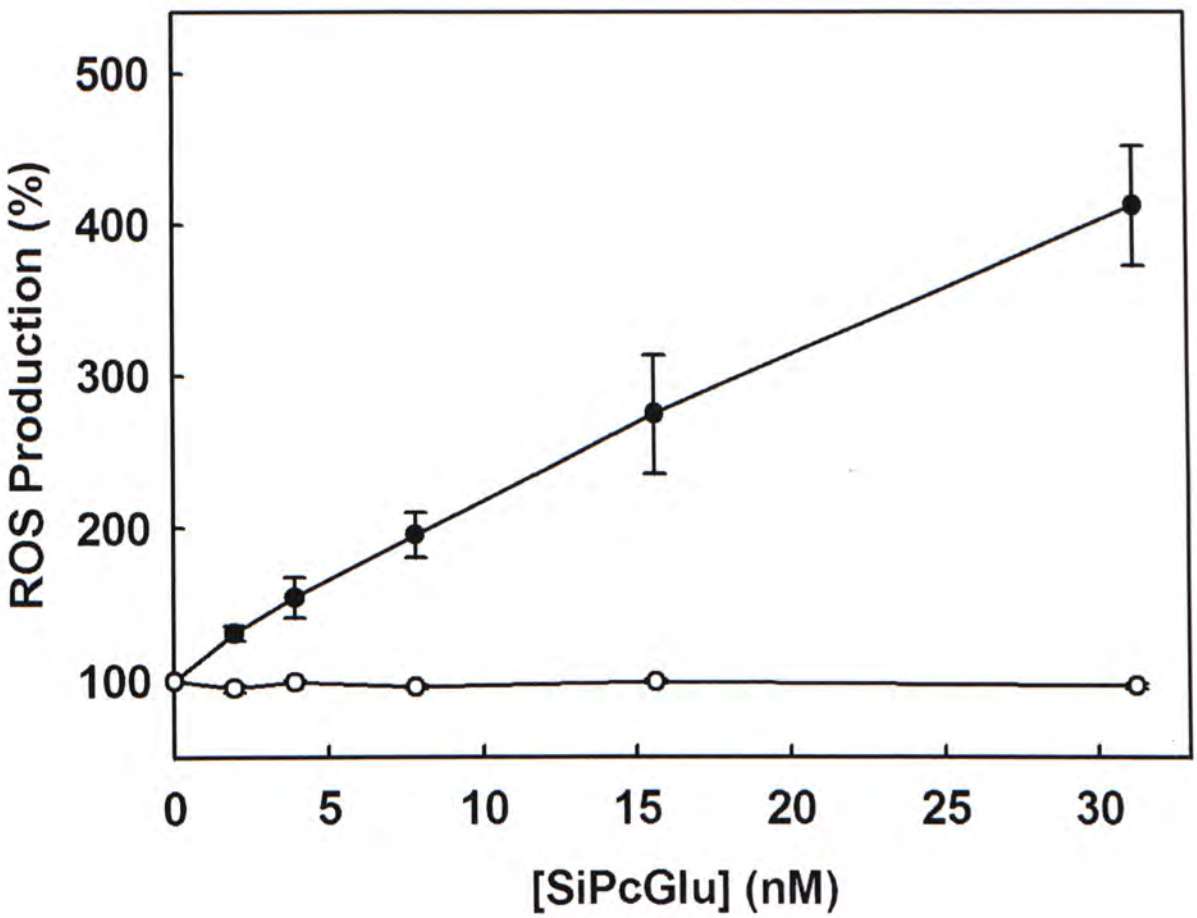

Figure 3.4 SiPcGlu-PDT-induced ROS production. The cells were incubated with different concentrations of SiPcGlu, followed by staining with DCFDA in the presence (●) or absence (○) of light illumination with halogen lamp (48 J/cm^2). ROS production was determined by using a fluorescence plate reader with excitation and emission filters at 485 and 535 nm respectively. The data are Mean ± S.E.M. from three independent experiments, each performed in quadruplicates.

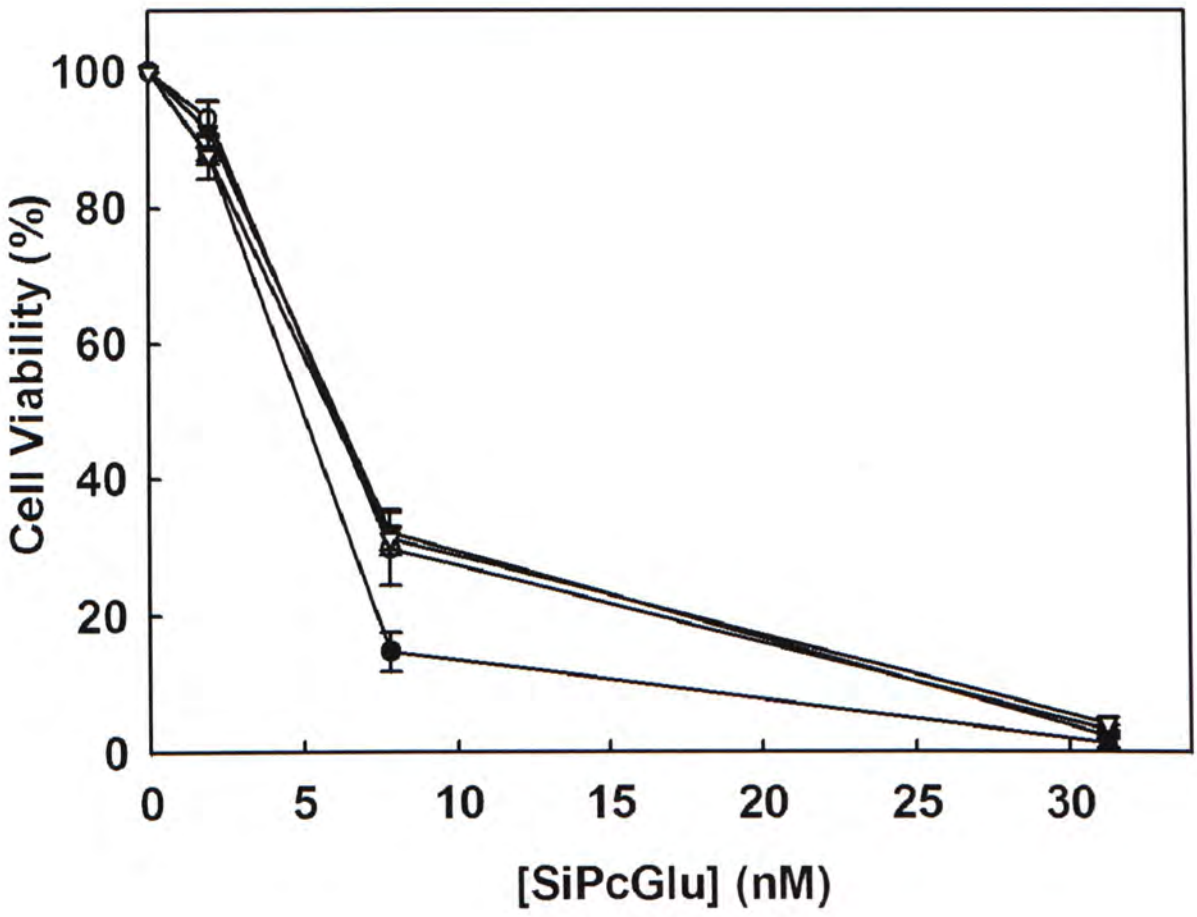

Figure 3.5 SiPcGlu-PDT-induced cell death via Type I and Type II photoreactions. Antioxidants were added to HT29 cells and incubated with different concentrations of SiPcGlu. The 4 groups of treatments included no antioxidant control (●), and cells treated with 50 mM D-mannitol (○), 100 μM L-histidine (▼) and 200 μM vitamin C (▽). The cells were illuminated with halogen lamp (48 J/cm^2). Cell viability was determined by MTT assay. The data are Mean ± S.E.M. from three independent experiments, each performed in quadruplicates.

3.1.5 ROS production after SiPcGlu-PDT

Zorov et al. (2000) have reported that the photodynamically produced ROS causes post-PDT ROS production inside the cells. Therefore, to study whether ROS was produced after SiPcGlu-PDT, DCFDA was added to the HT29 cells after SiPcGlu-PDT, followed by 1 hr incubation. Figure 3.6 shows that after SiPcGlu-PDT, there is a dose-dependent increase in ROS production. Since mitochondria is a major source of endogenous ROS which may be related to respiratory chain, investigation was performed to see whether oxidative insult caused by SiPcGlu-PDT leads to interrelated intramitochondrial generation of superoxide anion and other ROS (Mukhopadhyay et al., 2007). We applied MitoSOX^{TM} Red mitochondrial superoxide indicator which allows highly selective and quantitative detection of superoxide in the mitochondria of live cells by flow cytometry. Result shows that after SiPcGlu-PDT, there is a significant increase in mitochondrial superoxide production in a dose-dependent manner (8.82 ± 2.97% for control cells; 18.61 ± 1.15% and 43.85 ± 6.31% in 6 nM and 12nM SiPcGlu-PDT-treated cells respectively) (Figure 3.7). The mitochondrial ROS production can further be confirmed by staining the cells with MitoSOX^{TM} Red and using confocal microscopy. Confocal microscopic imaging shows a significant increase in mitochondrial fluorescence intensity of MitoSOX^{TM} Red in HT29 after 12 nM SiPcGlu-PDT (Figure 3.8), which is in agreement with the results by flow cytometric measurement.

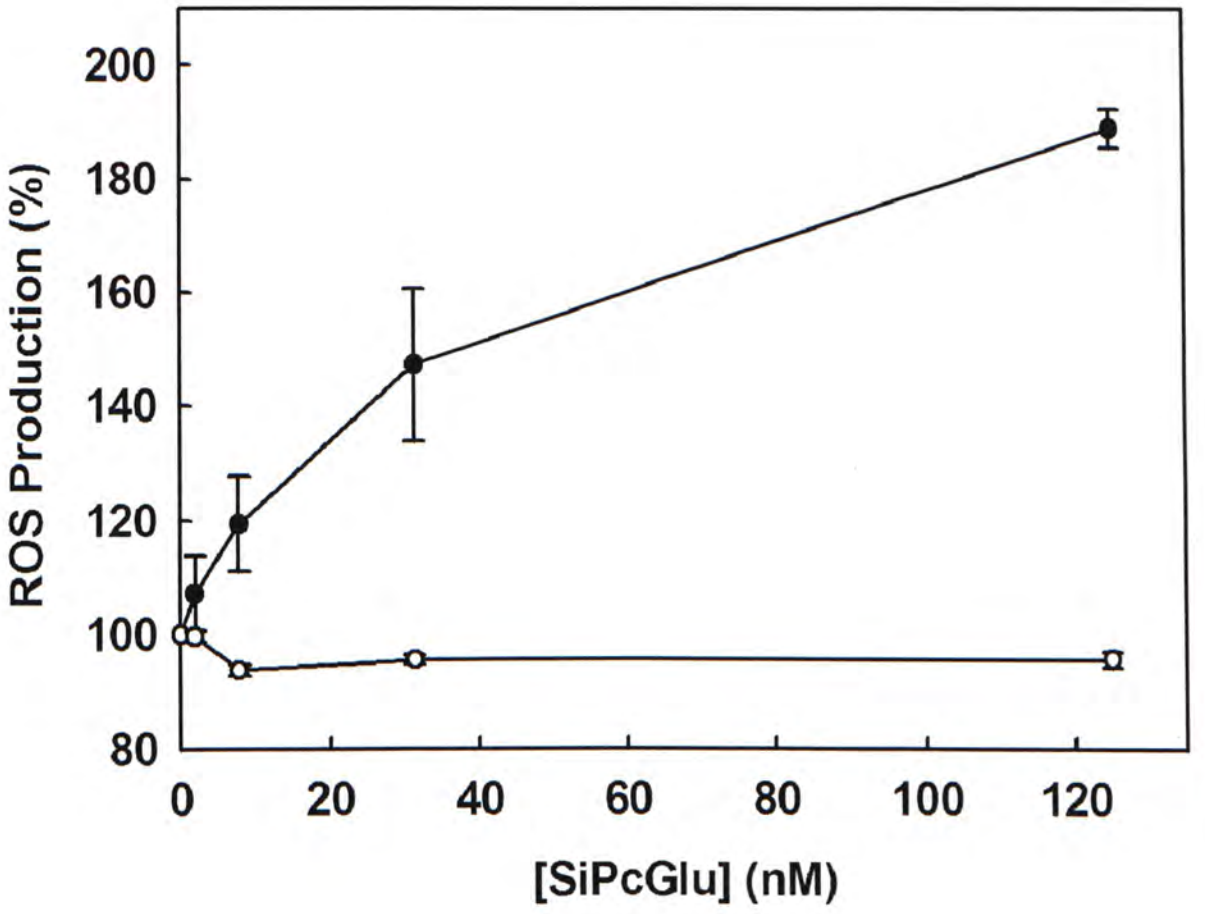

Figure 3.6 ROS production after SiPcGlu-PDT. The cells were treated with different concentrations of SiPcGlu. After light illumination, the cells were stained with DCFDA for 1 h. ROS production was determined by using a fluorescence plate reader with excitation and emission filters at 485 and 535 nm respectively. The data are Mean ± S.E.M. from three independent experiments, each performed in quadruplicates.

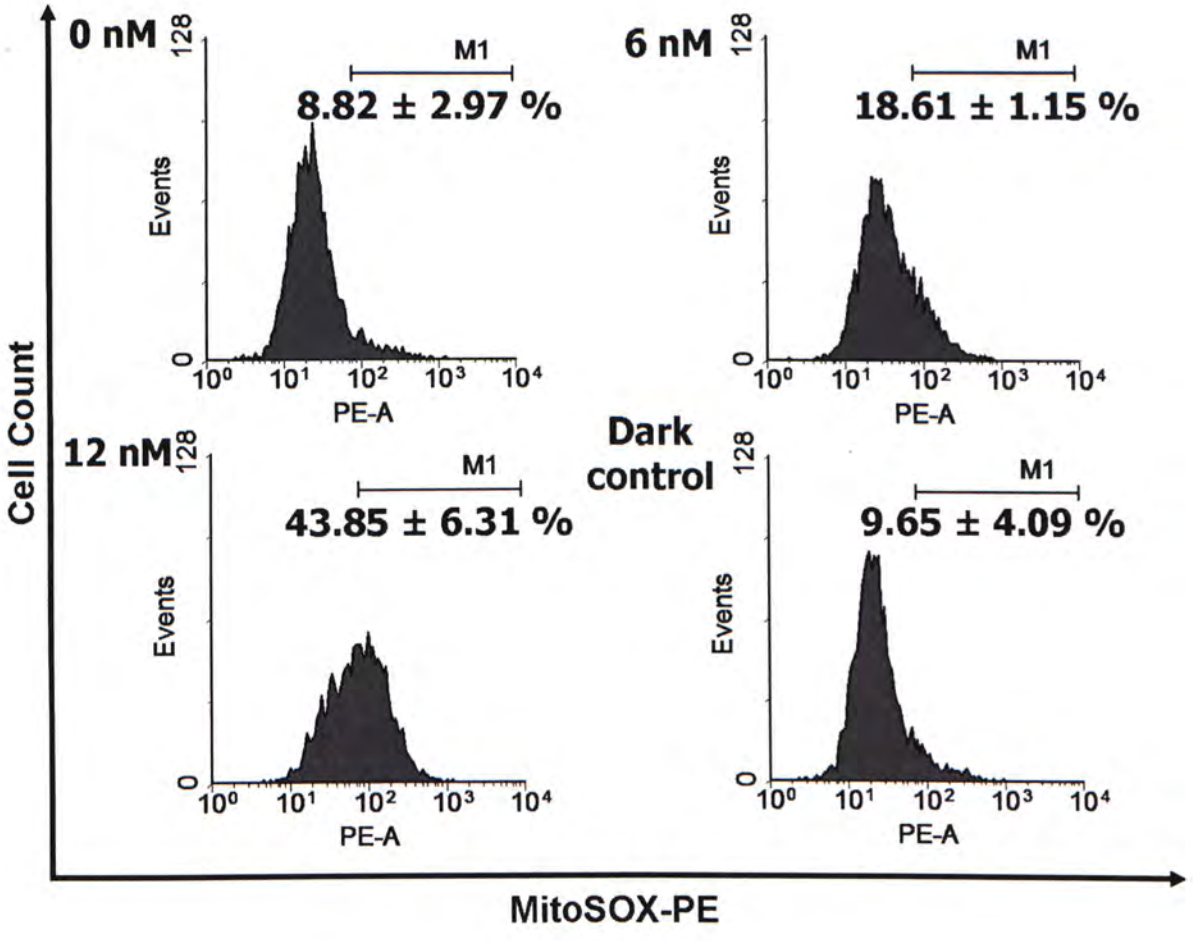

Figure 3.7 SiPcGlu-PDT-induced mitochondrial superoxide production as analyzed by flow cytometry. The cells were treated with different concentrations of SiPcGlu. After illumination, the cells were stained with MitoSOX™ Red mitochondrial superoxide indicator. The dark controls were cells treated with 12 nM SiPcGlu without illumination. The emitted fluorescence due to superoxide production was detected by the PE channel of the BD FACSCanto™ flow cytometer. The pattern shown is a representative from three independent experiments while the data are Mean ± S.D. from 3 independent experiments.

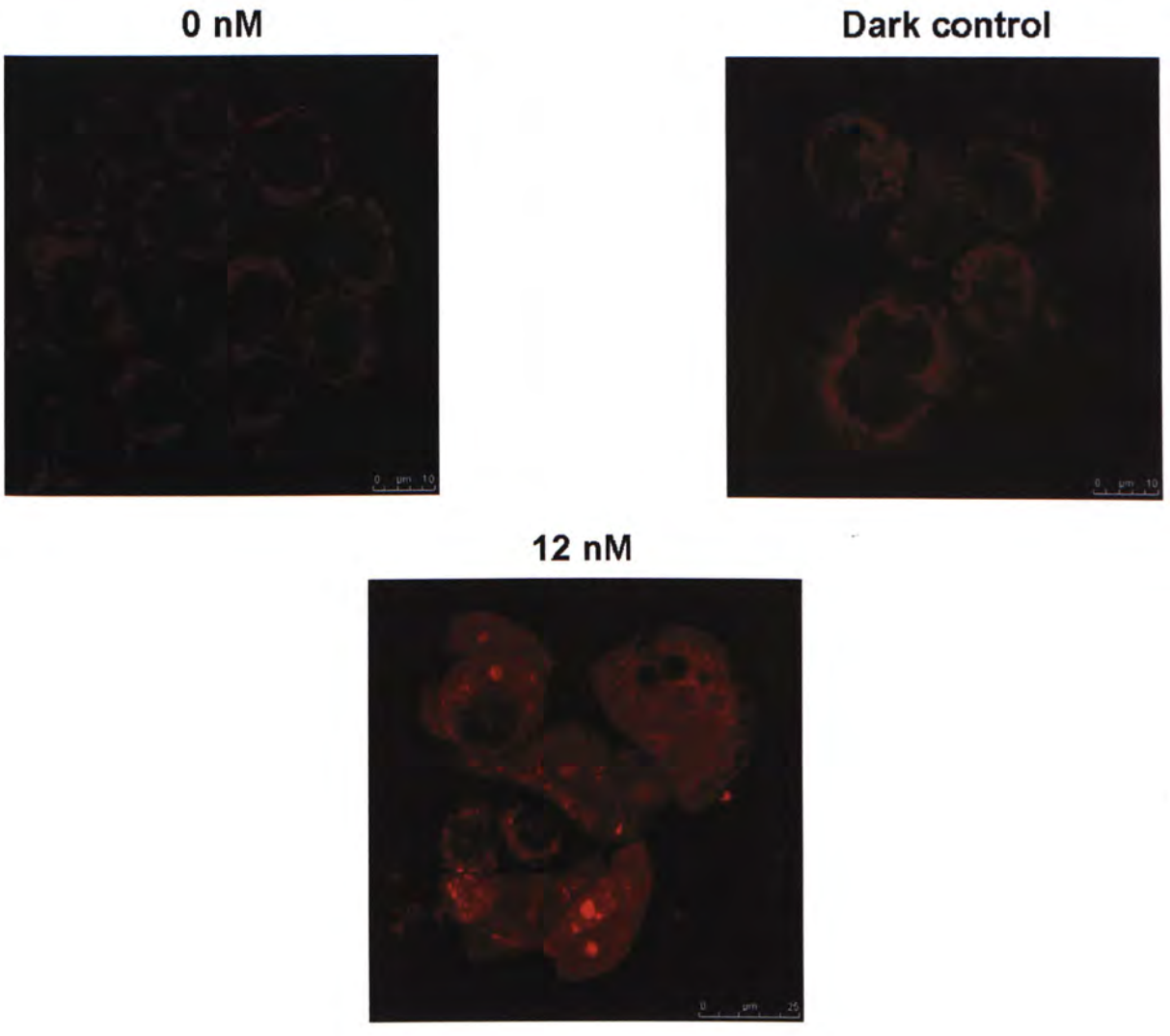

Figure 3.8 SiPcGlu-PDT-induced mitochondrial superoxide production as analyzed by confocal microscopy. The cells were treated with different concentrations of SiPcGlu. After illumination, the cells were stained with MitoSOX^{TM} Red mitochondrial superoxide indicator. The dark control refers to cells treated with 12 nM SiPcGlu without illumination. The emitted fluorescence due to superoxide production was detected by Leica SP5 Confocal Laser Scanning Microscope. MitoSOX^{TM} Red was excited by argon/krypton laser at 514 nm. The emitted fluorescence was detected at 580 nm.

3.1.6 Glucose competitive Assay

To better understand the role of glucose moiety in the structure of SiPcGlu, a competitive assay was performed. Glucose solutions (1 or 100 mM) were added and incubated with different concentrations of SiPcGlu. Twenty-four h after PDT, MTT assay was performed to determine whether glucose could inhibit the photocytotoxicity induced by SiPcGlu-PDT. Figure 3.9 shows that the cell viability was virtually identical in the presence or absence of glucose, which implies that the GLUTS may not be involved in the uptake of SiPcGlu.

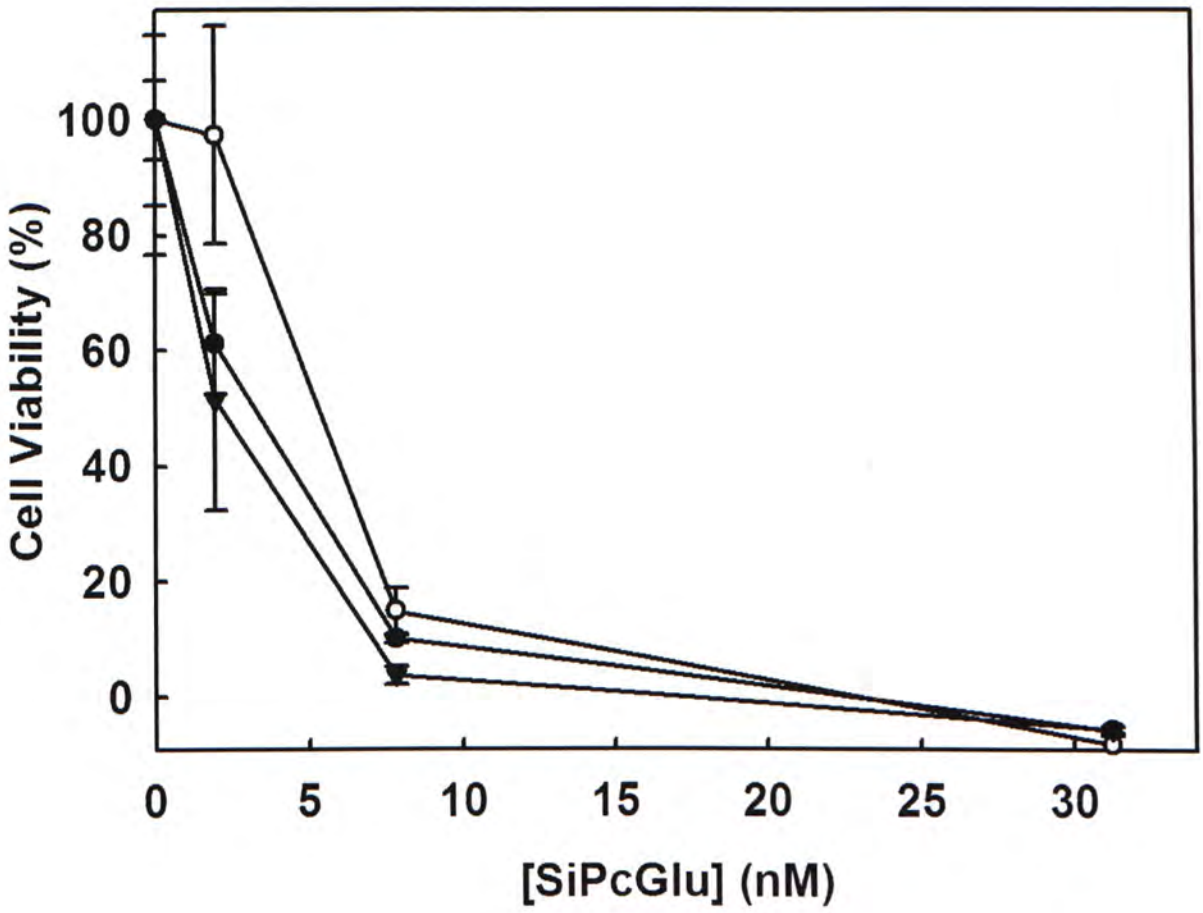

Figure 3.9 Glucose competitive assay. Glucose solutions (1 or 100 mM) were added and incubated with different concentrations of SiPcGlu. The 3 groups of treatments included no glucose control (●), and cells treated with 100 mM glucose solution (▼) and 1 mM glucose solution (○). The cells were illuminated with halogen lamp (48 J/cm^2). Cell viability was determined by MTT assay. The data are Mean ± S.D., n = 4.

3.1.7 SiPcGlu-PDT induced apoptosis in HT29 cells

To study whether SiPcGlu-PDT induces cell death via apoptosis, 24 h after SiPcGlu-PDT, the cells were subjected to TUNEL, annexin V & propidium iodide staining and DNA fragmentation assays. For the TUNEL assay, the DNA breaks of dead cells can be stained with fluorescein-2'-deoxyuridine 5'-triphosphate (FITC-dUTP). Figure 3.10 shows that there was an obvious increase in the FITC intensity, in a dose-dependent manner (31.4 ± 7.26% and 89.36 ± 6.19% in 6 nM and 12nM SiPcGlu-treated cells, respectively). The dark or light control cells only showed low FITC intensity (< 2%). To investigate whether the dead cells are apoptotic or necrotic cells, DNA laddering assay was performed. A typical DNA ladder pattern, a hallmark of apoptosis, was observed at either 24 or 48 h after treating the cells with 12nM SiPcGlu-PDT (Figure 3.11). To further differentiate the live, apoptotic and necrotic cells in the HT29 cell populations, annexin V & propidium iodide staining assay was performed to detect early apoptotic cells which have phosphatidyl serine externalization but do not have DNA leakage. The percentage of such cells in the population increased in a dose-dependent manner from <10 % for the controls to 27.87 ± 1.91% and 66.58 ± 5.92% after treatment with 6 nM and 12 nM SiPcGlu-PDT respectively (Figure 3.12).

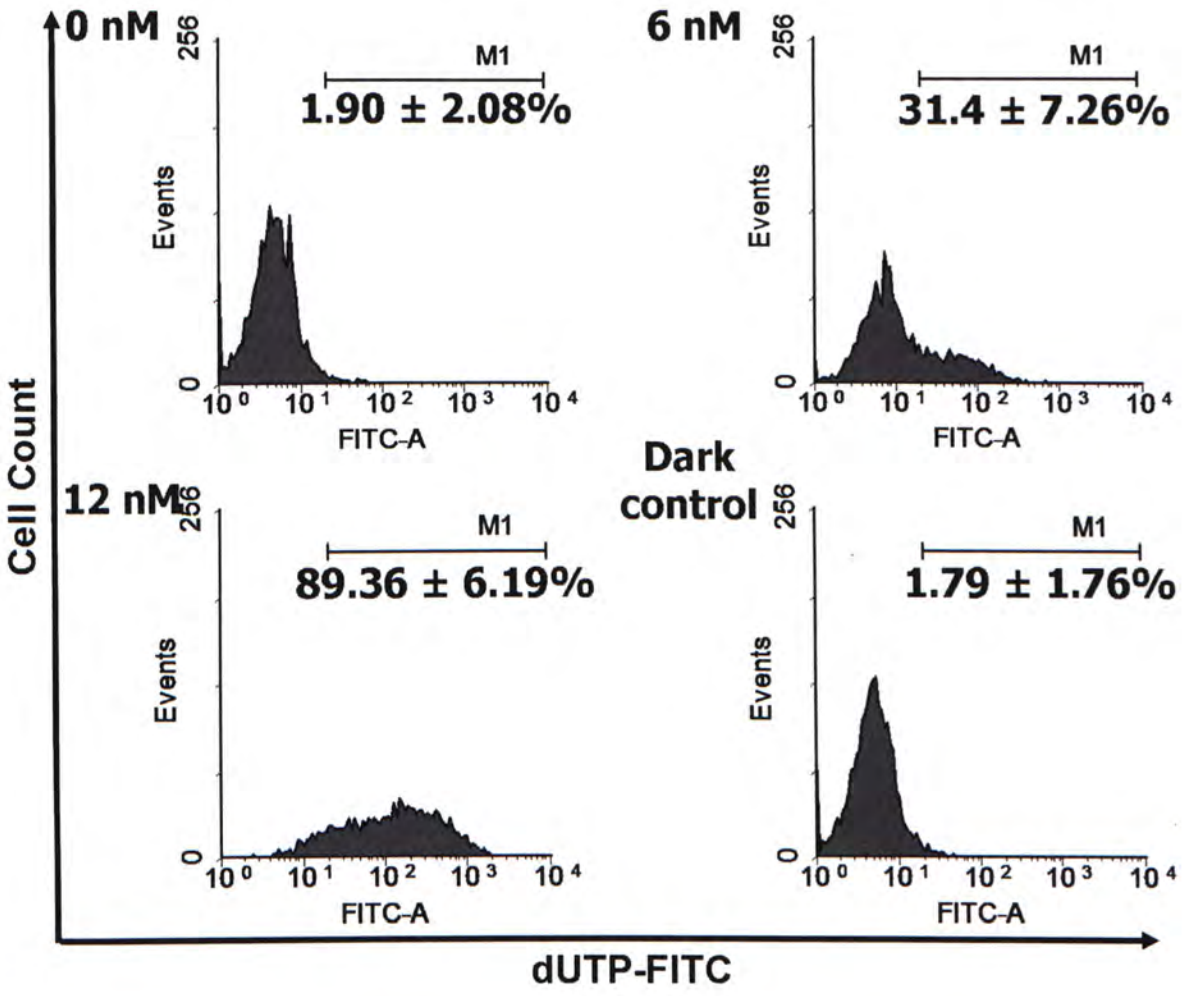

Figure 3.10 SiPcGlu-PDT-induced apoptosis in HT29 cells as analyzed by TUNEL assay.

The cells were treated with different concentrations of SiPcGlu. Twenty-four h after illumination, the cells were treated with the *In Situ* Cell Death Death Detection Kit, Fluorescein. The dark control refers to cells treated with 12 nM SiPcGlu without illumination. The emitted fluorescence due to fragmented DNA was detected by the FITC channel of the BD FACSCanto™ flow cytometer. The pattern shown is a representative from three independent experiments while the data are Mean ± S.D. from 3 independent experiments.

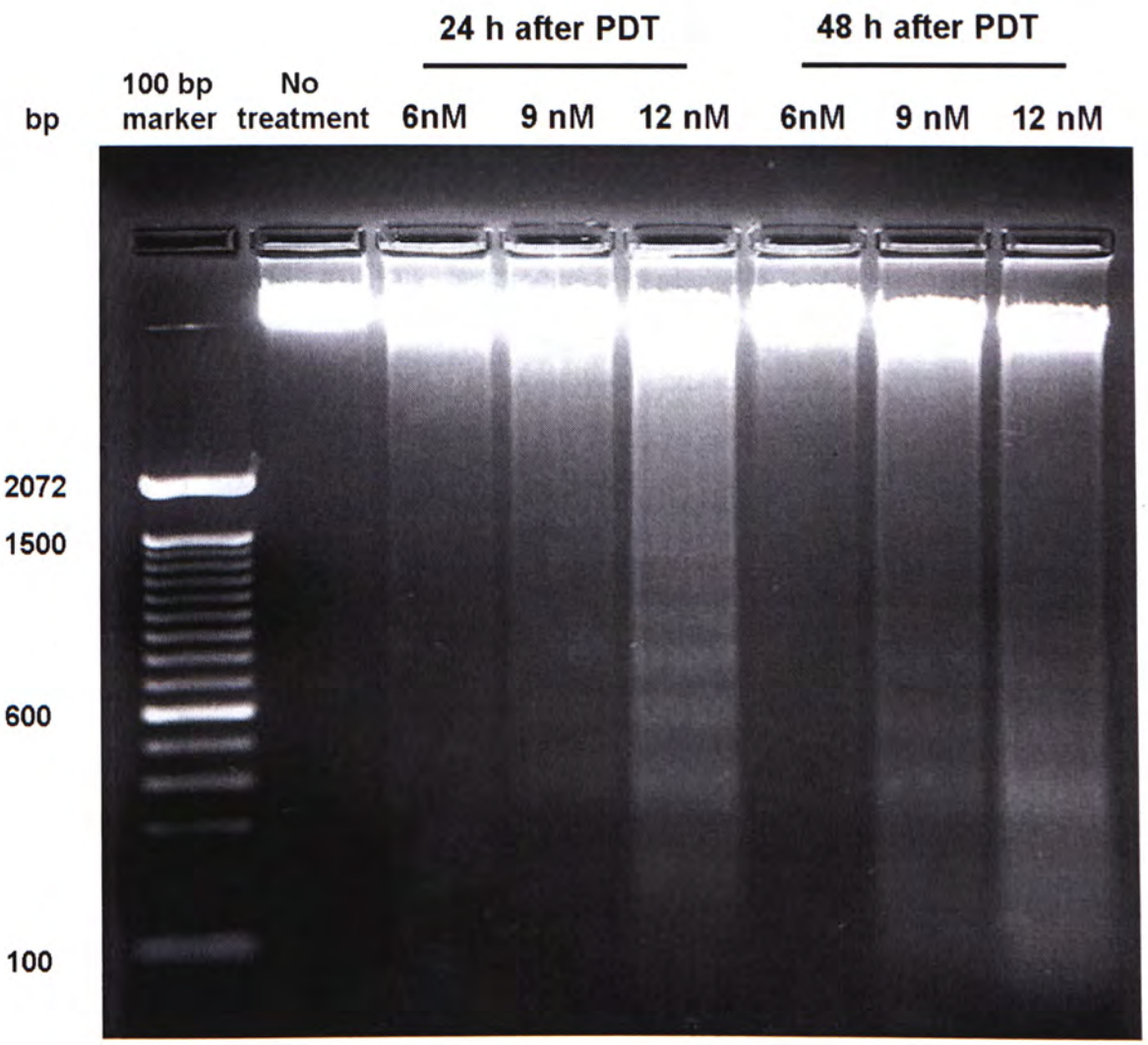

Figure 3.11 SiPcGlu-PDT-induced apoptosis in HT29 cells as analyzed by DNA laddering assay. The cells were treated with different concentrations of SiPcGlu. Twenty-four and forty-eight h after illumination, DNA was extracted and analyzed by electrophoresis in a 2% agarose gel containing ethidium bromide.

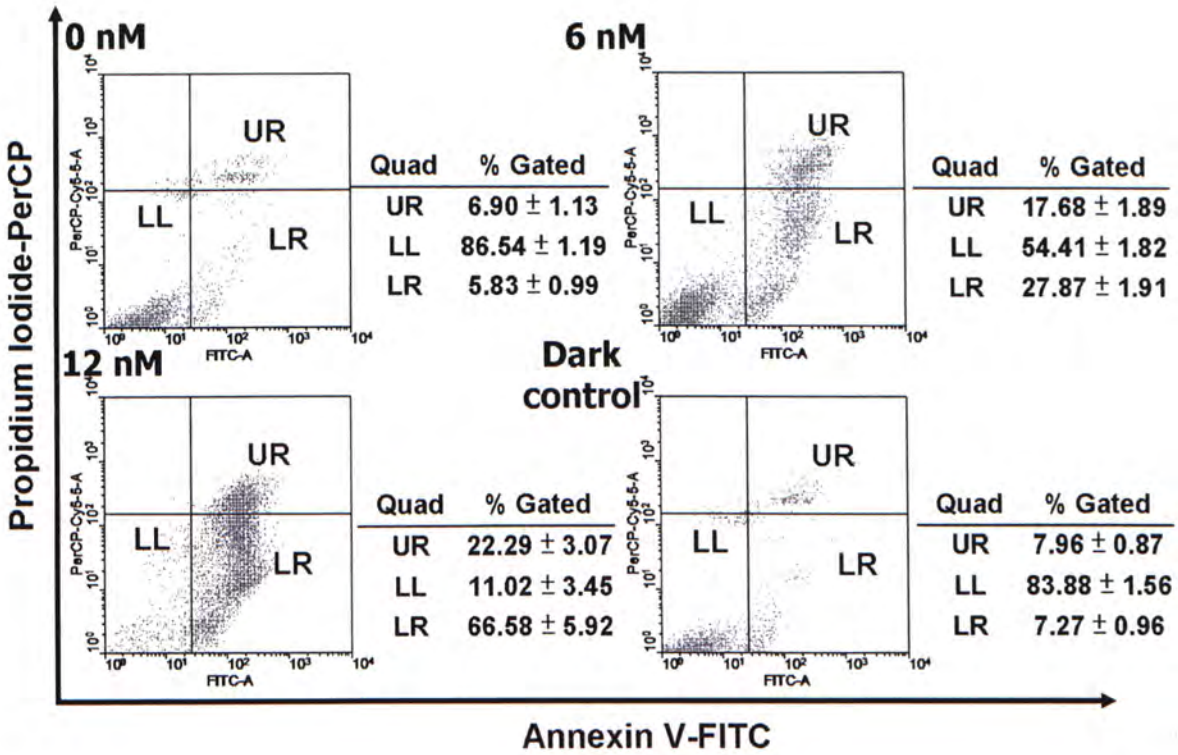

Figure 3.12 SiPcGlu-PDT-induced apoptosis in HT29 cells as analyzed by annexin V & propidium iodide assay. The cells were treated with different concentrations of SiPcGlu. Twenty-four h after illumination, the cells were stained with annexin V & propidium iodide solutions. The dark control refers to cells treated with 12 nM SiPcGlu without illumination. The emitted fluorescence was detected by the by the PerCP vs FITC channels of the BD FACSCanto™ flow cytometer. The percentage of the population of apoptotic cells (LR), normal cells (LL) and necrotic cells (UR) are shown. The pattern shown is a representative from three independent experiments while the data are Mean ± S.D. from 3 independent experiments.

3.1.8 Subcellular localization of SiPcGlu

Since ROS is only short-lived and has very short migration distance, it is crucial to find out the intracellular localization of photosensitizer where it exerts its primary photodamage. It was done by co-staining HT29 with SiPcGlu and organelle-specific probes. SiPcGlu did not specifically localize in a single organelle. Instead, the confocal overlay fluorescence images show that SiPcGlu partially overlapped with different organelle-specific probes, including those for ER, mitochondria, lysosome and Golgi body (Figures 3.13 to 3.16). Their line profiles were also drawn and it is shown that SiPcGlu has a partial localization in these membranous organelles.

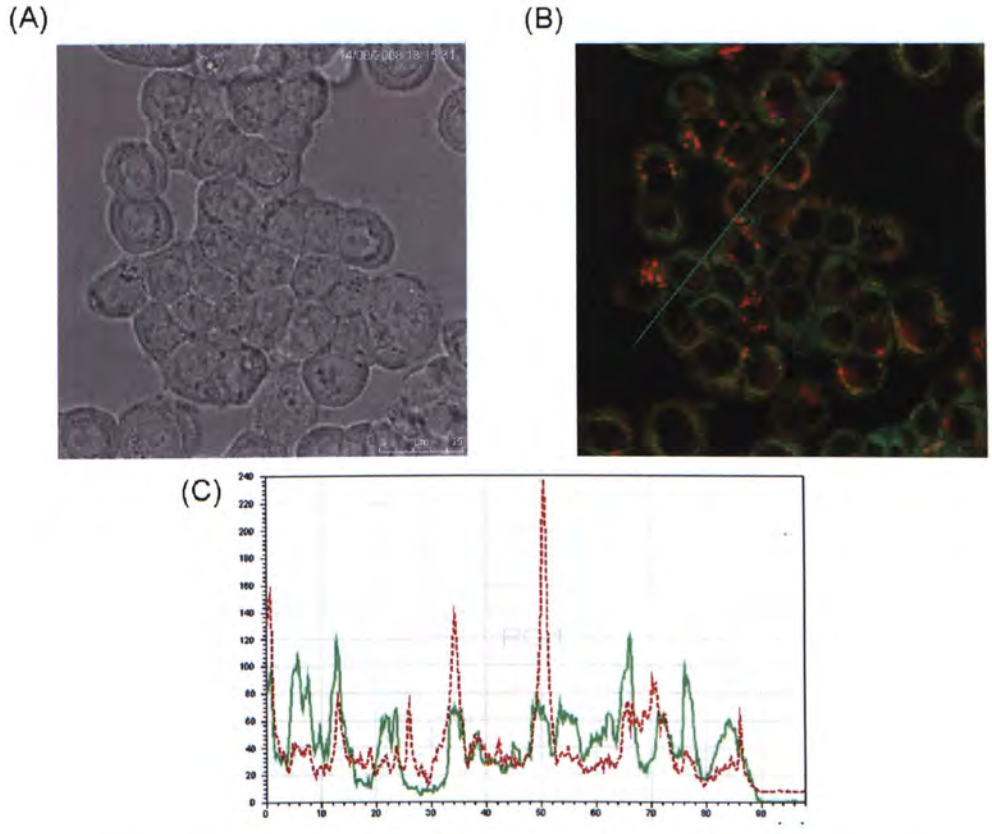

Figure 3.13 Subcellular localization of SiPcGlu in HT29 cells (ER). The cells were incubated with 0.5 μM SiPcGlu for 90 min and then ER-Tracker™ Green probe for further 30 min. The cells were visualized with a Leica SP5 Confocal Laser Scanning Microscope. An argon/krypton laser of 488 nm and a helium/neon laser of 633 nm were used. Their emitted fluorescences (detected at 516 nm for the ER-Tracker™ Green probe and 673 nm for SiPcGlu) were captured. (A) The bright field image of HT29 cells. (B) The confocal fluorescence image of SiPcGlu (red) and ER-Tracker™ Green probe (green). (C) The fluorescence line intensity profiles of HT29 cells double-stained with SiPcGlu (dotted line) and ER-Tracker™ Green probe (solid line). The line indicates the analyzed longitudinal transcellular zone.

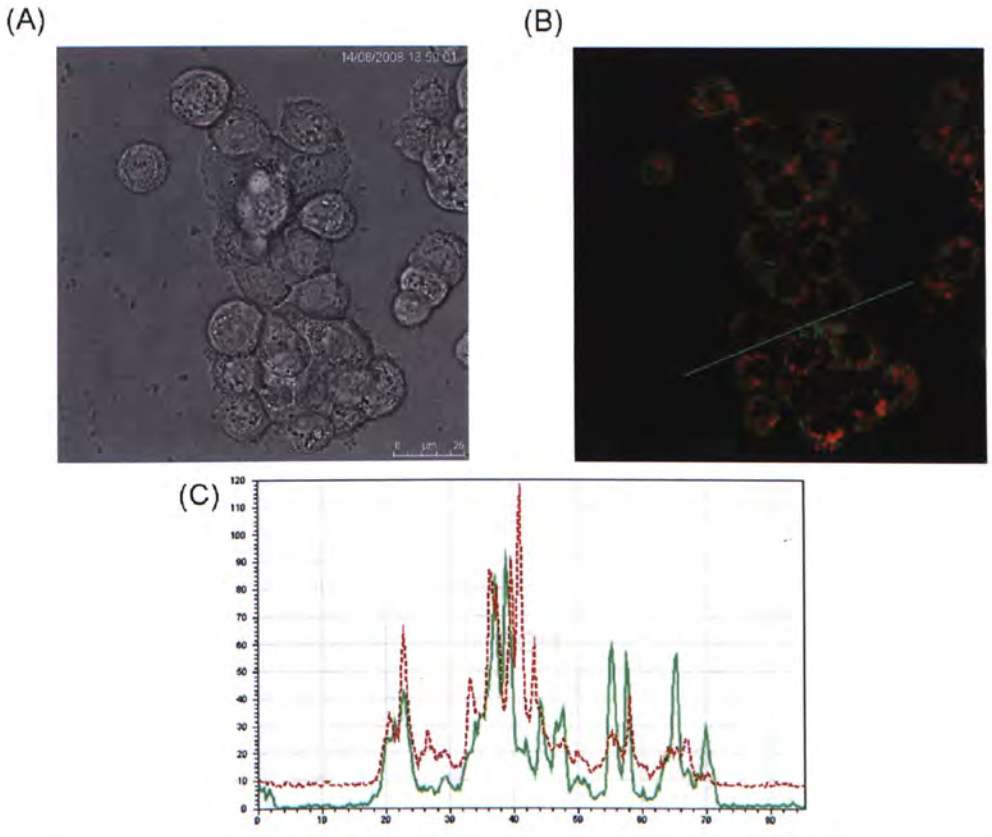

Figure 3.14 Subcellular localization of SiPcGlu in HT29 cells (mitochondria). The cells were incubated with 0.5 μM SiPcGlu for 90 min and then with MitoTracker Green probe for another 30 min. The cells were visualized with a Leica SP5 Confocal Laser Scanning Microscope. An argon/krypton laser of 488 nm and a helium/neon laser of 633 nm were used. Their emitted fluorescences (detected at 516 nm for the MitoTracker Green probe and 673 nm for SiPcGlu) were captured. (A) The bright field image of HT29 cells. (B) The confocal fluorescence image of SiPcGlu (red) and MitoTracker Green probe (green). (C) The fluorescence line intensity profiles of HT29 cells double-stained with SiPcGlu (dotted line) and MitoTracker Green probe (solid line). The line indicates the analyzed longitudinal transcellular zone.

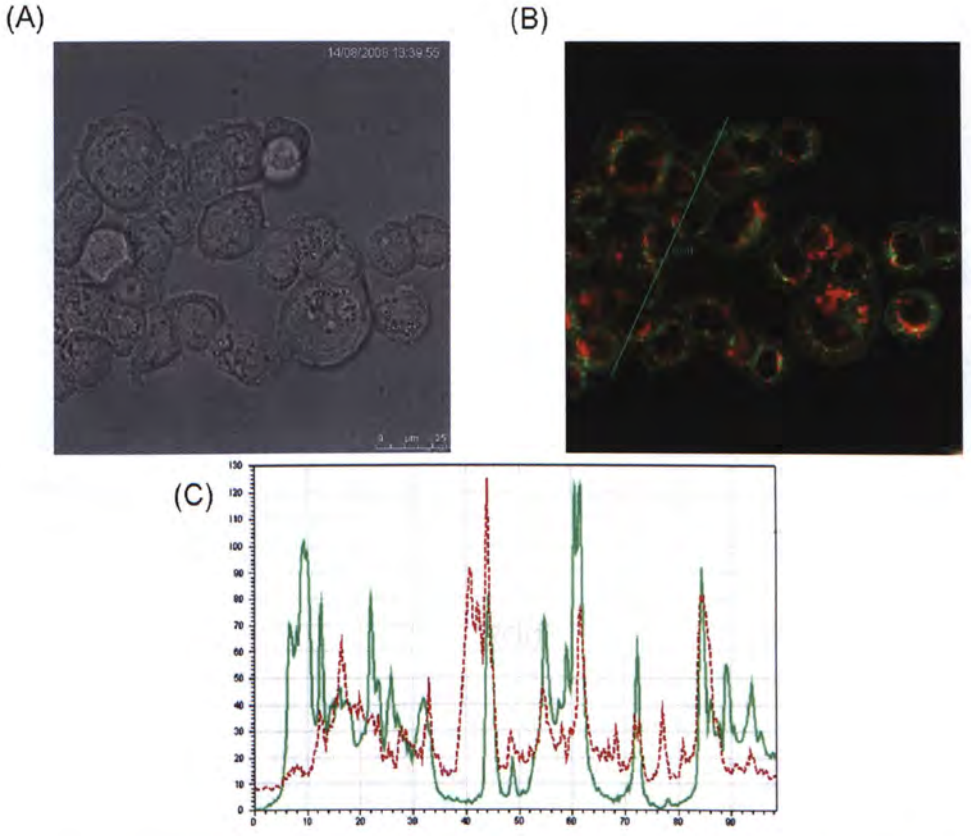

Figure 3.15 Subcellular localization of SiPcGlu in HT29 cells (Golgi body). The cells were incubated with 0.5 μM SiPcGlu for 90 min and then with BODIPY® FL C5-ceramide for another 30 min. The cells were visualized with a Leica SP5 Confocal Laser Scanning Microscope. An argon/krypton laser of 488 nm and a helium/neon laser of 633 nm were used. Their emitted fluorescences (detected at 516 nm for the BODIPY® FL C5-ceramide and 673 nm for SiPcGlu) were captured. (A) The bright field image of HT29 cells. (B) The confocal fluorescence image of SiPcGlu (red) and BODIPY® FL C5-ceramide (green). (C) The fluorescence line intensity profiles of HT29 cells double-stained with SiPcGlu (dotted line) and BODIPY® FL C5-ceramide (solid line). The line indicates the analyzed longitudinal transcellular zone.

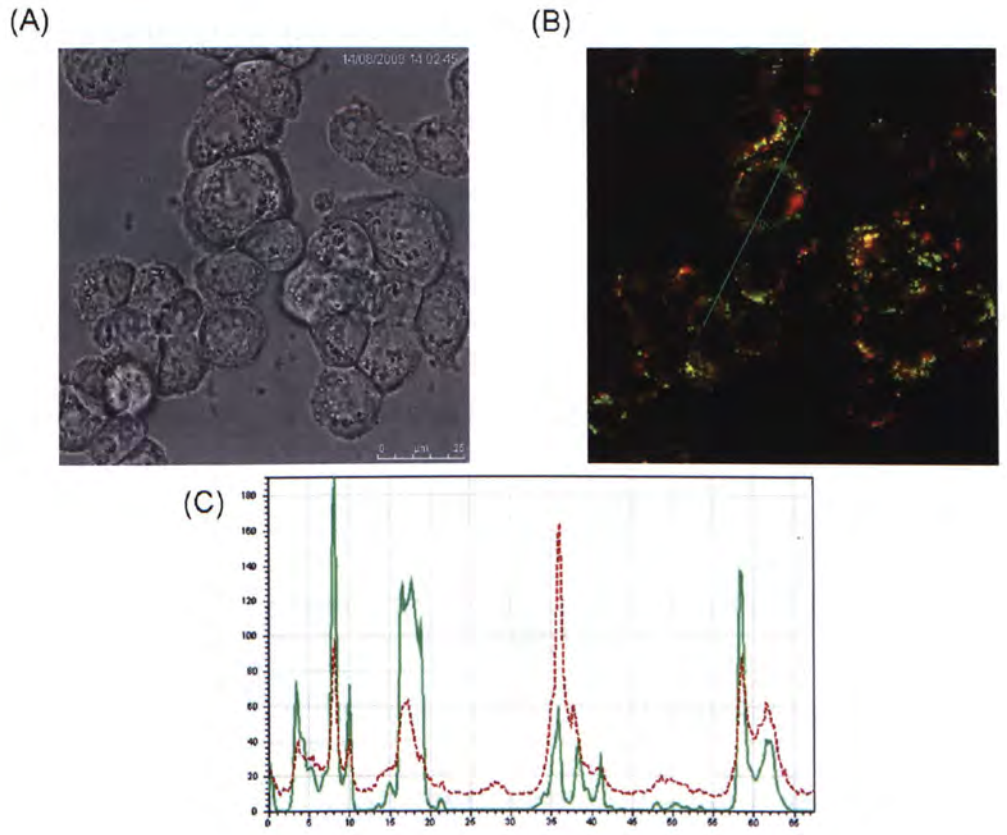

Figure 3.16 Subcellular localization of SiPcGlu in HT29 cells (lysosome). The cells were incubated with 0.5 μM SiPcGlu for 90 min and then with LysoTracker® Green probe for another 30 min. The cells were visualized with a Leica SP5 Confocal Laser Scanning Microscope. An argon/krypton laser of 488 nm and a helium/neon laser of 633 nm were used. Their emitted fluorescences (detected at 516 nm for the LysoTracker® Green probe and 673 nm for SiPcGlu) were captured. (A) The bright field image of HT29 cells. (B) The confocal fluorescence image of SiPcGlu (red) and LysoTracker® Green probe (green). (C) The fluorescence line intensity profiles of HT29 cells double-stained with SiPcGlu (dotted line) and LysoTracker® Green probe (solid line). The line indicates the analyzed longitudinal transcellular zone.

3.1.9 SiPcGlu-PDT induced mitochondrial changes

Since mitochondria is one of the primary photodamage sites by SiPcGlu-PDT, JC-1 staining assay was performed to determine whether mitochondrial membrane potential was collapsed, which could be indicated by the decrease in ratio of JC-1 red fluorescence to JC-1 green fluorescence. Figure 3.17 shows that immediately after SiPcGlu-PDT, there was a decrease in the red to green fluorescence ratio, which means that immediate collapse of mitochondrial membrane potential happened in a dose-dependent manner [12.53 ± 2.54% and 41.96 ± 11.88% of HT29 cells had their mitochondrial membranes depolarized after treatment with 6 nM and 12 nM SiPcGlu-PDT, respectively when compared with the control cells (~5%)].

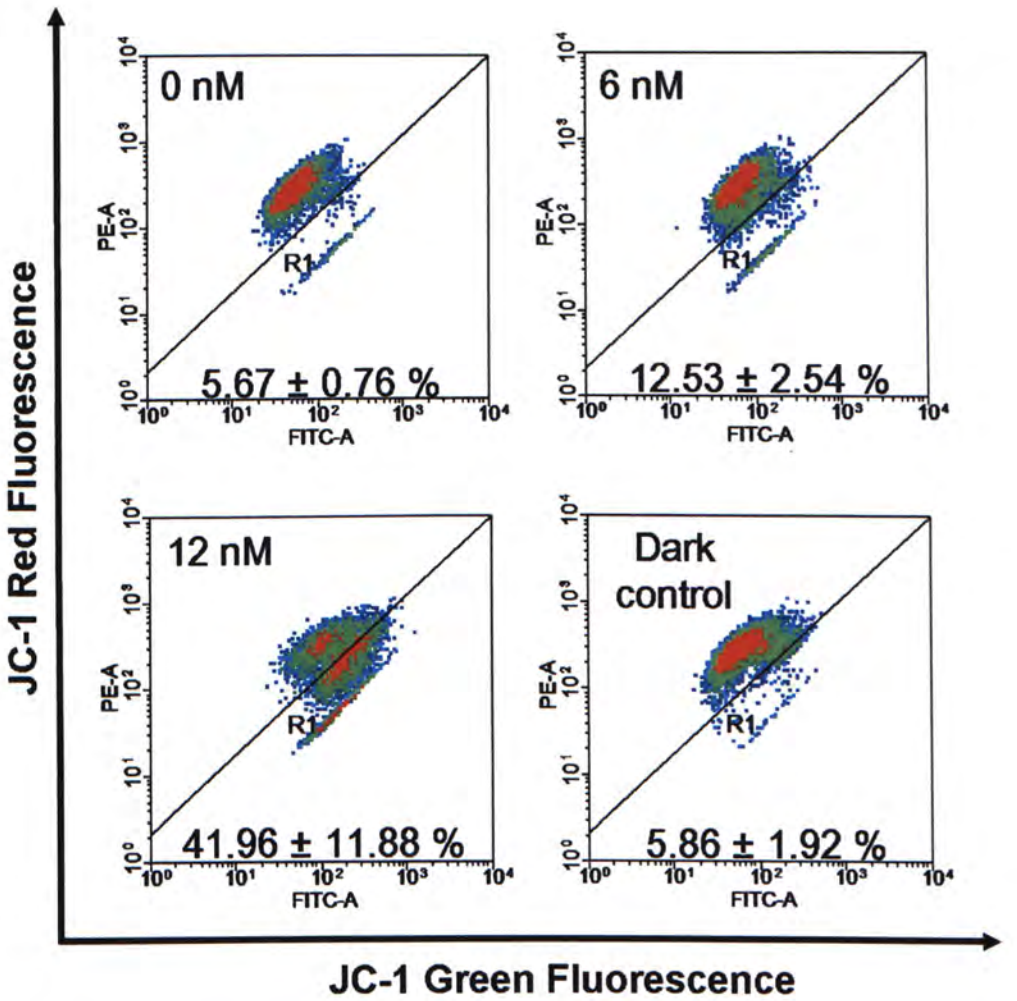

Figure 3.17 SiPcGlu-PDT-induced mitochondrial membrane depolarization. The cells were treated with different concentrations of SiPcGlu. After illumination, the cells were stained with JC-1 solution. The dark control refers to cells treated with 12 nM SiPcGlu without illumination. The emitted fluorescences were detected by the PE vs FITC channels of the BD FACSCanto™ flow cytometer. The percentage of cells with decrease in the red to green fluorescence ratio is shown. The pattern shown is a representative from three independent experiments while the data are Mean ± S.D. from 3 independent experiments.

3.1.10 SiPcGlu-PDT induced caspase activation

Release of cytochrome c and the activation of caspases were investigated after mitochondrial membrane depolarization. The cytosolic fractions of HT29 cells were extracted after treatment with SiPcGlu-PDT. Figure 3.18 shows that there was a significant increase in cytochrome c protein level in cytosol of HT29 cells treated with 12nM SiPcGlu-PDT in a time-dependent manner. Since cytochrome c can trigger the formation of apoptosome and activate the caspase cascade, caspase-3 activity assay was performed to see whether cleavage of fluorogenic substrate Ac-DEVD-AMC into fluorescent AMC by active caspase-3 occurred. Figure 3.19 shows that there is a significant increase in the fluorescence intensity after treatment with SiPcGlu-PDT which indicates that active caspase-3 was present. Another evidence of caspase-3 activation was illustrated by the Western blot analysis. After treatment with 9 nM or 12 nM SiPcGlu-PDT, there was a decrease in the protein expression of procaspase-3 while that of active caspase-3 increased (Figure 3.20). The activation of caspase-3 in photosensitized cells leads to the cleavage of a number of cellular proteins which eventually leads to apoptosis. In the present study, the cleavage of PARP, a DNA repair enzyme, was studied. Figure 3.20 shows that after treatment with 9 nM and 12 nM SiPcGlu-PDT, the protein level of intact PARP was decreased while that of cleaved PARP was elevated, which subsequently leads to DNA fragmentation and apoptosis.

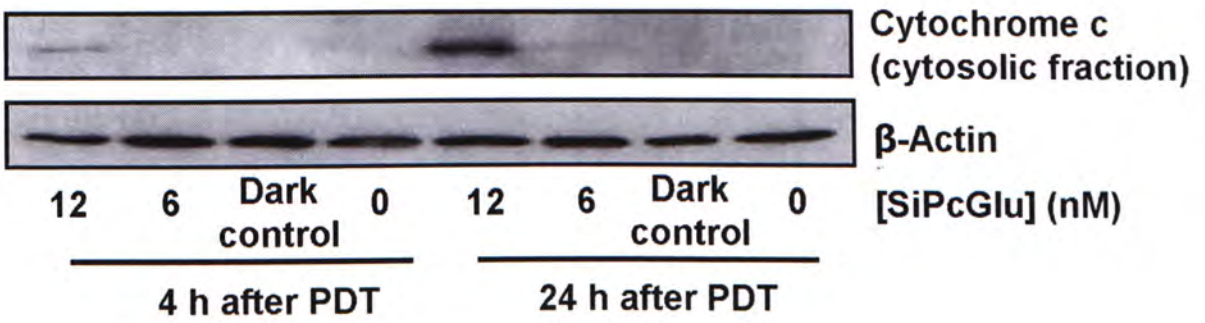

Figure 3.18 SiPcGlu-PDT-induced release of cytochrome c to cytosol in HT29 cells. The cells were treated with different concentrations of SiPcGlu. Four and twenty-four h after illumination, the cytosolic fraction of HT29 cells was obtained by the Cytosol/Particulate Rapid Separation Kit. SDS-polyacrylamide gel electrophoresis was carried out, followed by Western blot analysis. The dark control refers to cells treated with 12 nM SiPcGlu without illumination. The pattern shown is a representative from three independent experiments.

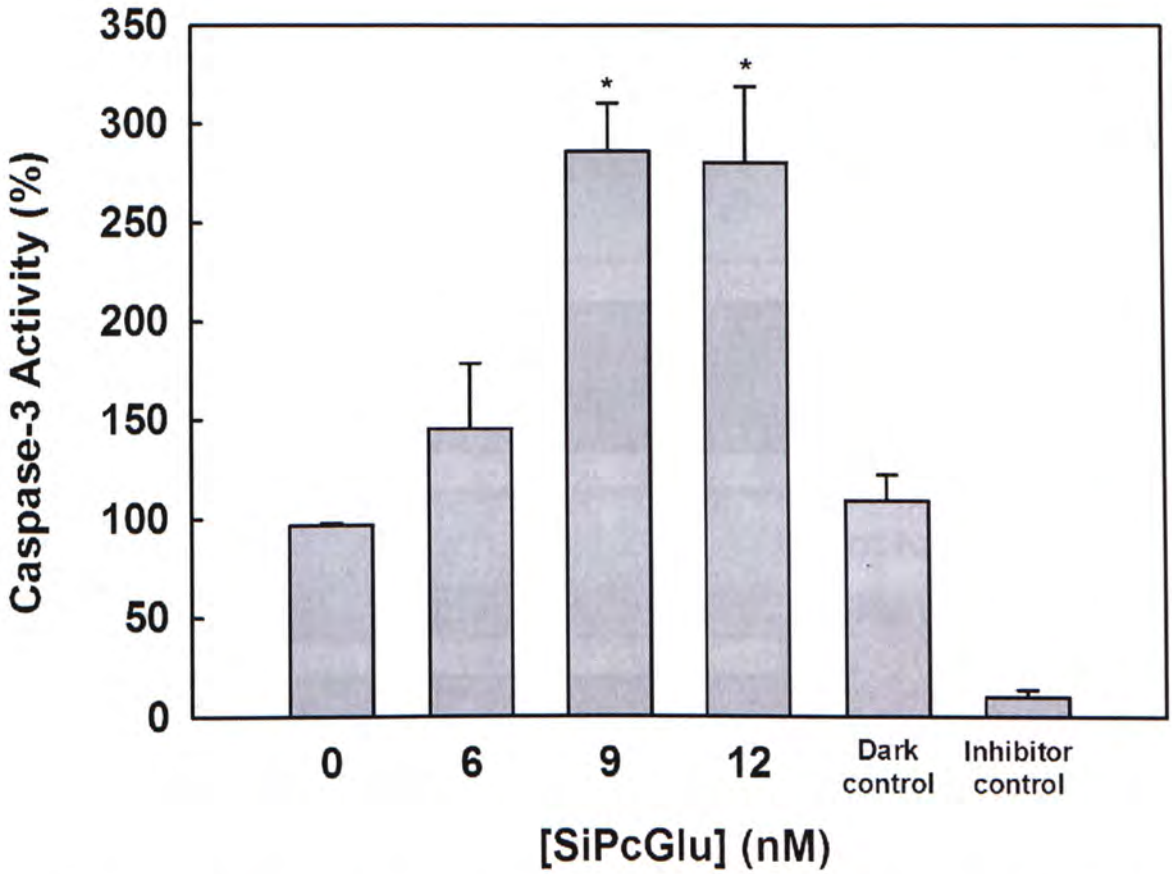

Figure 3.19 SiPcGlu-PDT-induced caspase-3 activation in HT29 cells (fluorogenic substrate). The cells were treated with different concentrations of SiPcGlu. Twenty-four h after illumination, the caspase-3 activity was determined by using caspase-3 assay kit. The amount of fluorescent product AMC liberated from the substrate Ac-DEVD-AMC by active caspase-3 was measured by a spectrofluorometer with excitation and emission wavelengths of 380 nm and 440 nm, respectively. The dark control refers to cells treated with 12 nM SiPcGlu without illumination, while the inhibitor control refers to cells treated with 12 nM SiPcGlu-PDT in the presence of Ac-DEVD-CHO, a synthetic tetrapeptide inhibitor of caspase-3 activity.The data represent Mean ± S.E.M. from three independent experiments, * $p < 0.05$ (Student's t-test) when compared with the light control (0 nM SiPcGlu).

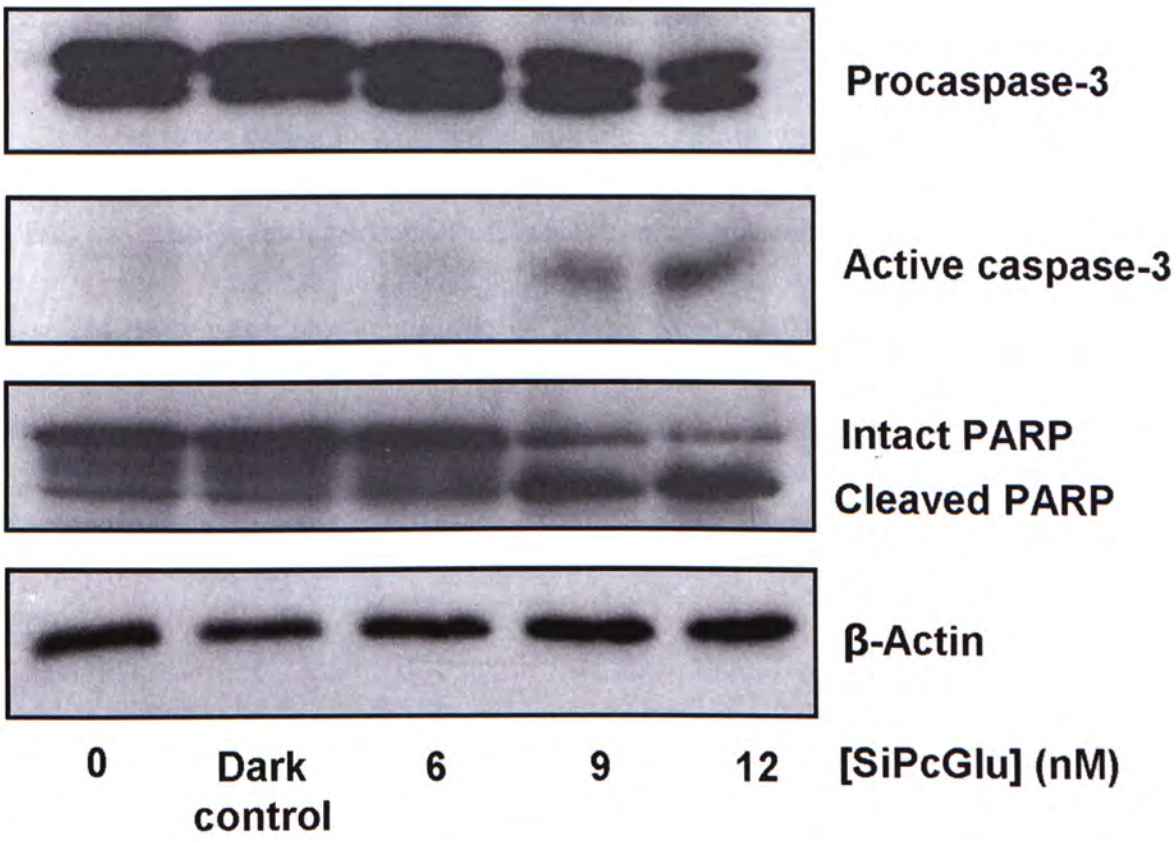

Figure 3.20 SiPcGlu-PDT-induced caspase-3 activation in HT29 cells (Western blot analysis). The cells were treated with different concentrations of SiPcGlu. Twenty-four h after illumination, whole cell lysate of HT29 cells was obtained. SDS-polyacrylamide gel electrophoresis was carried out, followed by Western blot analysis. The dark controls were cells treated with 12 nM SiPcGlu without illumination. The pattern shown is a representative from three independent experiments.

3.1.11 SiPcGlu-PDT increased expression of ER chaperone GRP78

Due to the partial localization of SiPcGlu in ER, the involvement of ER in SiPcGlu-PDT was also investigated. GRP78, an ER stress-induced molecular chaperone, was assessed by Western blot analysis at 24 h after SiPcGlu-PDT. For all the SiPcGlu-PDT treated cells, there was an abrupt elevation in the GRP78 protein level when compared with the control cells (Figure 3.21), which may suggest that ER stress was induced by SiPcGlu-PDT.

3.1.12 SiPcGlu-PDT induced release of Ca^{2+} from ER

As ER is a major Ca^{2+} store, ER stress may trigger the release of Ca^{2+} into cytosol which may initiate apoptosis. The cytosolic Ca^{2+} level was investigated using the Fluo-3, AM probe. Figure 3.22 shows a dose-dependent increase in Fluo-3 FITC intensity which indicates that the cytosolic Ca^{2+} level increased after treatment with SiPcGlu-PDT. The results may suggest that the elevation in cytosolic Ca^{2+}, probably from ER Ca^{2+} stores, may initiate apoptosis in HT29 after SiPcGlu-PDT.

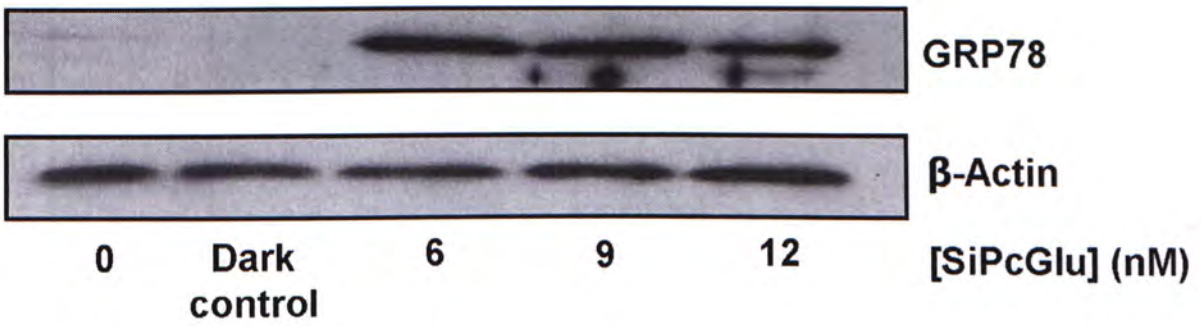

Figure 3.21 SiPcGlu-PDT-induced elevation of GRP78 expression in HT29 cells. The cells were treated with different concentrations of SiPcGlu. Twenty-four h after illumination, whole cell lysate of HT29 cells were obtained. SDS-polyacrylamide gel electrophoresis was carried out, followed by Western blot analysis. The dark control refers to cells treated with 12 nM SiPcGlu without illumination. The pattern shown is a representative from three independent experiments.

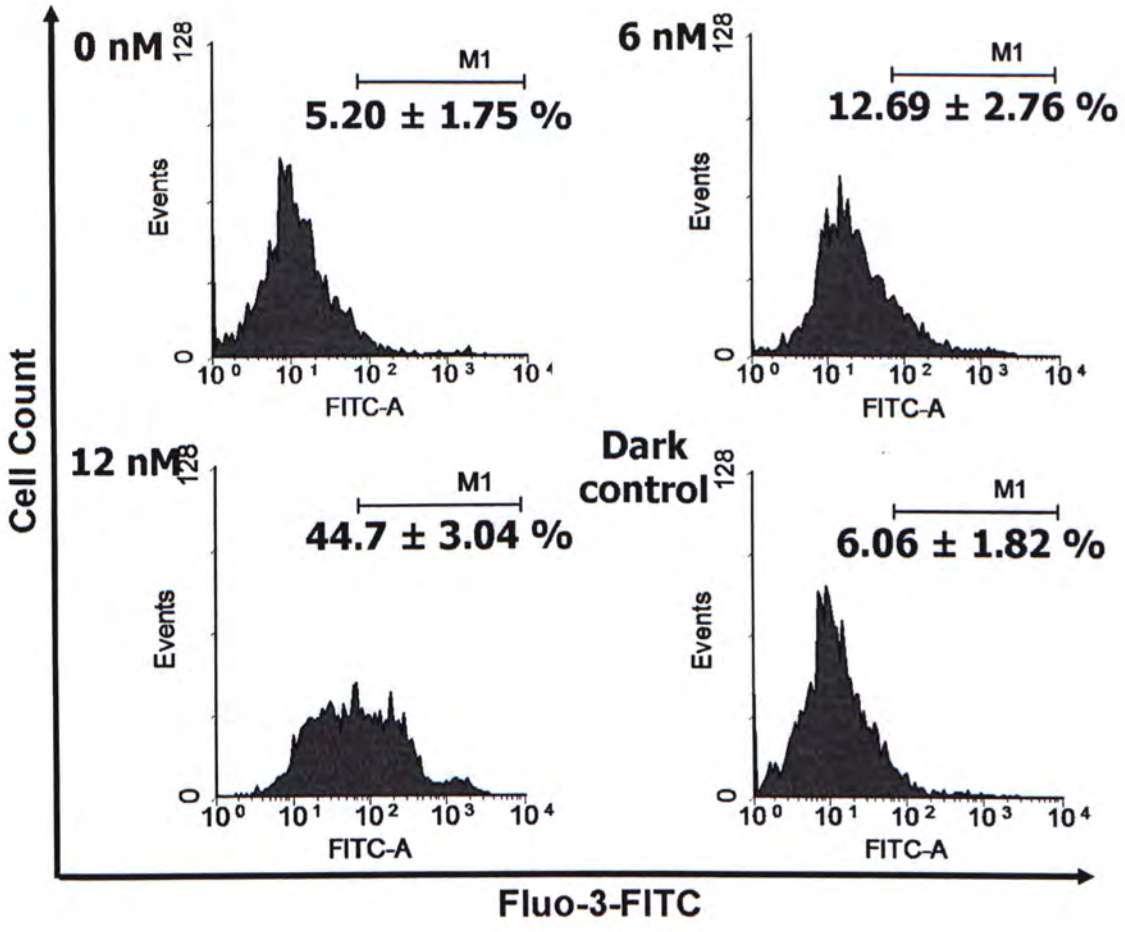

Figure 3.22 SiPcGlu-PDT-induced release of Ca^{2+} from ER into cytosol. The cells were treated with different concentrations of SiPcGlu. After illumination, the cells were stained with Fluo-3, AM probe. The emitted fluorescence due to Ca^{2+} release from ER was detected by the FITC channel of the BD FACSCanto™ flow cytometer. The dark control refers to cells treated with 12 nM SiPcGlu without illumination. The pattern shown is a representative from three independent experiments while the data are Mean ± S.D. from 3 independent experiments.

3.2 *In vivo* studies

3.2.1 *In vivo* photodynamic activities

To evaluate whether SiPcGlu has the potential to reach clinical studies, animal experimentation was done by using a HT29 tumor-bearing nude mice model. Before SiPcGlu-PDT, tumor cells were injected subcutaneously into the mice and the volumes of the tumor grown at the back of the nude mice were ranged from 51 to 117 mm^3 on day 8. The tumor volumes of different groups on day 8 were taken as 100%. On day 9, SiPcGlu was injected intravenously into the tail vein and laser was spotted onto the tumor after 24 h. After SiPcGlu-PDT, for the control groups, the tumor grew normally and reached 4-fold increase on day 25. On the contrary, for mice treated with 1 μmole SiPcGlu per kg body weight, the tumor growth was significantly retarded on day 13. From then on, the tumor volume remained more or less the same and only reached 1.7 fold increase on day 25 (Figure 3.23). In most cases, oedema of the tumor appeared immediately after irradiation and generally disappeared in the following days. Scars were present at 24 h after irradiation which normally persisted for about a week and recovered at the end of the experimental period.

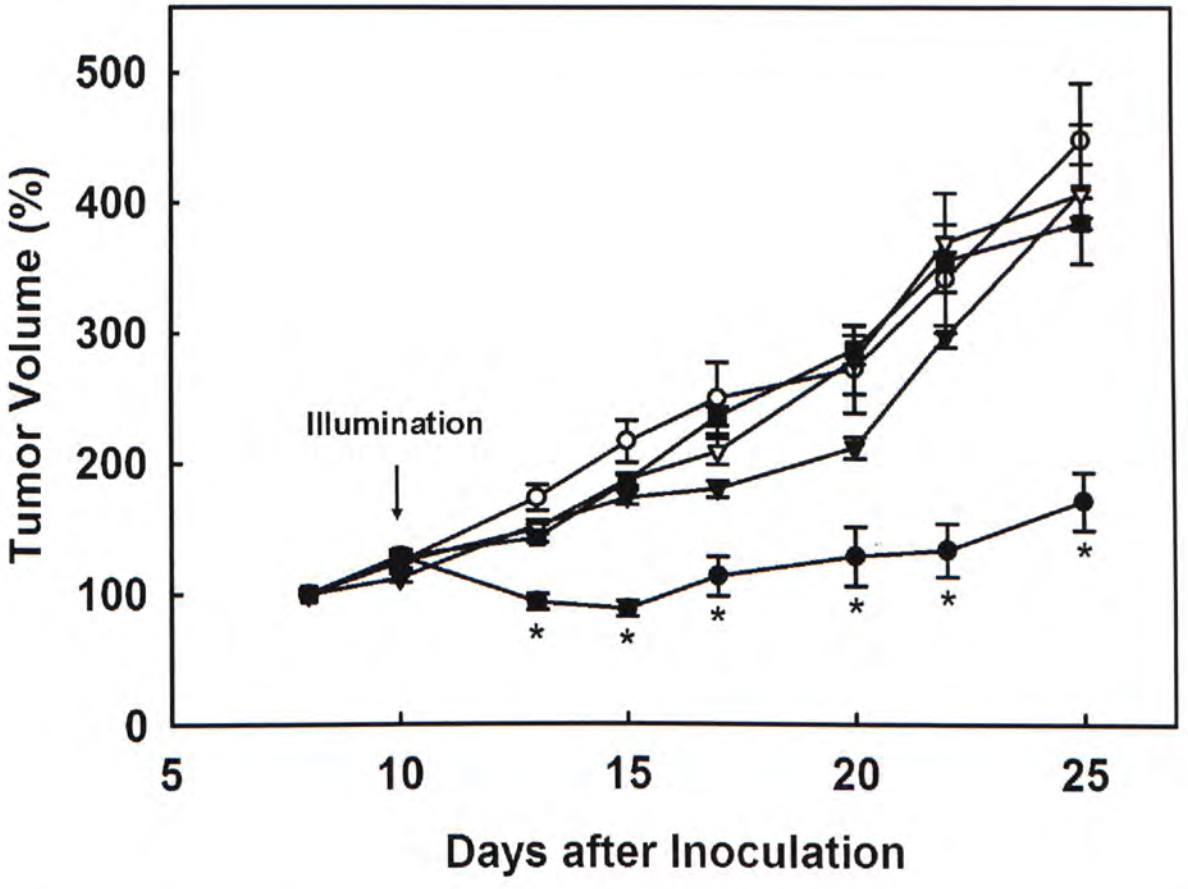

Figure 3.23 SiPcGlu-PDT-induced tumor growth retardation on the HT29 tumor-bearing nude mice. SiPcGlu was intravenously injected into the tail vein of the mice and the tumors were illuminated at 24 h with a diode laser (30 J/cm^2). The tumor volumes were followed for 25 days. The five groups of mice included SiPcGlu-PDT-treated (1 μmole/kg body weight, ●), dark control (with SiPcGlu, without illumination, ▽), light alone control (without SiPcGlu, with illumination, ▼), solvent control (with illumination, ○) and no treatment control (without SiPcGlu and illumination, ■). The data are Mean ± S.E.M. (n = 6 for each group of mice). * $p < 0.05$ (One-way ANOVA with Holm-Sidak method) when the PDT-treated group was compared with all the four control groups.

3.2.2 Biodistribution of SiPcGlu

In the hope that the glucose moieties of SiPcGlu may promote photosensitizer uptake by the tumor through the GLUTS, which are over-expressed in tumor cells, biodistribution study of SiPcGlu was performed in the tumor-bearing nude mice. The greatest retention of SiPcGlu was found in skin, kidney and tissues of the reticulo-endothelial system, viz. liver and spleen. For muscle and lung, there was only a relatively small portion of SiPcGlu accumulated, which was similar to the pharmacokinetic profile of tumor (Figure 3.24).

3.2.3 Analysis of intrinsic toxicity

In order to evaluate the safety use of SiPcGlu for clinical application, a preliminary intrinsic toxicity analysis of SiPcGlu, particularly in liver, was evaluated. ALT and AST were used to evaluate whether hepatic injury was induced. The increase in their plasma levels will suggest the presence of liver damage. CK was also used to evaluate whether cardiac injury was induced and any increase in its level suggests the presence of heart damage. The plasma of nude mice was obtained 15 days after PDT. The enzyme activities of ALT, AST and CK of plasma were evaluated and their levels in SiPcGlu-PDT treated mice were similar to all the control groups (Figure 3.25), suggesting that there was no significant acute hepatic or cardiac injuries induced by SiPcGlu.

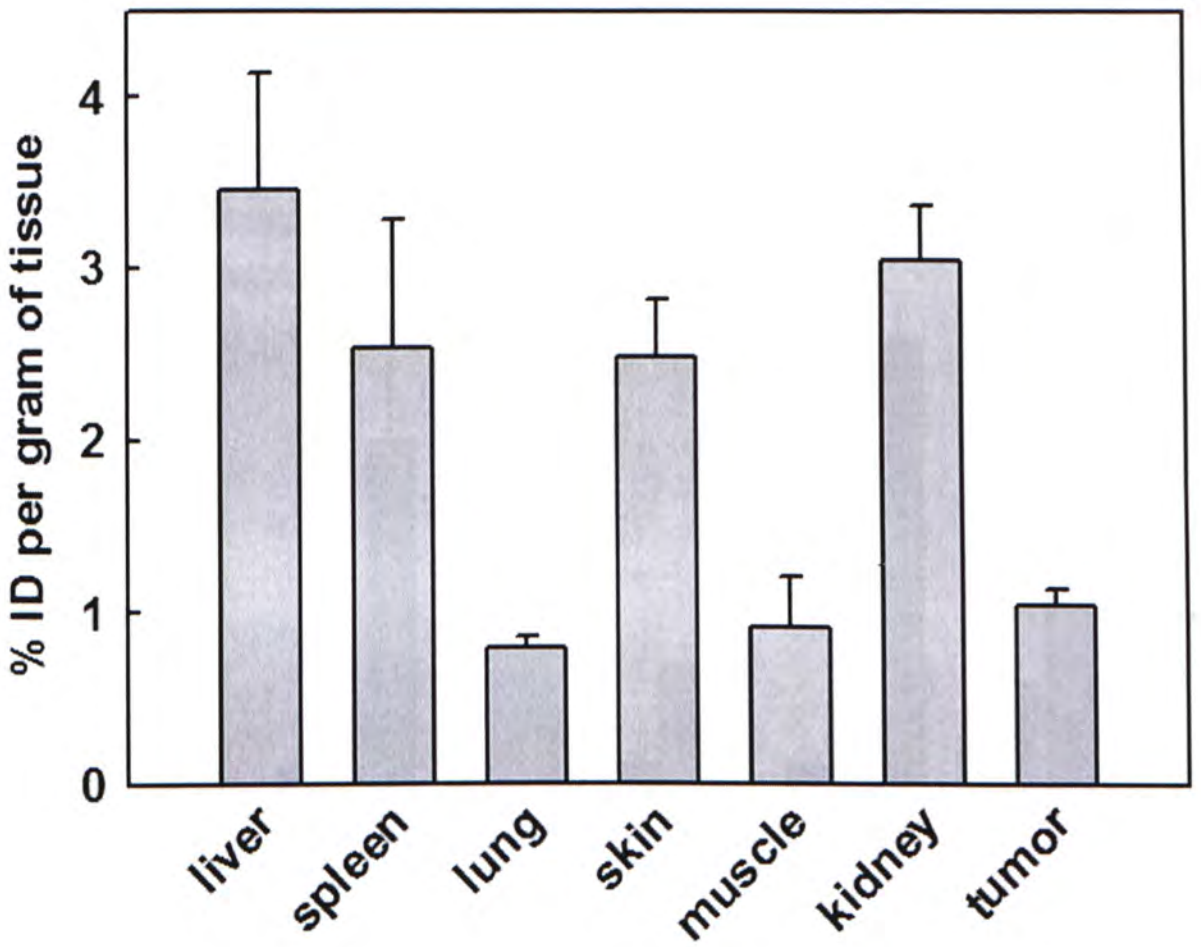

Figure 3.24 Tissue distribution of SiPcGlu in HT29 tumor-bearing nude mice. SiPcGlu was injected intravenously into the tail vein of the HT29 tumor-bearing nude mice. After 24 h, different organs/tissues were excised and homogenized with DMF. The peak fluorescence intensity of the extract was recorded by scanning the fluorescence emission spectrum from 610 nm to 900 nm using an excitation wavelength at 608 nm with a spectrofluorometer. Amount of SiPcGlu present in the sample was determined with reference to the standard curves of different organs/tissues. % ID per gram of tissue was calculated. Data are the Mean ± S.E.M., n = 6.

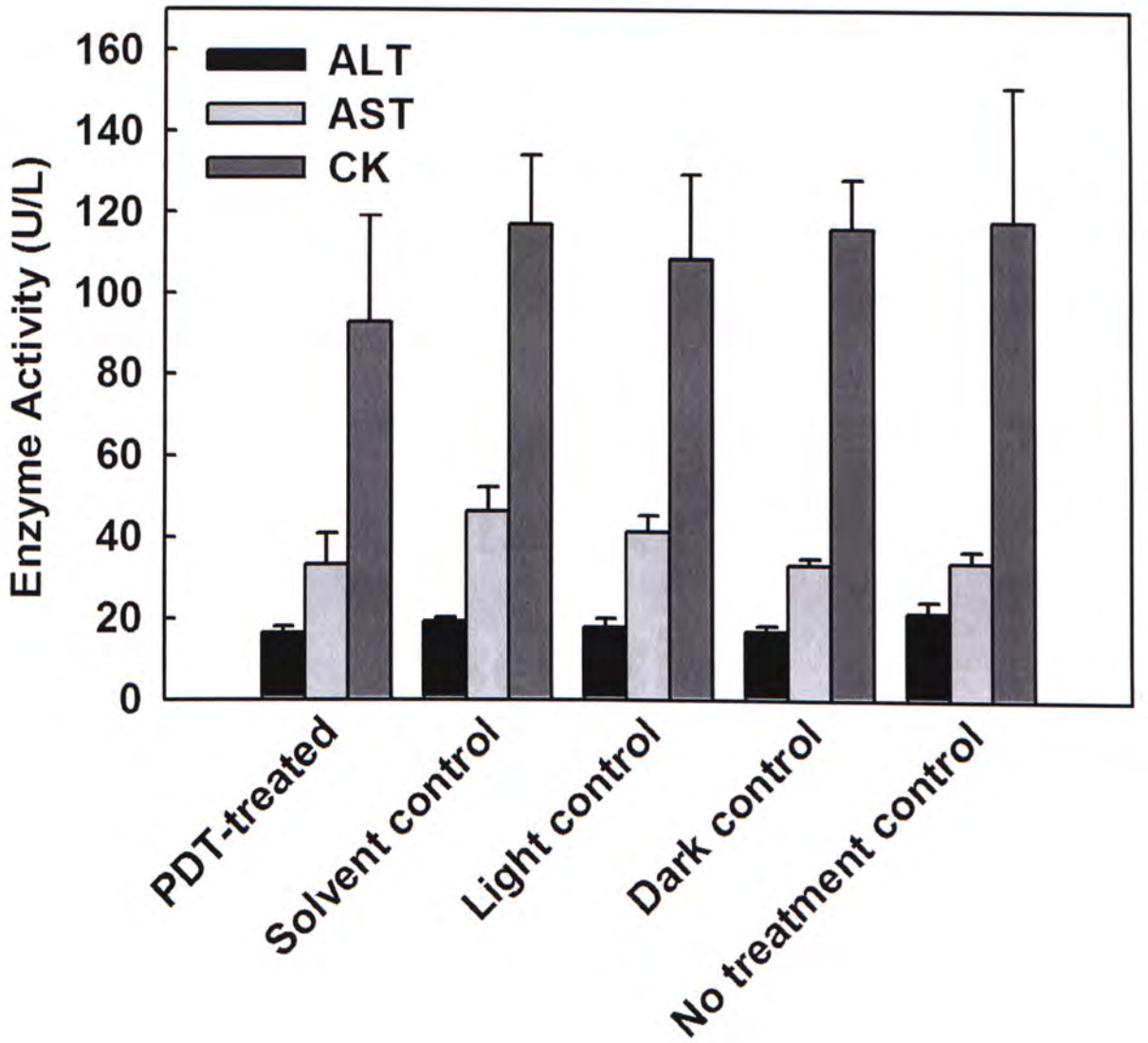

Figure 3.25 Plasma enzyme activity assay. Plasma samples were obtained by cardiac puncture of mice at 15 days after SiPcGlu-PDT. The five groups of mice included SiPcGlu-PDT-treated (1 μmole/kg body weight), dark control, light control, solvent control and no treatment control. The ALT, AST and CK activities were determined by using commercially available enzyme assay kits. Data represent Mean ± S.E.M., n = 6.

Chapter 4
Discussion

In recent years, PDT has emerged as a promising therapy for treatment of malignant and non-malignant diseases. Due to the drawbacks of the most commonly prescribed photosensitizer Photofrin®, ongoing research has been conducted to develop potential photosensitizers for cancer treatment. In our laboratory we have synthesized a number of glycosylated silicon(IV) and zinc(II) phthalocyanines (Choi et al., 2008; Liu et al., 2009; Lo et al., 2008). Most of them possess desirable physical properties and potent photodynamic activities. Among them the SiPcGlu is the most potent one (Figure 1.7, IC_{50} is 6 nM against HT29 and HepG2) (Lo et al., 2007). To further investigate whether SiPcGlu has the potential for clinical applications in cancer treatment, both *in vitro* and *in vivo* studies were performed.

4.1 Physical Properties of SiPcGlu

Conjugating photosensitizers with saccharides such as glucose and galactose can prevent their aggregation, increase water solubility and biological efficacy (Maillard et al., 1989). Our laboratory has previously described the preparation of silicon(IV) phthalocyanine conjugated to galactose via axial coordination and found that these compounds are highly soluble in most organic solvents and remain essentially non-aggregated in solution. Moreover, these compounds show an improvement in cellular uptake and enhanced photocytotoxicities against HepG2 (Lee et al., 2005). We have

employed glucose as an axial ligand to silicon(IV) phthalocyanine. It was hoped that this biocompatible moiety can enhance water solubility, minimize self-aggregation and thus potentiate photocytotoxicity of silicon(IV) phthalocyanine. SiPcGlu is soluble in organic solvents and exhibits substantial solubility in water. It is noteworthy that the original silicon(IV) phthalocyanine is completely insoluble in water and even in many organic solvents, therefore the protected glucose can greatly enhance the hydrophilicity of SiPcGlu and also the uptake of drug into the cells, which may explain its high photocytotoxicity against both HepG2 and HT29 cells. Moreover, the electronic absorption spectra of SiPcGlu in DMF or culture medium show an intense and sharp Q-band at 673 nm (Lo et al., 2007). This strong absorption peak in the far-red region of the visible spectra can ensure deeper penetration of light into the skin and thus trigger photoreaction more efficiently (Lane, 2003).

4.2 *In vitro* studies

4.2.1 SiPcGlu-PDT exhibits a high potency in killing HT29 cells

SiPcGlu is highly potent against HT29 with the IC_{50} and IC_{90} values down to 6 (7.8 ng/ml) and 12 nM respectively under the illumination of halogen lamp of 48 J/cm^2 (Lo et al., 2007). To compare the photocytotoxicity with the commonly prescribed photosensitizer Photofrin®, the same experimental setup was used and the IC_{50} of Photofrin® in killing

HT29 was ~5 μg/ml, which is much less potent than SiPcGlu. The cytotoxicity of SiPcGlu without irradiation was investigated to determine whether it is essentially non-toxic in darkness. Results of MTT assay reveals that SiPcGlu alone do not produce any cytotoxicity (Figures 3.1 and 3.2).

The absorption peak of SiPcGlu is 673 nm (Lo et al., 2007). For the light source that we used (Halogen lamp, $\lambda > 610$ nm), only a narrow region of the light (at ca. 610-700) was absorbed by SiPcGlu to initiate the photodynamic action. Therefore the total energy required to produce the cytotoxicity effect should be much lower. In order to study the actual amount of light dose required for SiPcGlu-PDT, the cells were illuminated with a monochromatic diode laser which can generate light with wavelength (675 ± 3 nm) very close to the excitation maxima of SiPcGlu. Figure 3.3 shows that a total fluence of 8 J/cm^2 (power = 0.2 W, time = 40 s) is sufficient to attain a similar effect.

4.2.2 ROS production is responsible for the cytotoxicity effect of SiPcGlu

It is well-known that ROS generated by PDT via Type I or Type II photoreaction is the main cause of cell death. In both reactions, different types of ROS are produced. Superoxides, hydroperoxyl, radicals and peroxides are formed in Type I photoreaction while singlet oxygen (the most damaging ROS) are formed in Type II photoreaction

(Calzavara-Pinton et al., 2007; Triesscheijn et al., 2006). In order to study the action mechanism of SiPcGlu-PDT, we have employed the fluorescent probe DCFDA to investigate whether ROS was produced during PDT. DCFDA can only be deacetylated by intracellular esterase to 2',7'-dichlorofluorescein (DCF) which is then oxidized by ROS to give the characteristic fluorescence. Figure 3.4 shows that photodynamic treatment with SiPcGlu induced a dose-dependent increase in ROS production. Therefore, it is believed that ROS is produced during SiPcGlu-PDT. To elucidate whether ROS is the cause of cell death by SiPcGlu-PDT, the cell survival and ROS production curves were compared. The dose-dependent curve for the survival of HT29 correlates well with the ROS production curve. Hence it is believed that the photodynamic treatment results in the production of ROS which then triggers the process to cell death.

Type I and Type II photoreactions can occur simultaneously, and the ratio between these two processes depends on the sensitizer, substrate and oxygen concentration (Jakus et al., 2005). It has been generally accepted that the Type II reaction predominates in oxygenated systems while the Type I reaction prevails under hypoxic conditions (Baumler et al., 1999; Chan and Wu, 2004; Ding et al., 2004). In order to investigate whether Type I or Type II photoreactions are the predominant mechanism of action, a quencher of hydroxyl radical, D-mannitol and quenchers of singlet oxygen, L-histidine or vitamin C were used. Chan and Wu (2004) reported that the apoptotic effects caused by Rose Bengal-PDT can be

blocked by singlet oxygen scavangers L-histidine and α-tocopherol, but not by hydroxyl radical scavenger D-mannitol, indicating that singlet oxygen (Type II photoreaction) is responsible for photocytotoxicity. On the other hand, Ding et al. (2004) reported that the singlet oxygen quencher sodium azide or the hydroxyl radical scavenger D-mannitol could protect HeLa cells from apoptosis and necrosis induced by hematoporphyrin monomethyl ether (HMME)-PDT, showing that hydroxyl radical (Type I photoreaction) and singlet oxygen (Type II photoreaction) play a decisive role in HMME-PDT-induced HeLa cells death. Figure 3.5 shows that both the hydroxyl radical scavenger D-mannitol, and the singlet oxygen quenchers L-histidine and vitamin C could slightly inhibit the HT29 cells from photodamage by SiPcGlu-PDT. These results suggest that ROS initiates cell death of HT29 and it is believed that both hydroxyl radical and singlet oxygen are involved, via Type I and Type II photoreactions.

4.2.3 SiPcGlu-PDT induced apoptosis in HT29 cells

Apoptosis is an ATP-requiring process which is morphologically characterized by cell shrinkage, plasma membrane blebbing, formation of apoptotic bodies with membrane integrity and cleavage of chromosomal DNA into internucleosomal fragments. *In vivo*, the apoptotic bodies are scavenged by phagocytes, inflammation is prevented and cells die under "immunological control" (Buytaert et al., 2007). At the biochemical level, apoptosis

may recruit the activation of caspases which are endopeptidases that employ cysteine at the active site and cleave their targets at aspartic acid residues (Leist and Jaattela, 2001). All caspases are synthesized as proenzymes or zymogens and are activated in response to the apoptotic signals by proximity-induced dimerization at a multimeric protein complex (initiator caspases) or by limited proteolysis by upstream caspases (effector caspases) (Boatright and Salvesen, 2003; Luthi and Martin, 2007). Proteolytic cleavage of cellular substrates by the effector caspases determines the features of apoptotic cell death.

After SiPcGlu-PDT, HT29 cells underwent apoptosis as evidenced by three assays. The first evidence is the presence of TUNEL positive cells. After PDT, the cells were incubated with the TUNEL reaction mixture containing terminal deoxynucleotidyl transferase (TdT) and FITC-dUTP. TdT can catalyze the attachment of FITC-dUTP to free 3'OH ends of the DNA breaks in dead cells. Figure 3.10 shows that upon SiPcGlu-PDT, there was an elevation of FITC fluorescence intensity due to increase in the number of TUNEL-positive cells. However DNA breaks caused by necrosis can also be stained by TUNEL assay. To avoid ambiguity, DNA fragmentation, a hallmark of apoptosis, was studied by gel electrophoretic analysis. DNA ladder pattern shown in Figure 3.11 clearly reveals the presence of nucleosomal DNA fragmentation after SiPcGlu-PDT. Another hallmark of apoptosis is the externalization of phosphotidylserine into the leaflet of the plasma membrane with no DNA leakage, which can be observed by simultaneous staining

of annexin V & propidium iodide. The flow cytometric analysis of both fluorescence signals indicates that the cells undergo apoptosis after SiPcGlu-PDT, as evidenced by the increase in cell populations having annexin V binding and no significant change in propidium iodide staining (Figure 3.12).

4.2.4 SiPcGlu is localized in various membranous organelles

The subcellular localization of the photosensitizers is of special importance, since it determines the primary site of photodamage which triggers different types of cell death. Singlet oxygen is very short-lived and can only damage biomolecules in their close proximity. The cellular structures having both a high photosensitizer and a high oxygen concentration will preferentially be damaged. The important structural features of photosensitizers are (a) the net ionic charge, (b) the degree of hydrophobicity expressed as the logarithm of the octanol/water partition coefficient, (c) the degree of asymmetry present in the molecule. Different structural features of photosensitizers will lead to different subcellular localization. Many hydrophobic photosensitizers localize in mitochondria or membranous organelles and exert their primary damage there (Moor, 2000). They can be specifically localized in one organelle or non-specifically in several organelles. Our previous study has shown that the unsymmetrical BAM-SiPc is localized in the mitochondria specifically (Lo et al., 2004). Noodt et al. (1999) reported that the

hydrophobic tetra(3-hydroxyphenyl)porphyrin (3THPP) is localized in intracellular membranes of Chinese hamster lung fibroblasts (V79) cells. Silicon phthalocyanine also exhibits a preferential localization in mitochondria, Golgi body and endoplasmic reticulum of epidermoid carcinoma (A431) cells (Lam et al., 2001). These mitochondria-localized photosensitizers can trigger cell death via apoptosis after photoactivation. On the other hand, photosensitizers which are hydrophilic in nature tend to localize in lysosome by endocytosis or distributed homogenously throughout the cytoplasm and nucleoplasm. One example of hydrophilic photosensitizer is tetraphenylporphyrin which can be taken up into lysosomes by endocytosis in V79 cells (Noodt et al., 1993). Lysosome-localized photosensitizers can trigger cell death via necrosis or apoptosis. Photosensitizers can also be localized on the plasma membrane. Hsieh et al. (2003) revealed that plasma membrane of A431 cells are the primary targets of Photofrin® which can cause cell death via necrosis upon photoactivation. Recent study has hypothesized that the similarity in structures of photosensitizers and cellular structures could promote the formation of preferred molecular complex. Ho et al. (2009) reported that hypericin and cholesterol molecules, which share common molecular morphology of rigid planar configuration, provided the driving force for the lipid-mediated preferential localization of hypericin in lipid membranes.

Confocal laser scanning fluorescence microscopy is usually used for the determination of intracellular localization of photosensitizers. Co-staining of subcellular

organelle-specific probes with photosensitizers of different fluorescence emission maxima can be used to identify the site of localization. In this study, confocal microscopic investigation of SiPcGlu's intracellular localization was done by co-staining with MitoTracker® Green FM, ER-Tracker™ Green, BODIPY® FL C5-ceramide or LysoTracker® Green Probes. The confocal images show that all the organelle-specific probes had a partial overlap with SiPcGlu. The fluorescence line profile also reveals that all the organelle-specific probes had similar fluorescence profiles to that of SiPcGlu, indicating that SiPcGlu localizes different intracellular organelles (Figures 3.13 to 3.16). Therefore SiPcGlu-PDT can exert its photodamage effect in different cellular compartments. The hydrophobic silicon(IV) phthalocyanine exhibits a preferential localization in mitochondria, Golgi body and ER (Lam et al., 2001). Since SiPcGlu is axially conjugated with two glucose moiety in a symmetric manner, its hydrophilicity increases which may cause its localization in lysosomes as well.

4.2.5 SiPcGlu-PDT induced mitochondrial-mediated apoptosis

ROS production after SiPcGlu-PDT was also found in HT29 cells (Figure 3.6). Such increase may be due to the damage of mitochondrial respiratory chain caused by SiPcGlu-PDT and may result in higher oxygen tension (Varnes et al., 1999). This phenomenon was termed by Zorov et al. (2000) as "ROS-induced ROS release". It was found that after

photodynamic treatment with tetramethylrhodamine derivatives, the ROS production during PDT caused abrupt mitochondrial depolarization and a burst of mitochondrial ROS generation. The mechanisms of the ROS burst is believed to be due to the damage of mitochondrial respiratory chain, especially mitochondrial Complexes I and III which are the major sources of ROS. The induction of mitochondrial membrane depolarization can affect the proper function of these respiratory chains. Photodamage to these sites can cause ROS burst (Zorov et al., 2000).

In this study, it was found that SiPcGlu was partially localized in mitochondria, investigations were done to see whether SiPcGlu-PDT could affect the mitochondrial membrane depolarization by JC-1 staining. JC-1 exhibits potential-dependent accumulation in mitochondria, indicated by a fluorescence emission shift from green to red. When mitochondrial depolarization occurs, the red/green fluorescence intensity ratio will be decreased. Figure 3.17 shows that immediately after SiPcGlu-PDT, there was an increase in cell populations having red/green fluorescence ratio decreased, suggesting that HT29 cells undergo mitochondrial membrane depolarization after SiPcGlu-PDT.

We speculated that ROS insults to mitochondria by SiPcGlu-PDT may also induce ROS production by mitochondria to trigger apoptosis. MitoSOX^{TM} Red mitochondrial superoxide indicator was developed for selective detection of superoxide in the mitochondria of live cells. SiPcGlu-PDT caused immediate generation of ROS from

mitochondria in a dose-dependent manner, as demonstrated by the flow cytometric analysis of MitoSOX^{TM} Red at 30 min post irradiation (Figure 3.7). In addition, the confocal microscopic imaging reveals that there was a significant increase in mitochondrial fluorescence intensity of MitoSOX^{TM} Red after PDT (Figure 3.8), demonstrating that SiPcGlu-PDT induces mitochondrial ROS production. However, it is noteworthy that nuclear and cytosolic staining by MitoSOX^{TM} Red could also be observed. The reason for nuclear staining is that MitoSOX^{TM} Red can bind to DNA following oxidation while cytosolic staining may be due to the oxidation of MitoSOX^{TM} Red during its transport from cell membrane to mitochondria. However, this level of cytosolic oxidized MitoSOX^{TM} Red is much less when compared with the fluorescence detected in mitochondria (Mukhopadhyay et al., 2007)

Many hydrophobic photosensitizers are localized in mitochondria and elicit rapid mitochondria-mediated apoptosis after PDT. Moreover, for photosensitizers which localize in other intracellular organelles such as endoplasmic reticulum, lysosomes or Golgi body, photodamage may also be propagated to mitochondria by various means. Foscan®, a photosensitizer localized in ER and Golgi body, can result in mitochondrial depolarization and cytochrome c release in a fluence-dependent manner, after its photosensitization in human breast adenocarcinoma (MCF-7) cells (Teiten et al., 2003). Previous study has also reported that a lysosomal photosensitizer N-aspartyl chlorin e6 (NPe6) caused

mitochondrial membrane depolarization, cytochrome c release and triggered mitochondria-mediated apoptosis, through the release of lysosomal protease and Bid activation to trigger the mitochondrial alternations (Reiners et al., 2002).

Primary photodynamic damage by SiPcGlu-PDT to mitochondria causes immediate opening of the permeability transition pore complex and release of cytochrome c into the cytosol (Figure 3.18), which is the hallmark of mitochondria-mediated apoptosis. It is well-known that in the cytosol, cytochrome c can bind to apoptotic protease activating factor 1 (Apaf-1) and in the presence of dATP or ATP, Apaf-1 adopts a conformation to enhance its ability to associate with procaspase-9, which promotes the cleavage of procaspase-9 into active caspase-9 to cleave and activate procaspase-3 (Nunez et al., 1998; Porter and Janicke, 1999). Caspase-3 is a key player in executing apoptosis. It cleaves a number of proteins which are involved in cell structure and maintenance including DNA fragmentation factor and PARP. PARP is a DNA repair enzyme which acts by transferring ADP-ribose polymers to histones and other nuclear proteins. The cleavage of PARP will disrupt its function and may unleash endonuclease activity within dying cells and promote DNA fragmentation (Nicholson et al., 1995). In PDT, the cleavage of PARP has largely been documented. The photoactivated hypericin can induce cleavage of PARP under apoptotic conditions in cervical carcinoma (HeLa) cells (Vantieghem et al., 1998). For photodynamic treatment with the photosensitizer benzoporphyrin derivative monoacid ring A, activation of caspase-

3 and 6, as well as the cleavage of PARP were also found (Granville et al., 1999). In this study, it was found that the release of cytochrome c after SiPcGlu-PDT leads to the activation of caspase-3 and the cleavage of PARP, which results in DNA fragmentation (Figures 3.19 and 3.20).

4.2.6 SiPcGlu-PDT induced ER stress

Since SiPcGlu also localizes partially in ER, further studies were done to investigate the role of ER in triggering apoptosis by SiPcGlu-PDT. ER is the first compartment in an ordered membranous network called secretory pathway, which is responsible for the synthesis, modification and delivery of biologically active proteins to their proper target sites within the cells and the extracellular milieu, as well as regulation of intracellular Ca^{2+} levels. ER is important for the proper folding of protein. If the amount of unfolded polypeptides exceeds the folding and processing capacity of the ER, the normal physiological state of the ER is perturbed and this will cause ER stress. Under these conditions, unfolded protein response (UPR) is activated. UPR can increase the folding capacity of the ER through induction of ER-resident molecular chaperones and foldases, or downregulate the biosynthetic load of the ER through shut-off of protein synthesis at both transcriptional and translational levels. However, when these mechanisms do not remedy the excessive stress, apoptosis is initiated in higher eukaryotic organisms to eliminate

unhealthy or infected cells. (Mattson et al., 2000; Schroder and Kaufman, 2005; Sherman and Goldberg, 2001). During PDT, oxidative damage to ER can result in dramatic changes in ER homeostasis, which proceeds through disruption of Ca^{2+} homeostasis and accumulation of misfolded proteins (Buytaert et al., 2006; Kessel et al., 2005; Mak et al., 2004). Marchal et al. (2007) had reported that photoactivation by the ER-localized photosensitizer Foscan® in MCF-7 cells exhibited upregulation of GRP78 protein, which is a chaperone protein known to be induced by the UPR, thus assuming a classic ER oxidative stress response following PDT. Since SiPcGlu also localizes in ER, it is believed that SiPcGlu-PDT can also induce oxidative stress to ER. We studied the protein expression of GRP78 and its elevation may suggest that a classic ER stress response can be induced following SiPcGlu-PDT (Figure 3.21).

The role of ER in triggering apoptosis by SiPcGlu-PDT was also studied. ER is a major Ca^{2+} store. Induction of the molecular chaperones helps to control intracellular Ca^{2+} homeostasis (Mak et al., 2004). A possible reason for the depletion of Ca^{2+} from ER stores may be related to sarco/endoplasmic reticulum Ca^{2+} ATPase ($SERCA_2$) degradation. $SERCA_2$ is located on the ER membrane and pumps cytosolic Ca^{2+} into ER to maintain Ca^{2+} homeostasis within the cells. $SERCA_2$ is highly sensitive to PDT which eventually leads to release of Ca^{2+} from ER. Previous studies have shown that both the hypericin and verteporfin-mediated PDT could immediately cause photodamage of $SERCA_2$ pump and

deplete ER-Ca^{2+} stores into cytosol, committing cells to death (Buytaert et al., 2006; Granville et al., 2001). Endonucleases in many model systems were found to be dependent on Ca^{2+} for internucleosomal cleavage of DNA. Therefore, it was suggested that increased Ca^{2+} may be necessary to allow nuclease activity. Other types of Ca^{2+}-dependent enzymes such as the neutral protease calpains are also implicated in apoptosis, which can activate subsequent caspase cascade and trigger apoptosis (Nakagawa and Yuan, 2000; Tan et al., 2006). The role of Ca^{2+} in triggering apoptosis was also previously studied by the use of an ER stress reagent. The Ca^{2+}-ATPase inhibitor thapsigargin, which depleted intracellular Ca^{2+} stores, induced large increase in cytosolic Ca^{2+} concentration and caused apoptosis in mouse T lymphoma (S49) cells (Bian et al., 1997). To study whether Ca^{2+} is released from ER to cytosol, Fluo-3 Ca^{2+} indicator was used. Upon binding to Ca^{2+}, Fluo-3 will exhibit large increase in fluorescence intensity. By analyzing the fluorescence intensity with flow cytometry, the cytosolic Ca^{2+} level in HT29 cells can be determined. Figure 3.22 shows that there is a dose-dependent increase in the Fluo-3 FITC intensity, which implies that there was an increase in the cytosolic Ca^{2+} level. This result indicates that the elevation of cytosolic Ca^{2+}, probably from ER Ca^{2+} stores, may initiate apoptosis in HT29 after SiPcGlu-PDT.

4.3 *In vivo* studies

4.3.1 SiPcGlu failed to target to tumor tissues

In the *in vitro* study we have shown that SiPcGlu exhibits excellent phototoxicity towards HT29 cancer cell lines. The development of new photosensitizer for PDT is complex, and multi-step preclinical experimental tests are required. Animal experimentation is the second chronological step in preclinical investigation (Longo et al., 2009). To evaluate whether SiPcGlu has the potential to reach clinical study, we investigated the *in vivo* efficacy of SiPcGlu-PDT by using HT29 tumor-bearing nude mice. One limitation of the conventional PDT approach for cancer treatment is the lack of selectivity towards tumor tissues. Unfortunately the majority of the photosensitizers are taken up non-selectively by all cell types and consequently they can accumulate in tumor and also in normal cells. There is a need for increased selectivity of photosensitizer for tumor tissue over healthy tissue; without this specificity, PDT has limited clinical applications (Josefsen and Boyle, 2008b). Therefore, in order for PDT to reach its full potential, there is a need for various photosensitizers and numerous targeting motifs so that all cell and tissue types can be selectively destroyed.

Several approaches were used to increase photosensitizer's selectivity to tumor tissues. One approach is to conjugate a targeting component such as antibody which can be directed against the tumor antigens or conjugate an antigen which can target the receptor-

binding sites on the tumor cells. In addition, molecular carriers such as liposome or targeted nanoparticles are also being extensively used in cancer therapy because they can enhance *in vivo* drug solubility by incorporating water-insoluble photosensitizers into their hydrophobic cores (Lassalle et al., 2009; Lee et al., 2009). Nanoscale polymeric carrier-encapsulated photosensitizer has prolonged circulation time, allowing them to accumulate in tumor tissue and avoiding the reticuloendothelial system. In recent years, a variety of carbohydrate-conjugated photosensitizers have been synthesized and evaluated for PDT efficacy (Pandey et al., 2007). One of the biochemical hallmarks of malignancy is enhanced tumor glycolysis, which is primarily due to the overexpression of GLUTS and increased activity of the mitochondrial-bound hexokinase. Various groups have studied the specificity of photosensitizer-saccharide conjugates in different cell lines. Fujimoto et al. (2002) have shown that galactoconjugated-tetraphenyl porphyrins but not glycoconjugated- tetraphenyl porphyrins showed specificity for rat hepatoma RLC-16 cells which have receptors for asialoglycoproteins. Chen et al. (2004) have demonstrated higher specificity and selectivity of a tetraglucose conjugate of tetra(pentafluorophenyl)porphyrin linked by a sulfur atom towards human breast cancer cells, when compared with the corresponding tetra-galactose conjugate. Pyropheophorbide 2-deoxyglucosamide is an example of incorporating 2 deoxyglucosamine moiety to a photosensitizer and was found to be selectively accumulated

inside the tumor compared to surrounding normal tissue, via the GLUT/hexokinase pathway. This selectivity could be competitively inhibited by 50 mM D-glucose (Zhang et al., 2003).

In our study, the strategy used to increase tumor selectivity is to conjugate glucose moiety to the photosensitizer. Glycoconjugation can modify the amphiphilicity of macrocycles and favor their interaction with the surface membrane of the tumor cells. The physical properties of SiPcGlu indicated that the glucose moiety can enhance the hydrophilicity of this compound. We hope that the protected glucose moieties of SiPcGlu may promote photosensitizer uptake by the tumor through the over-expressed GLUTS. Thus *in vitro* glucose competitive assay and *in vivo* biodistribution study were performed. In the *in vitro* glucose competitive assay, since D-glucose (25 mM) is present in the culture media, PBS was used to formulate the SiPcGlu and glucose solutions. The cytotoxicity was determined by MTT assay (Figure 3.9). The cell survival curves in the presence and absence of glucose are virtually identical and this result suggests that GLUT may not be involved in the uptake of SiPcGlu. To further verify whether the glucose moiety can enhance the uptake of SiPcGlu into the tumor, SiPcGlu was injected intravenouesly into the tail vein of the mice and its biodistributions in different organs /tissues were evaluated. SiPcGlu retained in different organs/tissues was extracted by homogenizing the tissues with DMF and quantified by spectrofluorometer excited at 673 nm, which is the absorption maximum wavelength of SiPcGlu. A significant accumulation of SiPcGlu was observed in various

organs such as lungs, muscle, spleen, skin, kidneys and especially liver, which exhibited the highest accumulation of SiPcGlu. Though SiPcGlu failed to specifically target to tumor tissues, a significant amount was found in tumor (Figure 3.24) which may be sufficient to inhibit tumor growth. Meanwhile, intrinsic toxicities analyses were done to investigate whether its highest accumulation in liver may pose hepatic damage to the nude mice.

4.3.2 SiPcGlu-PDT induced retardation in tumor growth

The efficacy of a photosensitizer depends on many critical parameters which include the molar absorption coefficient of the compound at the therapeutic window. It has been shown that wavelengths above 600 nm provide a more effective light penetration into the tissue since absorption and scattering of light by human tissue is less extensive in these circumstances (Delaey et al., 2003). SiPcGlu has a maximum absorption peak at 673 nm. In the *in vivo* study of SiPcGlu-PDT, we injected SiPcGlu into the tail vein of the nude mice and administered a single dose of irradiation at 24 h, which was delivered by an optic fiber onto the tumor. Four controls were done, namely (1) solvent control with irradiation, (2) light control, (3) SiPcGlu dark control and (4) no treatment control. The light source used in this study was a monochromatic laser, with a total fluence of 30 J/cm^2. With the use of an optic fibre, only a small area (~ 1 cm^2) could be illuminated, so that the illumination of healthy tissues could be minimized.

In the SiPcGlu-PDT treated groups, oedema of tumors appeared immediately after PDT, followed by significant inhibition of tumor growth in the following weeks when compared with the 4 control groups. The tumor volume only increased by 1.7 fold, which was significantly lower when compared with the control groups (4-fold increase). SiPcGlu alone, solvent with irradiation or light alone did not exert any cytotoxicity to the tumor cells. Inhibition in tumor growth was resulted when a combination of drug and light were applied onto the tumor (Figure 3.23). Direct photodamage can cause reduction in the number of clonogenic tumor cells. In our study, complete tumor eradication cannot be accomplished. The result is in accordance with the findings of other groups working on the HT29 tumor model. For example, tumor eradication cannot be fully achieved with the treatment of 30 mg/kg Photofrin® or 5 mg/kg diphenylchlorin photosensitizer of body weight (Bourre et al., 2003; Hajri et al., 2002). This observation could be attributed to the non-homogenous distribution of photosensitizer within the tumor or oxygen depletion since rapid and substantial reduction in the tissue oxygen tension appears during PDT (Chin et al., 2004; Dolmans et al., 2003). In addition, efficacy of PDT is limited by penetration of light into tissue (5-8 mm). Therefore the tumor beyond the penetration distance cannot be destroyed. It was believed that the presence of the remnant viable and uninjured tumor cells at their base was responsible for the delayed reappearance of tumor growth in PDT-treated mice (Hajri et al., 2002). However, in terms of therapeutic efficacy, it is believed that SiPcGlu is

a more potent one, in terms of photosensitizer and light dose, when compared with the commonly prescribed photosensitizers.

4.3.3 SiPcGlu is a safe photosensitizer for clinical PDT

Though SiPcGlu is a potent photosensitizer in inhibiting tumor growth, its high accumulation in liver is a major concern of safety in use. Therefore, whether SiPcGlu-PDT can cause intrinsic toxicity to the animal should be addressed before any clinical application. In this study, some preliminary intrinsic toxicity analyses were performed, especially those concerning hepatic injury due to its high accumulation in liver. It has been reported that hepatic injury was resulted with high dosage treatment of $ZnPcP_2S_2$ on Wistar rat (Zhang et al., 2006). Hepatic injury on Syrian golden hamster was also found when treated with verteporfin combined with high light dose (Ayaru et al., 2007). Plasma determinations were adopted to evaluate the levels of aspartate aminotransferase and alanine aminotransferase (AST and ALT), which are the biochemical markers of hepatic injury, as well as creatine kinase (CK), which is the biochemical marker of cardiac injury. These enzymes are predominantly present inside the cells. When hepatic or cardiac injuries are present, the levels of these enzymes in plasma will be elevated. After SiPcGlu-PDT, plasma of nude mice was obtained by intra-cardiac puncture and used for the enzyme activity assays. Figure 3.25 shows that the plasma levels of AST, ALT and CK were basically the same for the

different groups of mice, suggesting that the treatment does not cause any major hepatic and cardiac injuries to the nude mice. This preliminary toxicity test shows that SiPcGlu is a safe photosensitizer for clinical applications.

Chapter 5
Conclusion and Future Perspectives

5.1 Conclusion

SiPcGlu exhibits excellent physical properties as a photosensitizer, including its good water solubility, minimal self-aggregation and absorption maximum at 673 nm. In this study we have further evaluated the *in vitro* and *in vivo* efficacy of SiPcGlu-PDT in killing HT29 human colorectal adenocarcinoma. In the *in vitro* cytotoxicity assay we have shown that SiPcGlu is highly cytotoxic to HT29 in a dose-dependent manner with IC_{50} and IC_{90} as low as 6 nM and 20 nM respectively. *In vivo* tumor regression study has also revealed that SiPcGlu is effective in inhibiting tumor growth in the HT29 tumor-bearing nude mice model, as compared with the most conventionally prescribed photosensitizer Photofrin®. This compound does not cause toxicity in darkness, both *in vitro* and *in vivo*. We have also shown that its cytotoxic effects may be attributed to the production of ROS, as demonstrated by the correlation of cell survival and ROS production. Both hydroxyl radical and singlet oxygen may be involved in killing HT29 by SiPcGlu-PDT.

Similar to the action mechanism of most photosensitizers, the increased ROS production in SiPcGlu-PDT-treated cells leads to cell death via the apoptotic pathway, as evidenced by the presence of TUNEL positive cells, DNA ladder electrophoretic pattern and externalization of PS with no significant DNA leakage.

Subcellular localization studies show that SiPcGlu can be found in mitochondria, ER, Golgi body and lysosomes. It was found that both mitochondria and ER participate in

triggering apoptosis. A classical mitochondrial intrinsic pathway is triggered by SiPcGlu-PDT. SiPcGlu-PDT can cause immediate production of mitochondrial ROS and collapse of mitochondrial potential, followed by release of cytochrome c and caspase-3 activation to cleave PARP and result in DNA fragmentation. SiPcGlu-PDT can also cause ER oxidative stress response in HT29, as evidenced by the elevation of ER chaperone protein and the depletion of Ca^{2+} from ER store.

Although the glucose moiety of SiPcGlu is not able to target the photosensitizer to tumor tissue in HT29-tumor-bearing nude mice, this drug is potent enough in inhibiting tumor growth in nude mice. Despite the high accumulation of SiPcGlu in liver, the plasma enzyme activity assays of AST and ALT at the end of the experiment show that this drug does not cause hepatic injury. It also does not cause cardiac injury, as shown by the CK activity assay.

This study has demonstrated that SiPcGlu is an effective photosensitizer in treating HT29 cell lines and the preliminary animal study also shows that it is potent in inhibiting tumor growth in nude mice. However, its biodistribution problem highlights the need for further development of tumor-specific photosensitizer targeting for more effective PDT and new applications for photosensitizers.

5.2 Future Perspectives

In the future work regarding the study of SiPcGlu-PDT, more in-depth *in vitro* and *in vivo* studies should be done to comprehensively evaluate its potential to reach clinical application.

5.2.1 *In vitro* study

5.2.1.1 Lysosomal pathway to cell death

The accumulation of SiPcGlu in lysosomes may trigger a different cell death pathway. Some photosensitizers localize in lysosome and upon illumination they can cause cell death via two different routes, (1) via the release of lysosomal protease cathepsins in cytosol to trigger cytotoxicity or (2) via relocalization of the photosensitizer after illumination to other non-lysosomal targets (Moor, 2000). ATX-S10(Na) was found to be localized in mitochondria and lysosomes. Pharmacological inhibitions of lysosomal protease cathepsins, such as cathepsin B and D, could protect cells from apoptosis (Ichinose et al., 2006). In the future, further investigation on the role of lysosome in triggering cell death may be addressed.

5.2.2 *In vivo* studies

5.2.2.1 Pharmacokinetic studies

In this study, the laser irradiation was done at 24 h after SiPcGlu injection. However, in order to have a better understanding on the pharmacokinetics of this compound, the ratio of SiPcGlu in tumor to different organs, especially skin, at different time intervals could also be evaluated for best tumor response. Bourre et al. (2003) reported that 2,3-dihydro-5,15-di(3,5-dihydroxyphenyl)porphyrin (SIM01) exhibited the highest retention in tumor between 6 to 12 h post injection and the optimal PDT response occurred during this time interval. Lassalle et al. (2009) also reported that after administration of liposomal formulations of meta-tetra(hydroxyphenyl)chlorine (mTHPC) to the EMT6 mouse mammary carcinoma xenografted nude mice, the highest tumor to muscle ratios were observed at 6 and 15 h post injection, and the best tumor response was also obtained during this interval. These studies indicates that the higher the tumor/tissue ratio, the better the therapeutic outcome and less cytotoxic effects to healthy tissue. In addition the clearance rate should also be investigated to study whether SiPcGlu can be cleared from the body rapidly.

5.2.2.2 Eradication of HT29 tumor by repeated dose of SiPcGlu

Efficacy of PDT is limited by penetration of light into tissue (5-8 mm), so PDT can only be used for small lesions. Since PDT is a minimally invasive treatment and does not appear to succumb to multi-drug resistance and has no known cumulative dose ceiling as radiation and chemotherapy do, thus patients can be treated repeatedly as needed. Clinically, for the dosage and administration of photofrin®, a repeated light illumination can be applied 50-70 h after the first illumination (information from the website of Photofrin®, http://www.photofrin.com/patient_prescribing_information.php?lang=1). A repeated dose of topical methyl aminolevulinate-PDT has also been given to patients with nodular basal cell carcinoma in a previous clinical trial. The treatment was effective and exhibited a favorable cosmetic outcome (Rhodes et al., 2007).

In this study only a single dose of treatment was applied to the nude mice, which may not be enough for complete eradication of the tumor, therefore a repeated dose of SiPcGlu-PDT may be applied to investigate whether complete eradication can be achieved. The evaluation for possible repeated-dose toxicity should also be accompanied.

5.2.2.3 SiPcGlu-PDT-induced anti-tumor immunity

Apoptosis or necrosis occurred after receiving PDT can provoke acute inflammatory response at the site of damage. A lot of evidence shows that the outcome of PDT is greatly

dependent on the contribution of host response. Inflammatory cytokines and chemokines can also be attributed to the immune response after PDT. T-lymphocytes can also be activated to become effector T cells, attracted by chemokines, migrate to the tumor and kill the tumor cells. Therefore, further study on the anti-tumor immunity such as studying the level of the inflammatory cytokines or chemokines in the plasma of PDT-treated BALB/c mice may provide insight on how SiPcGlu-PDT works with the immune system to trigger anti-tumor effect.

5.2.2.4 Enhancement of tumor selectivity by conjugating with biomolecules

Although the glucose moiety of SiPcGlu can enhance the drug's water solubility, it failed to achieve tumor targeting. There is a need to formulate this compound by conjugating with other biomolecules, antibodies, tumor-specific antigens or encapsulating it with molecular carriers like nanoparticles or liposomes to enhance uptake specifically into tumor and so enhance therapeutic efficacy and minimize undesirable effects for further clinical applications.

References

Agostinis, P., Buytaert, E., Breyssens, H., Hendrickx, N., 2004. Regulatory pathways in photodynamic therapy induced apoptosis. Photochem Photobiol Sci 3, 721-729.

Allen, C.M., Langlois, R., Sharman, W.M., La Madeleine, C., van Lier, J.E., 2002. Photodynamic properties of amphiphilic derivatives of aluminum tetrasulfophthalocyanine. Photochem Photobiol 76, 208-216.

Allison, R. R., Downie, G.H., Cuenca, R., Hu, X. H., Childs, C. JH., Sibata, C. H., 2004. Photosensitizers in clinical PDT. Photodiagn Photodyn Ther 1, 27-42.

Ayaru, L., Wittmann, J., Macrobert, A.J., Novelli, M., Bown, S.G., Pereira, S.P., 2007. Photodynamic therapy using verteporfin photosensitization in the pancreas and surrounding tissues in the Syrian golden hamster. Pancreatology 7, 20-27.

Barge, J., Decreau, R., Julliard, M., Hubaud, J.C., Sabatier, A.S., Grob, J.J., Verrando, P., 2004. Killing efficacy of a new silicon phthalocyanine in human melanoma cells treated with photodynamic therapy by early activation of mitochondrion-mediated apoptosis. Exp Dermatol 13, 33-44.

Baumler, W., Abels, C., Karrer, S., Weiss, T., Messmann, H., Landthaler, M., Szeimies, R.M., 1999. Photo-oxidative killing of human colonic cancer cells using indocyanine green and infrared light. Br J Cancer 80, 360-363.

Bhatti, M., Yahioglu, G., Milgrom, L.R., Garcia-Maya, M., Chester, K.A., Deonarain, M.P., 2008. Targeted photodynamic therapy with multiply-loaded recombinant antibody fragments. Int J Cancer 122, 1155-1163.

Bian, X., Hughes, F.M., Jr., Huang, Y., Cidlowski, J.A., Putney, J.W., Jr., 1997. Roles of cytoplasmic Ca^{2+} and intracellular Ca^{2+} stores in induction and suppression of apoptosis in S49 cells. Am J Physiol 272, C1241-1249.

Boatright, K.M., Salvesen, G.S., 2003. Mechanisms of caspase activation. Curr Opin Cell Biol 15, 725-731.

Bonnett, R., 1995. Photosensitizers of the porphyrin and phthalocyanine series for photodynamic therapy. Chem Soc Rev 24, 19-33.

Bourre, L., Simonneaux, G., Ferrand, Y., Thibaut, S., Lajat, Y., Patrice, T., 2003. Synthesis, and in vitro and in vivo evaluation of a diphenylchlorin sensitizer for photodynamic therapy. J Photochem Photobiol B 69, 179-192.

Brown, S.B., Brown, E.A., Walker, I., 2004. The present and future role of photodynamic therapy in cancer treatment. Lancet Oncol 5, 497-508.

Buytaert, E., Callewaert, G., Hendrickx, N., Scorrano, L., Hartmann, D., Missiaen, L., Vandenheede, J.R., Heirman, I., Grooten, J., Agostinis, P., 2006. Role of endoplasmic reticulum depletion and multidomain proapoptotic BAX and BAK

proteins in shaping cell death after hypericin-mediated photodynamic therapy. FASEB J 20, 756-758.

Buytaert, E., Dewaele, M., Agostinis, P., 2007. Molecular effectors of multiple cell death pathways initiated by photodynamic therapy. Biochim Biophys Acta 1776, 86-107.

Calzavara-Pinton, P.G., Venturini, M., Sala, R., 2005. A comprehensive overview of photodynamic therapy in the treatment of superficial fungal infections of the skin. J Photochem Photobiol B 78, 1-6.

Calzavara-Pinton, P.G., Venturini, M., Sala, R., 2007. Photodynamic therapy: update 2006. Part 1: Photochemistry and photobiology. J Eur Acad Dermatol Venereol 21, 293-302.

Castano, A. P., Demidova, T. N., Hamblin M. R., 2004. Mechanisms in photodynamic therapy: part one-photosensitizers, photochemistry and cellular localization. Photodiagnosis Photodyn Ther 1, 279-293.

Castano, A.P., Mroz, P., Hamblin, M.R., 2006. Photodynamic therapy and anti-tumour immunity. Nat Rev Cancer 6, 535-545.

Chan, W.H., Wu, H.J., 2004. Anti-apoptotic effects of curcumin on photosensitized human epidermal carcinoma A431 cells. J Cell Biochem 92, 200-212.

Chatterjee, D.K., Fong, L.S., Zhang, Y., 2008. Nanoparticles in photodynamic therapy: an emerging paradigm. Adv Drug Deliv Rev 60, 1627-1637.

Chen, X., Hui, L., Foster, D.A., Drain, C.M., 2004. Efficient synthesis and photodynamic activity of porphyrin-saccharide conjugates: targeting and incapacitating cancer cells. Biochemistry 43, 10918-10929.

Chin, W., Lau, W., Cheng, C., Olivo, M., 2004. Evaluation of Hypocrellin B in a human bladder tumor model in experimental photodynamic therapy: biodistribution, light dose and drug-light interval effects. Int J Oncol 25, 623-629.

Choi, C.F., Huang, J.D., Lo, P.C., Fong, W.P., Ng, D.K., 2008. Glycosylated zinc(II) phthalocyanines as efficient photosensitisers for photodynamic therapy. Synthesis, photophysical properties and in vitro photodynamic activity. Org Biomol Chem 6, 2173-2181.

Delaey, E., Zupko, I., Chen, B., Derycke, A., van Laar, F., De Vos, D., De Witte, P., 2003. Comparison of hexamethylhypericin and tetrabromohypericin to hypericin for their in vivo efficacy as PDT tools. Int J Oncol 23, 519-524.

Ding, X., Xu, Q., Liu, F., Zhou, P., Gu, Y., Zeng, J., An, J., Dai, W., Li, X., 2004. Hematoporphyrin monomethyl ether photodynamic damage on HeLa cells by means of reactive oxygen species production and cytosolic free calcium concentration elevation. Cancer Lett 216, 43-54.

Dolmans, D.E., Fukumura, D., Jain, R.K., 2003. Photodynamic therapy for cancer. Nat Rev Cancer 3, 380-387.

Dougherty, T.J., Grindey, G.B., Fiel, R., Weishaupt, K.R., Boyle, D.G., 1975. Photoradiation therapy. II. Cure of animal tumors with hematoporphyrin and light. J Natl Cancer Inst 55, 115-121.

Dubuc, C., Langlois, R., Benard, F., Cauchon, N., Klarskov, K., Tone, P., van Lier, J.E., 2008. Targeting gastrin-releasing peptide receptors of prostate cancer cells for photodynamic therapy with a phthalocyanine-bombesin conjugate. Bioorg Med Chem Lett 18, 2424-2427.

Fujimoto, K.; Miyata, T.; Aoyama, Y., 2000. Saccharide-directed cell recognition and molecular delivery using macrocyclic saccharide clusters: masking of hydrophobicity to enhance the saccharide specificity. J Am Chem Soc 122, 3558-3559.

Gollnick, S.O., Evans, S.S., Baumann, H., Owczarczak, B., Maier, P., Vaughan, L., Wang, W.C., Unger, E., Henderson, B.W., 2003. Role of cytokines in photodynamic therapy-induced local and systemic inflammation. Br J Cancer 88, 1772-1779.

Granville, D.J., Jiang, H., An, M.T., Levy, J.G., McManus, B.M., Hunt, D.W., 1999. Bcl-2 overexpression blocks caspase activation and downstream apoptotic events instigated by photodynamic therapy. Br J Cancer 79, 95-100.

Granville, D.J., Ruehlmann, D.O., Choy, J.C., Cassidy, B.A., Hunt, D.W., van Breemen, C., McManus, B.M., 2001. Bcl-2 increases emptying of endoplasmic reticulum Ca^{2+} stores during photodynamic therapy-induced apoptosis. Cell Calcium 30, 343-350.

Hajri, A., Wack, S., Meyer, C., Smith, M.K., Leberquier, C., Kedinger, M., Aprahamian, M., 2002. In vitro and in vivo efficacy of photofrin and pheophorbide a, a bacteriochlorin, in photodynamic therapy of colonic cancer cells. Photochem Photobiol 75, 140-148.

Ho, Y.F., Wu, M.H., Cheng, B.H., Chen, Y.W., Shih, M.C., 2009. Lipid-mediated preferential localization of hypericin in lipid membranes. Biochim Biophys Acta. 1788, 1287-1295.

Hsieh, Y.J., Wu, C.C., Chang, C.J., Yu, J.S., 2003. Subcellular localization of Photofrin determines the death phenotype of human epidermoid carcinoma A431 cells triggered by photodynamic therapy: when plasma membranes are the main targets. J Cell Physiol 194, 363-375.

Ichinose, S., Usuda, J., Hirata, T., Inoue, T., Ohtani, K., Maehara, S., Kubota, M., Imai, K., Tsunoda, Y., Kuroiwa, Y., Yamada, K., Tsutsui, H., Furukawa, K., Okunaka, T., Oleinick, N.L., Kato, H., 2006. Lysosomal cathepsin initiates apoptosis, which is regulated by photodamage to Bcl-2 at mitochondria in photodynamic therapy using a novel photosensitizer, ATX-s10 (Na). Int J Oncol 29, 349-355.

Jori, G., 2006. Photodynamic therapy of microbial infections: state of the art and perspectives. J Environ Pathol Toxicol Oncol 25, 505-519.

Josefsen, L.B., Boyle, R.W., 2008a. Photodynamic therapy and the development of metal-based photosensitisers. Met Based Drugs 2008, 276109.

Josefsen, L.B., Boyle, R.W., 2008b. Photodynamic therapy: novel third-generation photosensitizers one step closer? Br J Pharmacol 154, 1-3.

Kalka, K., Ahmad, N., Criswell, T., Boothman, D., Mukhtar, H., 2000. Up-regulation of clusterin during phthalocyanine 4 photodynamic therapy-mediated apoptosis of tumor cells and ablation of mouse skin tumors. Cancer Res 60, 5984-5987.

Kessel, D., Castelli, M., Reiners, J.J., 2005. Ruthenium red-mediated suppression of Bcl-2 loss and Ca(2+) release initiated by photodamage to the endoplasmic reticulum: scavenging of reactive oxygen species. Cell Death Differ 12, 502-511.

Kessel, D., Poretz, R.D., 2000. Sites of photodamage induced by photodynamic therapy with a chlorin e6 triacetoxymethyl ester (CAME). Photochem Photobiol 71, 94-96.

Khdair, A., Gerard, B., Handa, H., Mao, G., Shekhar, M.P., Panyam, J., 2008. Surfactant-polymer nanoparticles enhance the effectiveness of anticancer photodynamic therapy. Mol Pharm 5, 795-807.

Konopka, K., Goslinski, T., 2007. Photodynamic therapy in dentistry. J Dent Res 86, 694-707.

Korbelik, M., 2006. PDT-associated host response and its role in the therapy outcome. Lasers Surg Med 38, 500-508.

Korbelik, M., Krosl, G., Krosl, J., Dougherty, G.J., 1996. The role of host lymphoid populations in the response of mouse EMT6 tumor to photodynamic therapy. Cancer Res 56, 5647-5652.

Lam, M., Oleinick, N.L., Nieminen, A.L., 2001. Photodynamic therapy-induced apoptosis in epidermoid carcinoma cells. Reactive oxygen species and mitochondrial inner membrane permeabilization. J Biol Chem 276, 47379-47386.

Lane, N., 2003. New light on medicine. Sci Am 288, 38-45.

Lassalle, H.P., Dumas, D., Grafe, S., D'Hallewin, M.A., Guillemin, F., Bezdetnaya, L., 2009. Correlation between in vivo pharmacokinetics, intratumoral distribution and photodynamic efficiency of liposomal mTHPC. J Control Release 134, 118-124.

Lee, P. P. S., Lo, P. C., Chan, E. Y. M., Fong, W. P., Ko, W. H. and Ng, D. K. P., 2005. Synthesis and in vitro photodynamic activity of novel galactose-containing phthalocyanines. Tetrahed Lett 46, 1551-1554.

Lee, S.J., Park, K., Oh, Y.K., Kwon, S.H., Her, S., Kim, I.S., Choi, K., Kim, H., Lee, S.G., Kim, K., Kwon, I.C., 2009. Tumor specificity and therapeutic efficacy of photosensitizer-encapsulated glycol chitosan-based nanoparticles in tumor-bearing mice. Biomaterials 30, 2929-2939.

Leist, M., Jaattela, M., 2001. Four deaths and a funeral: from caspases to alternative mechanisms. Nat Rev Mol Cell Biol 2, 589-598.

Lipson, R.L., Baldes, E.J., Olsen, A.M., 1961. The use of a derivative of hematoporhyrin in tumor detection. J Natl Cancer Inst 26, 1-11.

Liu, J.Y., Lo, P.C., Fong, W.P., Ng, D.K., 2009. Effects of the number and position of the substituents on the in vitro photodynamic activities of glucosylated zinc(II) phthalocyanines. Org Biomol Chem 7, 1583-1591.

Lo, P.C., Chan, C.M., Liu, J.Y., Fong, W.P., Ng, D.K., 2007. Highly photocytotoxic glucosylated silicon(IV) phthalocyanines. Effects of peripheral chloro substitution on the photophysical and photodynamic properties. J Med Chem 50, 2100-2107.

Lo, P.C., Fong, W.P., Ng, D.K., 2008. Effects of peripheral chloro substitution on the photophysical properties and in vitro photodynamic activities of galactose-conjugated silicon(IV) phthalocyanines. Chem Med Chem 3, 1110-1117.

Lo, P.C., Huang, J.D., Cheng, D.Y., Chan, E.Y., Fong, W.P., Ko, W.H., Ng, D.K., 2004. New amphiphilic silicon(IV) phthalocyanines as efficient photosensitizers for photodynamic therapy: synthesis, photophysical properties, and in vitro photodynamic activities. Chemistry 10, 4831-4838.

Longo, J.P., Lozzi, S.P., Simioni, A.R., Morais, P.C., Tedesco, A.C., Azevedo, R.B., 2009. Photodynamic therapy with aluminum-chloro-phthalocyanine induces necrosis and vascular damage in mice tongue tumors. J Photochem Photobiol B 94, 143-146.

Luthi, A.U., Martin, S.J., 2007. The CASBAH: a searchable database of caspase substrates. Cell Death Differ 14, 641-650.

MacDonald, I.J., Dougherty, T.J., 2001. Basic principles of photodynamic therapy. J Porphyrins Phthalocyanines 5, 105-129.

Maillard, P., Gaspard, S., Guerquin-Kern, J. L., Momenteau, M., 1989. Glycoconjugated tetrapyrrolic macrocycles. J Am Chem Soc 111, 9125–9127.

Mak, N.K., Li, K.M., Leung, W.N., Wong, R.N., Huang, D.P., Lung, M.L., Lau, Y.K., Chang, C.K., 2004. Involvement of both endoplasmic reticulum and mitochondria in photokilling of nasopharyngeal carcinoma cells by the photosensitizer Zn-BC-AM. Biochem Pharmacol 68, 2387-2396.

Marchal, S., Francois, A., Dumas, D., Guillemin, F., Bezdetnaya, L., 2007. Relationship between subcellular localisation of Foscan and caspase activation in photosensitised MCF-7 cells. Br J Cancer 96, 944-951.

Mattson, M.P., LaFerla, F.M., Chan, S.L., Leissring, M.A., Shepel, P.N., Geiger, J.D., 2000. Calcium signaling in the ER: its role in neuronal plasticity and neurodegenerative disorders. Trends Neurosci 23, 222-229.

Miller, J.D., Baron, E.D., Scull, H., Hsia, A., Berlin, J.C., McCormick, T., Colussi, V., Kenney, M.E., Cooper, K.D., Oleinick, N.L., 2007. Photodynamic therapy with the phthalocyanine photosensitizer Pc 4: the case experience with preclinical mechanistic and early clinical-translational studies. Toxicol Appl Pharmacol 224, 290-299.

Moor, A.C., 2000. Signaling pathways in cell death and survival after photodynamic therapy. J Photochem Photobiol B 57, 1-13.

Mukhopadhyay, P., Rajesh, M., Yoshihiro, K., Hasko, G., Pacher, P., 2007. Simple quantitative detection of mitochondrial superoxide production in live cells. Biochem Biophys Res Commun 358, 203-208.

Nagata, S., Obana, A., Gohto, Y., Nakajima, S., 2003. Necrotic and apoptotic cell death of human malignant melanoma cells following photodynamic therapy using an amphiphilic photosensitizer, ATX-S10(Na). Lasers Surg Med 33, 64-70.

Nakagawa, T., Yuan, J., 2000. Cross-talk between two cysteine protease families. Activation of caspase-12 by calpain in apoptosis. J Cell Biol 150, 887-894.

Nicholson, D.W., Ali, A., Thornberry, N.A., Vaillancourt, J.P., Ding, C.K., Gallant, M., Gareau, Y., Griffin, P.R., Labelle, M., Lazebnik, Y.A., et al., 1995. Identification and inhibition of the ICE/CED-3 protease necessary for mammalian apoptosis. Nature 376, 37-43.

Nishiyama, N., Nakagishi, Y., Morimoto, Y., Lai, P.S., Miyazaki, K., Urano, K., Horie, S., Kumagai, M., Fukushima, S., Cheng, Y., Jang, W.D., Kikuchi, M., Kataoka, K., 2009. Enhanced photodynamic cancer treatment by supramolecular nanocarriers charged with dendrimer phthalocyanine. J Control Release 133, 245-251.

Noodt, B.B., Berg, K., Stokke, T., Peng, Q., Nesland, J.M., 1999. Different apoptotic pathways are induced from various intracellular sites by tetraphenylporphyrins and light. Br J Cancer 79, 72-81.

Noodt, B.B., Kvam, E., Steen, H.B., Moan, J., 1993. Primary DNA damage, HPRT mutation and cell inactivation photoinduced with various sensitizers in V79 cells. Photochem Photobiol 58, 541-547.

Novichenko, N.L., Mamchur, A.A., Lisniak, I.O., Gamaliya, M.F., 2008. Study of photodynamic efficiency of the hematoporphyrin conjugated with antibody to VEGF in mouse Lewis carcinoma. Exp Oncol 30, 315-318.

Nunez, G., Benedict, M.A., Hu, Y., Inohara, N., 1998. Caspases: the proteases of the apoptotic pathway. Oncogene 17, 3237-3245.

Pandey, S.K., Zheng, X., Morgan, J., Missert, J.R., Liu, T.H., Shibata, M., Bellnier, D.A., Oseroff, A.R., Henderson, B.W., Dougherty, T.J., Pandey, R.K., 2007. Purpurinimide carbohydrate conjugates: effect of the position of the carbohydrate moiety in photosensitizing efficacy. Mol Pharm 4, 448-464.

Plaetzer, K., Kiesslich, T., Krammer, B., Hammerl, P., 2002. Characterization of the cell death modes and the associated changes in cellular energy supply in response to AlPcS4-PDT. Photochem Photobiol Sci 1, 172-177.

Porter, A.G., Janicke, R.U., 1999. Emerging roles of caspase-3 in apoptosis. Cell Death Differ 6, 99-104.

Reiners, J.J., Jr., Caruso, J.A., Mathieu, P., Chelladurai, B., Yin, X.M., Kessel, D., 2002. Release of cytochrome c and activation of pro-caspase-9 following lysosomal photodamage involves Bid cleavage. Cell Death Differ 9, 934-944.

Rhodes, L.E., de Rie, M.A., Leifsdottir, R., Yu, R.C., Bachmann, I., Goulden, V., Wong, G.A., Richard, M.A., Anstey, A., Wolf, P., 2007. Five-year follow-up of a randomized, prospective trial of topical methyl aminolevulinate photodynamic therapy vs surgery for nodular basal cell carcinoma. Arch Dermatol 143, 1131-1136.

Schroder, M., Kaufman, R.J., 2005. ER stress and the unfolded protein response. Mutat Res 569, 29-63.

Sharman, W.M., van Lier, J.E., Allen, C.M., 2004. Targeted photodynamic therapy via receptor mediated delivery systems. Adv Drug Deliv Rev 56, 53-76.

Sherman, M.Y., Goldberg, A.L., 2001. Cellular defenses against unfolded proteins: a cell biologist thinks about neurodegenerative diseases. Neuron 29, 15-32.

Sibani, S.A., McCarron, P.A., Woolfson, A.D., Donnelly, R.F., 2008. Photosensitiser delivery for photodynamic therapy. Part 2: systemic carrier platforms. Expert Opin Drug Deliv 5, 1241-1254.

So, C.W., Tsang, P.W., Lo, P.C., Seneviratne, C.J., Samaranayake, L.P., Fong, W.P., 2009. Photodynamic inactivation of *Candida albicans* by BAM-SiPc. Mycoses (in press).

Song, L., Li, H., Sunar, U., Chen, J., Corbin, I., Yodh, A.G., Zheng, G., 2007. Naphthalocyanine-reconstituted LDL nanoparticles for in vivo cancer imaging and treatment. Int J Nanomedicine 2, 767-774.

Sun, S.C., Xiao, G., 2003. Deregulation of NF-kappaB and its upstream kinases in cancer. Cancer Metastasis Rev 22, 405-422.

Tan, Y., Dourdin, N., Wu, C., De Veyra, T., Elce, J.S., Greer, P.A., 2006. Ubiquitous calpains promote caspase-12 and JNK activation during endoplasmic reticulum stress-induced apoptosis. J Biol Chem 281, 16016-16024.

Teiten, M.H., Marchal, S., D'Hallewin, M.A., Guillemin, F., Bezdetnaya, L., 2003. Primary photodamage sites and mitochondrial events after Foscan photosensitization of MCF-7 human breast cancer cells. Photochem Photobiol 78, 9-14.

Triesscheijn, M., Baas, P., Schellens, J.H., Stewart, F.A., 2006. Photodynamic therapy in oncology. Oncologist 11, 1034-1044.

Vantieghem, A., Assefa, Z., Vandenabeele, P., Declercq, W., Courtois, S., Vandenheede, J.R., Merlevede, W., de Witte, P., Agostinis, P., 1998. Hypericin-induced photosensitization of HeLa cells leads to apoptosis or necrosis. Involvement of cytochrome c and procaspase-3 activation in the mechanism of apoptosis. FEBS Lett 440, 19-24.

Varnes, M.E., Chiu, S.M., Xue, L.Y., Oleinick, N.L., 1999. Photodynamic therapy-induced apoptosis in lymphoma cells: translocation of cytochrome c causes inhibition of respiration as well as caspase activation. Biochem Biophys Res Commun 255, 673-679.

Whitacre, C.M., Feyes, D.K., Satoh, T., Grossmann, J., Mulvihill, J.W., Mukhtar, H., Oleinick, N.L., 2000. Photodynamic therapy with the phthalocyanine photosensitizer Pc 4 of SW480 human colon cancer xenografts in athymic mice. Clin Cancer Res 6, 2021-2027.

Yom, S.S., Busch, T.M., Friedberg, J.S., Wileyto, E.P., Smith, D., Glatstein, E., Hahn, S.M., 2003. Elevated serum cytokine levels in mesothelioma patients who have undergone pleurectomy or extrapleural pneumonectomy and adjuvant intraoperative photodynamic therapy. Photochem Photobiol 78, 75-81.

Zhang, M., Zhang, Z., Blessington, D., Li, H., Busch, T.M., Madrak, V., Miles, J., Chance, B., Glickson, J.D., Zheng, G., 2003. Pyropheophorbide 2-deoxyglucosamide: a new photosensitizer targeting glucose transporters. Bioconjug Chem 14, 709-714.

Zhang, Z., Jin, H., Bao, J., Fang, F., Wei, J., Wang, A., 2006. Intravenous repeated-dose toxicity study of ZnPcS2P2-based-photodynamic therapy in Wistar rats. Photochem Photobiol Sci 5, 1006-1017.

Zorov, D.B., Filburn, C.R., Klotz, L.O., Zweier, J.L., Sollott, S.J., 2000. Reactive oxygen species (ROS)-induced ROS release: a new phenomenon accompanying induction of the mitochondrial permeability transition in cardiac myocytes. J Exp Med 192, 1001-1014.